INSTITUTE OF PHYSICS, POLISH ACADEMY OF SCIENCES

DOCTORAL THESIS

# Study of factors governing mechanism of protein aggregation by using computer simulation

*Author* Nguyen Truong Co

*Supervisor* Prof. dr hab. Mai Suan Li

*A thesis submitted in fulfillment of the requirements*

*for the degree of Doctor of Philosophy*

*in the Division of Theoretical Physics*

April 18, 2022

# Declaration

I, Nguyen Truong Co, declare that this thesis entitled, "Study of factors governing mechanism of protein aggregation by using computer simulation" and the work presented in it is my own. I confirm that:

- This work was done wholly or mainly while in candidature for a research degree at Institute of Physics, Polish Academy of Sciences.
- Where any part of this thesis has previously been submitted for a degree or any other qualification at this Institute or any other institution, this has been clearly stated.
- Where I have consulted the published work of others, this is always clearly attributed.
- Where I have quoted from the work of others, the source is always given or cited. With the exception of such quotations, this thesis is entirely my own work.
- I have acknowledged all main sources of help.
- Where the thesis is based on work done by myself jointly with others, I have made clear exactly what was done by others and what I have contributed myself.

---

Full Name Goes Here

---

Date

# Abstract

In the past few decades, despite many efforts, researchers have not found a cure for neurodegenerative diseases such as Alzheimer's disease and Parkinson's disease. The reason for these failures is probably because we do not understand the nature of these diseases. According to the amyloid hypothesis, neurodegenerative diseases are associated with the accumulation of proteins or peptides in the brain leading to neuronal death. For example, Alzheimer's disease can be caused by the aggregation of amyloid beta (Aβ) peptides between cells, while Parkinson's disease is caused by the aggregation of alpha-synuclein protein. If the amyloid hypothesis is correct, it will be important to find the factors that control the accumulation of insoluble fibrils. In addition, understanding the mechanisms that break down fibrils is useful work that can help us find ways to treat the disease. In this dissertation, we studied the role of beta content of a monomer and surface roughness in fibril formation of proteins. To study the kinetics of temperature-induced degradation of fibrils, a new phenomenological theory was developed and supplemented by simulations.

Previous studies showed that the environment properties (pH, protein concentration, salts, temperature ...) and intrinsic properties of proteins (hydrophobicity, electrical charge, propensity to fibrillate in the monomer state, etc) are factors that control the fibril formation rate of proteins. Experimentally resolved fibrillar structure of the protein consists of crossed β-sheets, which suggests that monomers with high β content are expected to fibrillate faster than monomers with a lower β composition. Therefore, studying the monomner structure can help infer information on the kinetics of the fibril formation process, but this relationship has not been clearly demonstrated. In this thesis, we collected the fibril formation rate from previous experimental works and calculated the β content in the monomer state for the Aβ42 wild type and its 19 mutations using replica exchange molecular dynamics (REMD) all-atom simulations with implicit water. The high correlation between the experimental aggregation rate and the β content allows confirming that the β structure in the monomer state is an important factor that controls the fibrillation rate of Aβ42. The higher the β content, the faster the fibril formation process and the dependence of the fibrillation rate on the β content can be described by an exponential function. Currently, the calculation of the fibril formation time of proteins using all-atom simulations is prohibited due to the large gap between the real time (days) and the computation time (ms). From this point of view, our result is very useful, as it opens up a new way to estimate the rate of fibril formation using β-content, which can be easily obtained using REMD simulations.

Protein aggregation can occur both in solution and on surfaces, for example, in the case of cell membranes. Self-assembly of proteins on various surfaces has been the subject of many experimental and theoretical studies, but the effect of surface roughness on the kinetics of this process has not been theoretically studied. Here, we have developed a simple lattice model that allows us to explore this problem in depth due to its low computational cost. For both

hydrophobic and hydrophilic smooth surfaces our model predicts that aggregation time increases with protein-surface interactions in weak (entropy-driven) and strong (energy-driven) interaction regimes. However, in the intermediate regime of interaction, aggregation is accelerated with increasing protein-surface interaction due to the competition between entropy and energy factors. It was shown that, in agreement with the experiment, a rough surface retards the fibril formation of polypeptide chains, and at high roughness this process is inhibited. One of the most interesting predictions followed from our model is that a weakly rough surface enhances the fibril formation rather than delaying it. This effect is possible when the protein-surface interaction is moderate and results from the trade-off of entropy and energy.

Protein aggregates or fibrils can degrade for various reasons such as the binding of other molecules, the presence of chemical denaturants, temperature increase, etc. Since the degradation of these complexes is one of the possible treatments for neurodegenerative diseases, understanding the molecular mechanisms underlying this process, is of great importance. Traditionally, ThT fluorescence assay has been used to study heat-induced degradation, and the decay of fibril content, proportional to the fluorescence signal, can be described by a bi-exponential function of time. Recently, tryptophan fluorescence has been used to control the amount of monomers belonging to the dominant cluster. Moreover, the engineered ZAβ3W protein was used to sequester the Aβ monomer, i.e. preventing it from rejoining the parent cluster. This scenario can be called degradation without recycling, which differs from the standard scenario, when the monomer released from the parent cluster can be re-associated with it. It was experimentally shown that without monomer recycling a single-exponential function can be used to fit the time dependence of the number of monomers of the dominant cluster provided that the proportion of bound monomers becomes less than a certain threshold. We developed a phenomenological theory and showed that the dependence of the number of monomers of the dominant cluster obeys a logistic function for both recycling and non-recycling cases. Above a certain threshold, this function becomes a single exponential, and this agrees with experiment. We performed lattice and all-atom simulations for 10 Aβ37–42 truncated peptides, which confirmed our theory.

# Publications associated with this thesis

1. Nguyen Truong Co, Mai Suan Li. *Effect of Surface Roughness on Aggregation of Polypeptide Chains: A Monte Carlo Study*. Biomolecules 11, 596 (2021)
2. Tran Thi Minh Thu, Nguyen Truong Co, Ly Anh Tu and Mai Suan Li *Aggregation rate of amyloid beta peptide is controlled by beta-content in monomeric state*,, J. Chem. Phys. 150, 225101 (2019)
3. Nguyen Truong Co, Pham Dang Lan, Pham Dinh Quoc Huy, and Mai Suan Li**,** *Heat-induced degradation of fibrils: Exponential vs logistic kinetics*, J. Chem. Phys. 152, 115101 (2020)

# Acknowledgement

I would like to express my gratitude to my supervisor prof. dr. hab. Mai Suan Li, who guided me to complete this thesis. I highly appreciate the fruitful collaboration with Dr. Pham Dinh Quoc Huy, Pham Dang Lan, Dr. Tran Thi Minh Thu, and Dr. Ly Anh Tu, which resulted in the three publications used in this thesis. Finally, I would like to say a big thanks to my big family, particularly my elder brother Xuan Ro and my younger brother Ngoc Luat for their special meaning in my life.

# Table of contents

# List of figures

# List of tables

# Chapter 1: Introduction

## 1.1 Motivation

It is assumed that many neurodegenerative diseases, such as Alzheimer's, Parkinson's, Huntington's, and others, are associated with protein aggregation, which, under suitable environmental conditions, can lead to the formation of amyloid fibrils [1-3]. Due to the urgent need to find effective treatments for these diseases, a huge amount of research has been carried out on the factors that control the kinetics of protein self-assembly, which is associated with neurotoxicity [4-6]. These factors can be divided into two groups: external factors and intrinsic (internal) ones. The first group includes environmental conditions such as protein concentration, pH, temperature, ionic strength, and presence of membranes, foreign surfaces or crowders. Intrinsic factors are the internal properties of proteins, including their sequences, charge, aromatic interaction, hydrophobicity, the population of fibril-prone structure in the monomer state, etc.

Since there is still no cure for neurodegenerative diseases, the discovery of new factors affecting protein aggregation has implications not only for basic research but also for applications. In this thesis, using all-atom simulation with implicit water and experimental results on the rate of fibril formation, we have proved that the fibril formation rate depends on the beta structure of the monomer state exponentially; the higher the beta content, the faster the fibrillation.

Another external factor of interest to us is how roughness of the foreign surface affects protein aggregation. This issue is important because biological processes occur in cells with different types of surfaces such as lipid bilayers and have been investigated experimentally but theoretically remain open. With today's computer capabilities, it is not possible to calculate fibrillization rates based on all-atom models, so to investigate this issue thoroughly we have developed a lattice model in the presence of the surface. Our model is an extension of the model developed by the group of Prof. M. S. Li and Prof. D. Thirumalai to study the protein aggregation in solution [7,8]. Using our model we performed Monte Carlo simulations and demonstrated that in general surface roughness impedes protein fibrillation and when the roughness is large enough this process is completely inhibited, which is consistent with experiment [9]. However, we predict that if the protein-surface interaction is moderate, the weak roughness might promote fibrillation rather than hinder it.

Since neurodegenerative diseases involve the formation of protein plaques/oligomers, disrupting these plaques is also one of the possible treatment options. One of the ways to break up aggregates is to increase the temperature, also known as heat-induced dissociation. Although this approach may not work because at high temperatures proteins will be inactivated, understanding the molecular mechanism underlying heat-induced dissociation is significant for basic research. It is well known that due to thermal fluctuations the content of fibril mass measured by ThT

fluorescence assay decays with time and the corresponding time dependence is described by a bi-exponential function [10]. In recent experiments, tryptophan fluorescence has been used to control the proportion of monomers belonging to the main cluster. Interestingly, it was found that the decay of this fraction over time obeys a single exponential rather than a bi-exponential function. To elucidate this issue, we have developed a phenomenological theory and showed that the time dependence of the number of monomers belonging to the main cluster is described by the logistic function. Above a certain threshold this function becomes a single exponential function and this is in agreement with the experiment. Our theory is applicable to both cases when the released monomer is allowed to return to the parent cluster or not allowed to return thanks to protein capture technique. We have also carried out both lattice and all-atom simulations to support our theory.

This thesis contains 5 chapters. A brief Introduction with motivation is given in Chapter 1. Chapter 2 is devoted to literature review, where we presented the kinetics of protein aggregation, the typical amyloid fibril structures, and their relation to various neurodegenerative diseases. The biological functions and potential applications of amyloid fibrils in materials science have been discussed. This chapter has also reviewed the main factors that control the aggregation process, as well as popular computational models used in studying the process of fibril formation. Chapter 3 describes the main computational methods used in this dissertation. Chapter 4 summarizes the results of three publications presented in this dissertation: the influence of foreign surfaces on protein aggregation with an emphasis on surface roughness [11], the correlation between beta content in the monomeric state and the rate of protein aggregation [12] , and the kinetics of thermal degradation of fibrils [13]. Conclusions and a plan for future work are presented in Chapter 5.

## 1.2 Other important information

My thesis is organized as follows:
Chapter 1: Introduction
Chapter 2: Literature review on protein aggregation, their association with diseases, main factors governing the fibril formation; computational models applied to study aggregation process**.**
Chapter 3: Computational techniques used in this thesis.
Chapter 4: Summary of publications
- 4.1 Effect of Surface Roughness on aggregation of polypeptide chains: A Monte Carlo Study
- 4.2 Aggregation rate of amyloid beta peptide is controlled by beta-content in monomeric state
- 4.3 Heat-induced degradation of fibrils: Exponential vs. logistic kinetics

Chapter 5: Conclusions and future work.

**List of publications presented in this thesis**

1 Nguyen Truong Co, Mai Suan Li. *Effect of Surface Roughness on Aggregation of Polypeptide Chains: A Monte Carlo Study*. Biomolecules 11, 596 (2021)

2 Tran Thi Minh Thu, Nguyen Truong Co, Ly Anh Tu and Mai Suan Li *Aggregation rate of amyloid beta peptide is controlled by beta-content in monomeric state*,, J. Chem. Phys. 150, 225101 (2019)

3 Nguyen Truong Co, Pham Dang Lan, Pham Dinh Quoc Huy, and Mai Suan Li**,** *Heat-induced-degradation of fibrils: Exponential vs logistic kinetics*, J. Chem. Phys. 152, 115101 (2020)

**Other publications**

1. Mai Suan Li, Nguyen Truong Co, Govardhan Reddy, Chin-Kun Hu, J.E.Straub and D. Thirumalai, *Factors governing fibrillogenesis of polypeptide chains revealed by lattice models*, Phys. Rev. Lett. 105, 218101(2010)
2. Nguyen Truong Co and M. S. Li, *New method for determining size of critical nucleus of fibril formation of polypeptide chains*, J. Chem. Phys. 137, 095101 (2012)
3. Nguyen Truong Co, Chin-Kun Hu, and Mai Suan Li, *Dual effect of crowders on fibrillation kinetics of polypeptide chains revealed by lattice models*, J. Chem. Phys. 138, 185101 (2013)
4. M. Kouza, Nguyen Truong Co, P.H. Nguyen, A. Kolinski, and Mai Suan Li, *Preformed template fluctuations promote fibril formation: Insights from lattice and all-atom models*, J. Chem. Phys. 142, 145104, (2015)
5. Maksim Kouza, Nguyen Truong Co, Mai Suan Li, Sebastian Kmiecik, Andrzej Kolinski, Andrzej Kloczkowski, and Irina Alexandra Buhimschi, *Kinetics and mechanical stability of the fibril state control fibril formation time of polypeptide chains: A computational study*, J. Chem. Phys. 148, 215106 (2018) (co-main author)

**Conference publications**

Nguyen Truong Co, Man Hoang Viet, Phan Minh Truong, Maksim Kouza, Mai Suan Li, Key Factors Governing *Fibril Formation of Proteins: Insights From Simulations And Experiments* Task Quarterly 18 No 3, 219-229 (2014)

**Book chapter**

Co N.T., Li M.S., Krupa P. (2022) *Computational Models for the Study of Protein Aggregation.* In: Li M.S., Kloczkowski A., Cieplak M., Kouza M. (eds) Computer Simulations of Aggregation of Proteins and Peptides. Methods in Molecular Biology, vol 2340. Humana, New York, NY

**Publication metrics**

Total number of citations without self-citations: 151
H-index: 6 (Web of Science, as of April 18th, 2022)

# Chapter 2: Literature Review

## 2.1 Protein self-assembly kinetics

Proteins are biomolecules that compose of amino acids (residues) connected by polypeptide bonds. They perform many important functions in organisms, such as building material for tissues, carrying out information transfer within the body, balancing the PH level, replicating DNA, etc. A protein functions correctly if it can adopt a specific compact and energetically favorable three-dimensional structure called a folded structure or native state. The path of protein evolution from the initial configuration, when the protein is synthesized in the ribosome, to its folded state in solution, passes through extremely complex intermediate states. In general, it is counterintuitive if a protein must sample all possible configurations to reach the native state, because in this case the required folding time can be astronomical. In reality, proteins reach their native states in milliseconds to seconds and this confliction was known as Levinthal's paradox [14]. One of the widely accepted scenarios for the protein folding kinetics has been proposed by Wolynes, Onuchic and Dill, which is called the funnel theory [15,16]. According to this theory, protein folding occurs along some pathways rather an exhaustive configuration sampling.

Although, the folding process is under the strict regulation of the cell quality control system under some environmental conditions, the protein cannot fold to its native state leading to misfolding and aggregation. Figure 1 shows the free energy landscape of both protein folding (purple funnel) and protein aggregation (pink) processes, in which protein folding and protein self-assembly are controlled by intra-molecular and inter-molecular contacts, respectively. The wide area at the top of the funnel means that when stretched or unfolded, the protein can adopt a large number of different high-entropy configurations. Folding intermediates and partially folded states correspond to local minima of the folding free energy landscape. While the folding funnel (purple) reflects interactions within a monomer, the aggregation funnel (pink) captures not only intrachain interactions but also interchain interactions, where misfolded proteins form diverse aggregates, including oligomers, amorphous aggregates or amyloids fibrils, depending on sequences and external conditions [17].

As briefly mentioned in the introduction, the association between fibril formation or, more broadly, protein aggregation, and many chronic neurodegenerative diseases such as Alzheimer's, Parkinson's, and Huntington's has catalyzed a vast amount of research aimed at unraveling the underlying mechanism and discovering effective treatments [2,3]. Furthermore, the diversity of amyloid morphologies [18-20], the high percent of hydrogen bonds in their structure, and their biocompatible properties indicate potential applications of amyloid fibrils in nanotechnologies and many other areas [21,22].

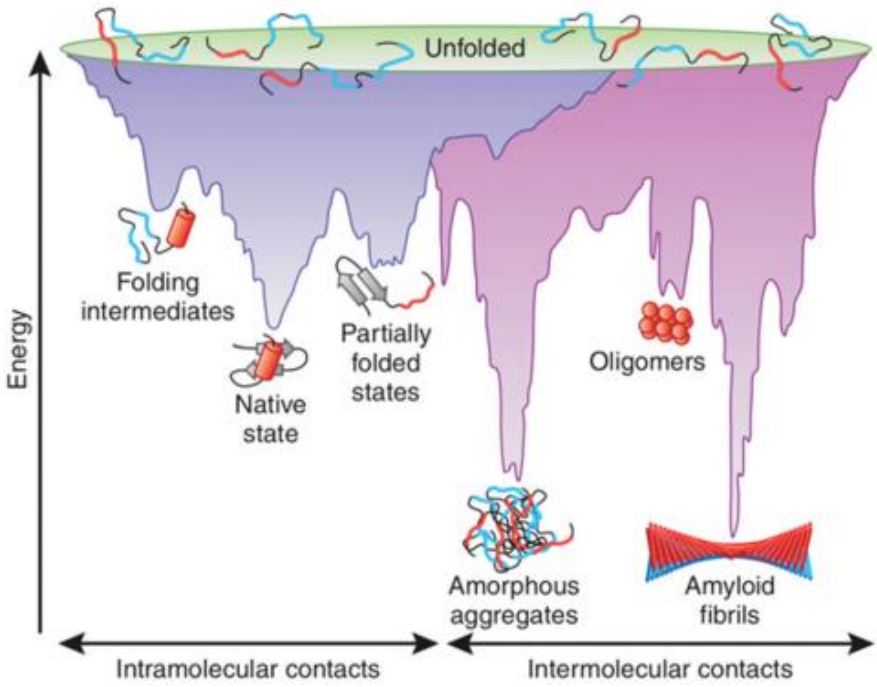


**Figure 1**: Presentation of protein folding, aggregation pathways and the free energy landscape [23]. The purple and pink colors correspond to the folding and aggregation funnels, respectively. More information can be visually obtained from the figure.

In the experiment, the concentration of fibrils in solution or fibril mass was controlled by the fluorescence intensity of binding dyes, for instance, Thioflavin-T (ThT), Congo red (CR). The time dependence of the fibril mass can be described as a sigmoidal curve with three typical phases (Figure 2). The lag phase corresponds to the early stage when self-assembly of proteins is thermodynamically unfavorable until the formation of critical nuclei, from which proliferation occurs. During the lag phase, the critical nucleus is created following one-step (1SN) or two-step (2SN) kinetics [24,25]. 1SN refers to a process in which two monomers with a high binding propensity are combined into a dimer with a high β-content, which plays the role of a critical nucleus and a growing template. Meanwhile, 2SN is a process in which many monomers combine into unstructured stable particles and then rearrange into a β-rich nucleus. The duration of the lag phase is characterized by the lag time, $t_{lag}$, which can be experimentally estimated by observing a decrease in the monomer concentration or the mass of aggregates [24]. The growth phase is recognized by the rapid increase in fibril mass. due to the incorporation of peptides into this template, which is regulated by many possible mechanisms, such as the dock-lock mechanism [26], secondary nucleation [27,28], fibril fragmentation [29], fibril elongation.

According to the dock-lock mechanism, fibril formation is a two-stage process has: proteins dock to a preformed template, which corresponds to the dock phase, then the nascent chain is rearranged to reach an optimal stable position on the template and this process is called the lock-phase. The dock-lock mechanism leads to the steady growth of protofibril, fibril as well as other

aggregated products [26]. In the mechanism of secondary nucleation, the appearance of various templates results in increasing number of surfaces that catalyze the formation of new oligomers, on which new self-assembly process possibly occur. This accelerates the formation of fibrils. Finally, the process gets saturation when the concentration of monomers reaches an equilibrium state, and the predominant product in solution mainly comprises of mature fibrils.

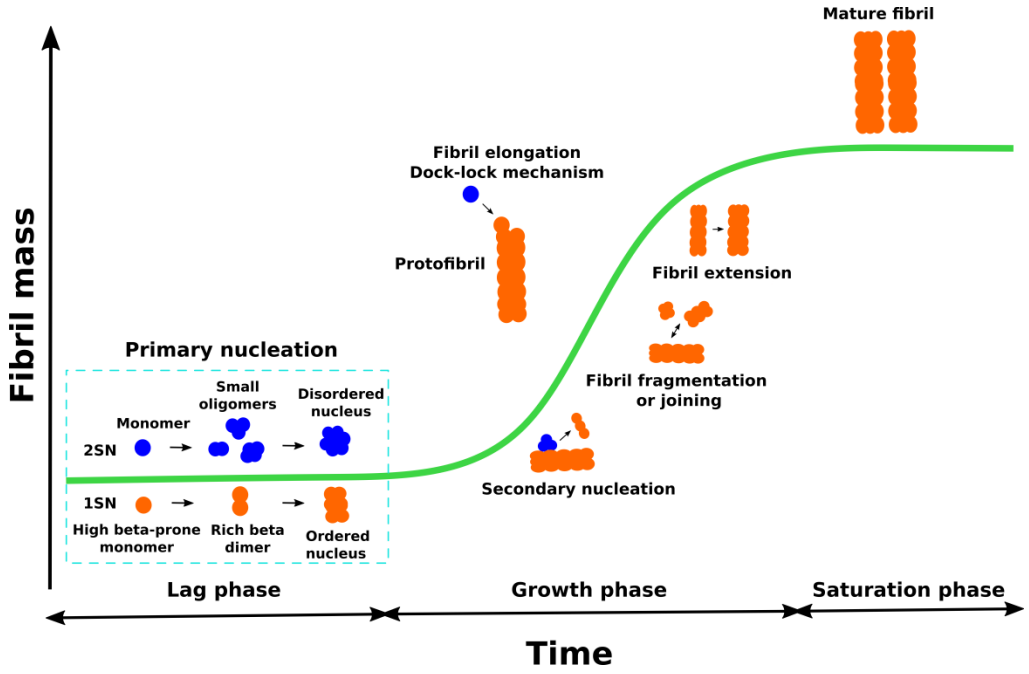


**Figure 2**: Typical sigmoidal shape of kinetics of protein aggregation [30].The blue and orange colors refer to poor and rich beta-content species, respectively. More information can be obtained directly from the picture

### *Structure of amyloid fibrils*

X-Ray diffraction (XRD) [31], solid-state nuclear magnetic resonance (ss-NMR)[32] and cryo-EM (Cryogenic Electron Microscopy)[33] are the three most common experimental methods for determining the amyloid fibril structures. Generally, amyloid fibrils have been experimentally observed as thread-line structures with approximate micron and 7-13 nm in length and diameter, respectively. They may consist of a single filament or a set of protofibrils twisted together in an ordered manner. Structurally, the protein arrangement in a fibril mainly takes form of cross-β structures, in which β-strands (the extended conformation of the polypeptide chain according to its backbone) are oriented perpendicularly to the fibril axis [1,3].

Stacking of β-strands leads to the formation of β-sheets, a process mainly governed by hydrogen bonds between protein backbones. β-sheets can interact and organize to create protofibrils or protofilaments ,which in turn continue assemble to higher order amyloid fibril structures. Due to the diversification of fibril formation pathways amyloid fibrils are polymorphic, which depends not only on specific amyloidogenic sequences, but also experimental conditions, as well as the fibril formation kinetics. Figure 3 shows various amyloid fibril structures of different Aβ-peptides. The most dominant sequences of this class are the Aβ40 and Aβ42 variants, which are supposed to be closely associated with Alzheimer's disease [1].

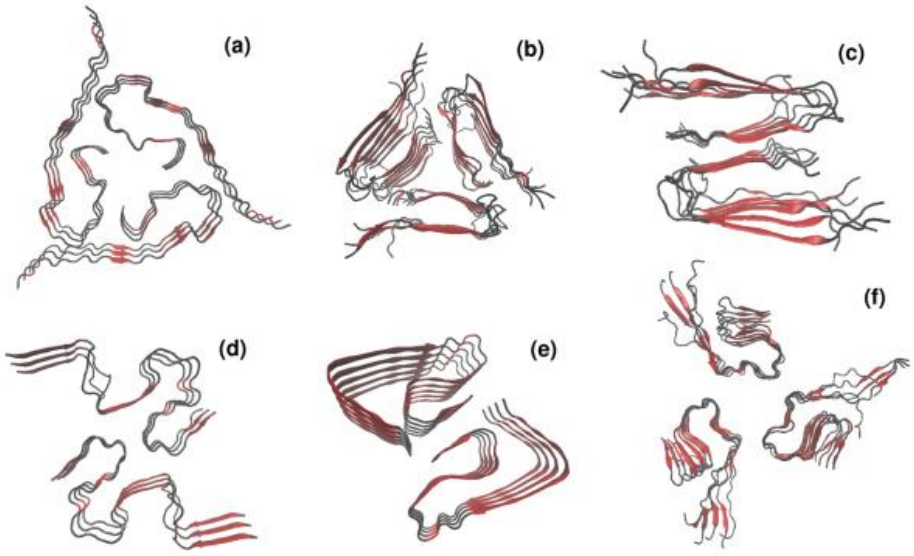


**Figure 3**: Different fibril morphologies of β-amyloid peptides [34]. U-shaped Aβ40 2M4J [35] (a) ; fibril structures of Aβ9-40: (PDB code 2LMP) [36] (b) and (c) 2LMO [36]; S-shaped 2NAO [37] (d), LS-shaped 5OQV [38] (e) fibril structures and out-of-register model fibril [39] (f) of *A*β42.

***Diseases related to amyloid-like deposit***

The aggregation of protein into an amyloid-like structure is thought to be associated with many diseases in humans. Most of the 37 proteins associated with human amyloid–associated diseases are rather short polypeptide chains containing less than 400 residues compared to the average length of human genome protein length of about 500 residues. These 37 proteins include 13 intrinsically disordered proteins, 9 proteins with unknown structure, 14 proteins with a well-defined native structure, and one with both disordered and globular domains in its structure.

Neurodegenerative diseases are associated with 7 proteins whose amyloid aggregates are located in the central nervous system, while the non-neuropathic disorder is associated with the remaining 30 proteins, of which 15 are deposited in multi-organs such as the liver, spleen, heart,

and the remaining 15 amyloid deposits in one of the specific tissues, causing various localized human pathologies [1]. One of the most common neurodegenerative diseases is Alzheimer's disease associated with the assembly of Aβ40, Aβ42 peptides and their variants into amyloid plaques with crossed β-structure [40]. Parkinson's disease is believed to be associated with α-synuclein (αS) deposition [41], and prion protein (PrP) aggregation leads to Creutzfeldt-Jakob disease [42]. Deposition of β2-microglobulin (β2-m), lysozyme (LYS), gelsolin fragments are associated with systemic dialysis amyloidosis [43], systemic lysozyme amyloidosis [44], and systemic familial amyloidosis [45], respectively. Localized disorders include type II diabetes induced by islet amyloid polypeptide deposition (IAPP) [46], medial aortic amyloidosis is closely associated with medin amyloid formation [47] or injectable localized amyloidosis associated with enfuvirtide peptide aggregation [1,48].

Non-amyloid deposits can also cause human diseases. Aggregation of the 2355-residue proteins Fibronectin (FN) is associated with FN glomerulopathy [49,50]; Hemoglobin misfolding leads to sickle cell anemia or Heinz body anemia [1,51]; deposition of cellular tumor antigens p53 may indicate cancer development [52,53].

Amyloid fibrils have received much attention due to their potential association with many serious illnesses, however, in nature, there is a class of amyloids involved in a wide range of functions in mammals, bacteria, fungi and insects called functional amyloids [17]. For example, amyloid of hormone signaling peptides stores, sorts or releases hormones in mammals [54]; Curli amyloid contributes to the construction of extracellular matrix [55]; the HIV virus exploits the amyloid deposition of prostatic acid phosphatase fragment and semenogelin for its infection [56].

Another positive aspect of amyloids is artificial amyloids created in vitro from non-toxic proteins. Artificial amyloids retain the typical beneficial characteristics of natural amyloid fibrils, including their extreme aspect ratio, surface chemistry coated with functional amino acids, or high quality tensile modulus elasticity, so they are used in many fields [17]. Artificial amyloids can serve as templates for fabricating new materials, devices, and nanotechnologies [20]. Decorating gold, silver, and palladium nanoparticles with amyloid fibrils improves the delivery of such particles to a living organism [57]. Cheetham et al. created drug-peptides whose nanofibrils and nanotubes acted as drug loading agents [58]. Artificial amyloids are also used for the synthesis of gels used in cell culture and growth [59], and are used as materials for the manufacture of optical devices such as organic/polymer light emitting diodes (OLED/PLED) [60], or for the creation of membranes based on amyloid for water purification [61].

## 2.2 Factors control the aggregation process

Proteins are divided into two classes: native or ordered and intrinsically disordered proteins (IDPs) [62]. Ordered proteins usually fold into their native state in which they function. By themselves, IDPs do not take a well-defined shape, but they can fold in the presence of other proteins. Under certain conditions, proteins misfold into off-pathway intermediates and

aggregate. Misfolding of proteins does not necessarily lead to aggregation, although in many cases the two processes are linked. Here we will review the main factors that affect protein aggregation. They are grouped into two categories: internal or intrinsic factors related to protein properties and external factors related to the environment.

### 2.2.1 External factors

***Temperature***

Assembling of monomers to higher-ordered structures is strongly influenced by temperature [63-65]. The aggregation rate of β-Lactoglobulin sharply increased as the temperature changed from $30^oC$ to $50^oC$ [66]. The acceleration of nucleation [67] and the elongation phase [68] for self-assembly of Aβ peptides was observed in the temperature range of 29-45$^o$ C and 4-40$^o$ C, respectively. Furthermore, some proteins exhibit cold-denaturation, in which their native structure loses stability at low temperatures that catalyzes condensation [69,70]. Ribosomal protein L9 exhibited a higher aggregated mass at $4^oC$ (76%) than at $25^oC$ (35%) [70], lowering the temperature from $37^oC$ to $5^oC$, which promoted the oligomerization of some monoclonal antibodies [71]. In a narrow temperature range, the temperature-dependent rate of aggregation of some proteins follows the traditional Arrhenius law [72-74]. However, over a wider temperature range, proteins may not obey this rule [5,65,75-77]. All direct or indirect effects of temperature on proteins complicatedly influent the whole self-assembly process. However, in general, the temperature dependence of aggregation time on temperature has a form of U-shape [78]. This is due to the competition between entropy and energy, since at high temperatures (entropy-driven regime) the system spends a lot of time reaching the fibril state among a huge number of states, and at low temperatures (energy-driven regime) thermal energy is not enough to escape local energy traps. Thus, in both regimes, the fibril formation time is long. Rapid aggregation occurs at the bottom of the U-curve when there is a trade-off between energy and entropy.

***Protein concentration***

Concentration of proteins is one of the most important factors affecting their self-assemble ability because increasing the protein concentration reduces the distance between proteins, enhances their interaction, and thereby improves their self-association[79,80]. Protein aggregation can occur above a concentration threshold that depends on proteins. The threshold of Aβ42, Aβ40 peptides is around μM [81,82] or even nM ranges [83], while PolyQ, β-Ovalbumin, and α-synuclein self-assemble at the concentration around 3μM [84], 7μM [85] and 0.7 μM [86], respectively. Increasing monomer concentration reduces the lag time and aggregation time in typical sigmoidal nucleus-dependent on-pathway aggregation due to the promotion of monomers collision [86]. However, in some cases [87,88], the aggregation slows down when adding more monomers to the solution due to the competition between the formation of clusters which do not contribute to the aggregation pathway (off-path way species) and the on-pathway species [89].

In protein aggregation that follows the primary nucleation mechanism, the dependence of any characteristic time ($\tau_F$) such as lag time, or half time, on the monomer concentration ($C$) is given by $\tau_F \approx C^{-(nc+1)/2}$ [90], where $n_c$ is the size of the critical nucleus of the aggregate. Different concentration dependence was observed for the secondary nucleation case [91].

***Pressure***

High hydrostatic pressure (HHP) [92-94] impacts on protein conformations, protein-protein interaction and further on their oligomeric or aggregated forms through volume changes [95]. Many studies [53,95] showed that, under high-pressure conditions, the change in volume due to expulsion of water from interior cavities of proteins [96], hydration of hydrophobic surfaces [97], dissociation, and breakage of associated ion-pair [98] are the cause of pressure-induced unfolding, and hence the aggregation rate and pathways [99-101].

***pH***

The pH level of the solution modulates the charge density of the protein surface. Environment with extreme pH leads to a high density of like charges on the surface of proteins leading to their strong repulsion, and reducing self-assembly. For example, self-assembly of Aβ42 peptide is inhibited at pH>9.5 due to electrical neutralization of the residue Ly28, which prevents the formation of a salt bridge between Ly28 and Asp23, which plays a key role in aggregation [102]. Generally, pH value around protein isoelectric point of a protein enhances protein aggregation [103].

***Ionic strength***

Just like pH, ionic strength of surrounding environment strongly influences the kinetics of protein self-assembly as well as aggregate morphology. Hover et al. observed various structures of α-synuclein deposits in NaCl and $MgCl_2$ solutions [104]; the presence of $SO4^{2-}$, $Cl^-$, $I^-$, $ClO4^-$ affected the amyloid formation of β2-microglobulin [105]. The effect of ionic strength on the aggregation propensity of β-lactoglobulin protein [106], islet amyloid polypeptide (IAPP) [107] , Aβ40 [108] or Aβ42 [109] have been investigated.

***Salts***

Salts dissolve in solution to cations and anions.These ions can bind unpaired charged residues or protein backbones leading to the change in protein conformations, solubility as well as inter-protein interactions, which affect the aggregation rate [110-112]. For example, rhGCSF self-assembly was enhanced in present of NaCl, but the addition of NaCl retarded aggregation of recombinant factor VIII SQ. Goto et. al. showed that modulation of NaCl concentration resulted in the competition between fibril formation and amorphous aggregates of β2-microglobulin [113]; Adding guanidinium hydrochloride (GdmCl) and $CaCl_2$ to solution of bovine serum albumin alters their aggregation behavior from a downhill to nucleated-dependent mechanism [114]; HCA

II aggregation kinetics changed from monophasic to biphasic kinetics at 328K under the effect of salt ions [115].

### *Crowding and confinement*

Proteins can misfold and aggregate when surrounded by various objects called crowders. In living organisms, crowders include proteins, sugar, lipid membranes, chaperons, DNA, RNA collagen, etc. which occupy up to 40% of a living solution [116-118]. In vitro, crowders can be artificial materials inserted to solution, such as nano particles [119] or other polymers [120]. Crowders can accelerate the protein self-assembly because their volume exclusion restricts accessible space of the protein reducing the protein entropic cost [121-125]. However, retardation of the aggregation process occurs in a crowding milieus of sufficiently small particles, where crowders limit the peptide diffusion [119,126,127] or deform proteins from their aggregation-prone state [128].

Crowding and confinement are often discussed together because of their close relationship. While crowders refer to molecules surrounding proteins which aggregate, confinement describes the boundary of rigid or fixed structures including chaperon, ribosome exit tunnel or cytoskeleton [129]. Typically, dependence of the protein aggregation rate on the confined volume (or size) can be described as a U-shape curve which results from the competition between the entropy and energy of proteins. A narrow confined space limits the conformational entropy of proteins, preventing them from assessing to an optimal energy state; therefore, the aggregation time rapidly increases. The protein conformational entropy sharply expands with an increase in the confinement volume, which leads to slowdown in the aggregation rate [126].

### *Foreign surfaces*

Protein is not only aggregate in solution but also in environment of various surfaces. We can consider foreign surfaces as crowders; however, not the same as crowding concept defined as the effect of the whole medium impacts on the protein self-assembly, the role of foreign surfaces on the process is being investigated more details because of their wide range applications including drug discovery, novel materials as well as polymer science [130-132]. Surfaces possibly accelerate the aggregation process such as many lipid membranes catalyze the fibril growth [133-135], mica and glass surfaces were reported to accelerate α-synuclein [136] and Aβ18-22 [137] fibrillations. By contrast, the presence of foreign surfaces can also restrict assembly of amyloid fibril; the misfolding of IAPP and Aβ42 to their fibril-like structures were restricted by appearance of the polymeric nanoparticles coverage [119] and the protein-coated surfaces of graphen oxide [138], respectively. Furthermore, the impact of surfaces can change the fibrillar morphologies [139,140] or even if completely alter them [141].

Protein aggregation also depends on the topologies [142] as well as roughness of surfaces [9,11]. Further discussion about effect of surfaces on protein self-assembly will be mentioned in section 4.2 of this thesis.

Other factors such as oxidative stress, organic solvent, ligands, freezing, thawing, metal ions, UV illumination, drying, pumping, surfactants, biopolymers, and mechanical-force-mediated amyloid formation have been studied [5,63,143].

The main external factors discussed above are *in vitro* factors. There are also *in vivo* factors affecting protein aggregation such as aging, over expression, oxidative stress, pathogenic mutations, impaired autophagy and proteasome impairment [143].

### 2.2.2 Protein intrinsic factors

#### *Mutations*

The aggregation ability of proteins strongly depends on their sequence. Therefore, it is natural that mutations that change the order and type of amino acids in the protein sequence have a huge impact not only on the kinetics, rate, but also on the morphology of the aggregated products of the self-assembly process [3,144]. For Aβ, mutations E22Q (Dutch mutation) and D23N showed a higher propensity to aggregate than its wild type [145-147], while substitutions H6R, D7N, K16N, E22Δ [148,149] alter fibrillar pathways, enhancing the formation toxic oligomers. Three mutations A53T, A30P and E46K in α-synuclein associated with Parkinson's disease slightly changed the structure of the monomer; A53T and E46K promote the kinetics of fibril formation, while A30P catalyzes the formation of oligomers [150-152]. In the case of the tau protein associated with Alzheimer's disease, some mutations interfere with the ability of tau to bind to microtubules or accelerate tau self-assembly, which reveals potentially pathology [153-155].

#### *Charge*

A high net charge enhances peptides the solubility due to its effect on promoting the repulsion between peptides, which slows down monomer aggregation [156,157]. Therefore, mutations that reduce the protein net charge can improve self-assembly. Otzen et.al [158] observed the tetramer formation of the non-amyloidogenic protein S6 from *Thermusthermophilus* after being replaced its 4 charge residues with non-polar neutral residues. The fibril formation rate of Aβ peptides rapidly increased as their net charge is reduced from -3e to -2e due to English [159] and Tottori mutations [160].However, in some cases, increasing protein local net charge was required for amyloid formation [8,161]

#### *Aromaticity and hydrophobicity*

In their study with different short amyloidogenic peptides, Gazit et. al. observed the π stacking interaction in aromatic residues which plays an important role in the arrangement, orientation and stabilization of amyloid structures [162]. Another example: under physical pH condition, the diphenylalanine peptide FF strongly favors self-assembly into stable nanotubes [163].However, the assumption that aromatic residues play a main role in the early stages of the aggregation process was challenged, because some observations showed that non-aromatic peptides derived by replacing aromatic side-chains by hydrophobic ones still retained their self-assemble ability

[164]. Although, this also indirectly indicated the catalyzing effect of hydrophobic residues on the process, the investigation of various truncated fragments such as Aβ16-22 suggested that the combination of aromatic, hydrophobic and even steric arrangement can promote fibril formation [165].

***Propensity of fibril-prone conformation in monomeric state***

The fibril-prone structure N* of the monomer is the structure of that monomer in its fibril state. The probability that a monomer is in the N* state is defined as the population of fibril-prone state $P_{N^*}$. Many studies [8,166] have shown that the higher the $P_{N^*}$ value, the faster the aggregation. Constraint of the D23-K28 salt bridge of Aβ40, which stabilized the fibril-prone state of the monomer, dramatically increases the rate of their aggregation compared to its wild type [167]. Self-assembly of Aβ40 peptides into a β-sheet fibril is much slower than that of Aβ42 due to a higher β-content of Aβ42 monomer than Aβ40 monomer [168,169]. Important simulation work by Li el. al. with a lattice model showed an exponential dependence of fibril formation time on $P_{N^*}$ [8].

***Mechanical stability of the fibril state***

Kinetics stability $G_{fib}$ of a fibril state is defined through probability to achieve fibril state $P_{fib}$ (Eq. 1) by Kouza et al. [34]. Through simulation, they found that the fibril formation time $\tau_{fib}$ did not correlate with either the fibril state energy $E_{fib}$ or the free energy $F$, but exhibited an exponential dependence on the kinetic stability $G_{fib}$ (Eq. 2). Such a relationship between $G_{fib}$ and $\tau_{fib}$ can be restated that the higher the kinetic stability of the fibril state, the faster the process of fibril formation.

Based on a natural inference, it was hypothesized that fibrillar structures readily accessible over long simulation times can optimize the arrangement of their peptides to resist degradation by external mechanical forces, i.e., are more stable in terms of mechanical stability [34].

$$G_{fib} = -k_B T ln P_{fib} \quad (1)$$

$$\tau_{fib} = \exp(a * G_{fib}) \quad (2)$$

Therefore, the kinetic stability of the fibril state can be related to its mechanical stability in such a way that the higher the kinetic stability, the higher the mechanical stability. Since the stability of the kinetics is associated with both mechanical stability and the rate of aggregation (Figure. 4), they conclude that the higher the mechanical stability, the faster the aggregation.

Because mechanical stability of a fibril can be accessed by Steer Molecular Dynamics (SMD) simulation, this result opens a new way to estimate the aggregate rate by using SMD instead of conventional MD that is much more expensive. The hypothesis about the relationship between the mechanical stability and fibril formation time was successfully confirmed for short peptides KLVFF and FVFLM, as well as for Aβ40 (2M4J) and Aβ42 (2NAO) [34]. For example, Aβ42 is

mechanically more stable than Aβ40 [34] and aggregates faster than Aβ40, which is consistent with the presented here hypothesis.

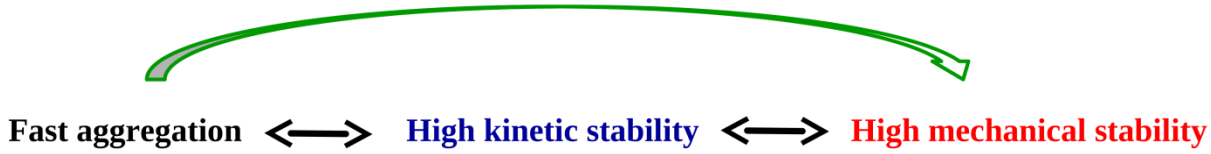


**Figure 4**: The relationship between the aggregation rate, kinetic stability and mechanical stability

***Beta content of the monomeric state***

Thu et al. have shown that the beta content of the monomer controls the propensity of a protein to aggregation [12]. This factor will be discussed in detail below as one of the main results of the thesis.

## 2.3 Computational models for studying protein aggregation

Many computational models have been developed to investigate the protein folding and aggregation. They range from low resolution models such as lattice and simple coarse-grained models to higher resolution models including systematic coarse-grained and especially all-atom models. Because of the limitation of computational resources the combination of different models has contributed to the understanding of protein self-assembly in many aspects [25,170].

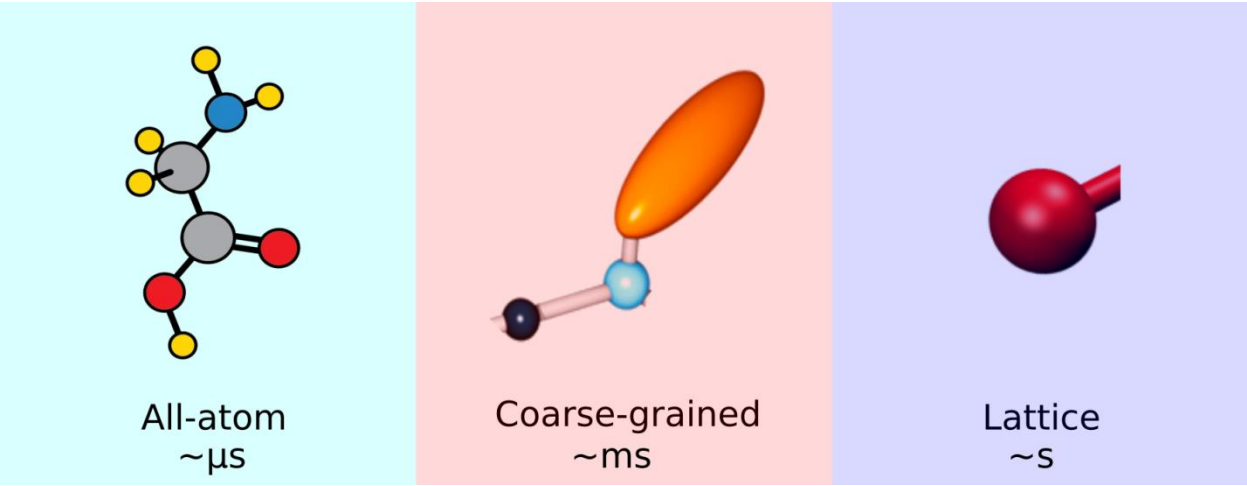


**Figure 5**: (Left) All-atom model for proteins, where all atoms are taken into account and the simulation time scale is of order of 1 μs on standard computers but one can perform simulations up to ms on special-purpose computers such as Anton designed and built by D. E. Shaw

Research. (Middle) Off-lattice coarse-grained model, which reduces the number of atoms for each amino acid and the simulation time scale, is on the order of 1 ms. (Right) Lattice model, in which each amino acid is replaced by a single bead and the simulation time scale ~ 1 s.

### 2.3.1 All-atom models

In this thesis we restrict ourselves to classical all-atom models used to study proteins, where each atom is considered as a particle without the internal structure (electrons and nucleus) and all atoms are taken into account (Figure 5). The interaction energy of atoms (force field) is given by the following equation

$$U(r) = U_{\text{stretch}} + U_{\text{bend}} + U_{\text{dihedral}} + U_{\text{electrostatic}} + U_{\text{vdW}}, \quad (3)$$

Where $U_{\text{bend}}$, $U_{\text{stretch}}$, $U_{\text{dihedral}}$ are bonded potentials, while electrostatic $U_{\text{electrostatic}}$ and van der Walls (vdW) term $U_{\text{vdw}}$ represent non-bonded potentials. The detail information about each term is showed in Figure 6.

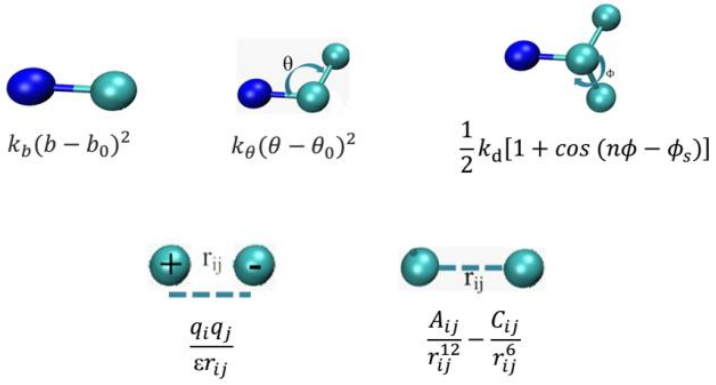


**Figure 6**: $U_{\text{stretch}} = k_b(b-b_0)^2$, where $k_b$ - bond stretching force constant, $b$ - bond length, $b_0$ - bond length in equilibrium. $U_{\text{bend}} = k_\theta(\theta-\theta_0)^2$, $k_\theta$ - angle bending force constant, $\theta$ - bending angle, $\theta_0$ - reference angle obtained in equilibrium. $U_{\text{dihedral}} = ½\ k_d[1+\cos(n\phi-\phi_s)]$, $k_d$ - dihedral angle force constant, $\phi$ - dihedral angle, $\phi_s$ - phase shift, $n = 1, 2, 3$ is a symmetry coefficient. $U_{\text{electrostatic}} = q_iq_j/\varepsilon r_{ij}$, $q_i$, $q_j$ - charge of atoms $i$ and $j$, $r_{ij}$ - distance between atom $i$ and $j$, ε - the electrical permittivity of medium. $U_{\text{vdW}} = (A_{ij}/r_{ij}^{12})-(C_{ij}/r_{ij}^{6})$, $A_{ij}$, $C_{ij}$ are coefficients of the Lennard-Jones potential, $r_{ij}$: distance between atom $i$ and $j$.

Different groups have developed different force fields (FFs) and the most frequently used FFs for studying proteins include Amber [171], CHARMM [172], GROMOS [173], and OPLS [174]. They are used with various explicit water models such as TIP3P [175], OPC [176], SPC [175] or implicit water models including the Generalized Born model (GB) [177], Poisson – Boltzmann (PB) model [178]. In addition, some FFs have been developed or modified to capture the behavior of IDPs , which are a99SB-disp [179], ff99SBnmr2 [180], CHARMM36IDPSFF [181] force fields. More information can be found in recent reviews [25,30,182].

Today, all-atom model are implemented in many convenient software, such as Gromacs [183], Amber [184], Charmm [172] or NAMD [185], which are widely used in scientific community. Concerning applications of all-atom models to study protein aggregation, we recommend recent reviews [25,182].

### 2.3.2 Coarse-grained models

Coarse-grained models are based on a reduction in the number of particles or degrees of freedom, which speeds up simulation and improves sampling (Figure 5). However, the use of such simplified models can lead to biased observations, which requires an appropriate choice of model for a given problem. Coarse-grained models are classified as off-lattice models and on-lattice models, in which particle motion is limited only by lattice nodes [30].

#### *Off-lattice coarse-grained models*

Several off-lattice coarse-grained force fields have been developed for biomolecules such as Martini [186,187], OPEP [188,189], UNRES [190,191], AWSEM [192]. AWSEM FF was used to build AWSEM Amylometer, a powerful tool to predict amyloidogenic proteins [193] and investigated the nucleus formation of Tau fibril formation process relating to Pick's and Alzheimer's diseases [194]. The OPEP force field was used to investigate the correlation between the β-sheet content and pH environments [195], the important role of β-barrel structure in early stage of NHVTLSQ oligomerization [196,197] and observed the presence of the pore and brand structures during aggregation of 1000 truncated Aβ16-22 [198].The dock-lock growth mechanism [199], role of α-to-β transition in the formation fibril structure [200] and morphologies of small oligomers [201] of truncated Aβ peptides have been explored by using UNRES FF.

Other more simplified off-lattice models also had the significant contribution to many aspects of the protein aggregation. Two-state model of Vacha and Frenkel considered monomers as patchy sphero-cylinder's shape. This model successfully captured two-filament amyloid-like configuration [202] and the nucleation-dependence mechanism of peptide aggregation [203,204], and explained the effect of foreign surfaces on protein aggregation [132], as well as provided much insight on dynamic of oligomer population [205]. A different patchy protein particle model designed to study self-assembly was built by Briels and his colleagues [206]. By conducting Brownian dynamics simulation, they reported that α-synuclein aggregation can occur according to a nucleation-dependent or two-step mechanism, the presence of a preform template increases the rate of transformation of disorder oligomers into fibril-like structures [206]. They also released a higher resolution version of this model, which allowed them to evaluate the process of adding a peptide at the fibril end [207]. Barz and Urbanc obtained various morphologies of aggregates in simulation with their homemade tetrahedron model, in which a monomer was constructed by 2 attractive and 2 repulsive beads forming a tetrahedron [208]. By modulating the

relationship between attraction and repulsion interactions, they assessed the fibril rupture propensity of various amyloidogenic protein sequences [194].

In the tube model developed by Hoang et.al., each polypeptide chain is defined as a self-avoiding flexible tube of identical Cα atoms [209]. The applications of this model include the investigation of nucleation and growth kinetics of the self-assembly process [210], studying the mechanism of formation of protofilaments from unstructured clusters [211] or observing the catalytic effect of a template formed by highly fibril-prone sequences on aggregation of poorly amyloidogenic sequences [212]. Another one-bead-per-residue Cα model constructed by Cieplak and Mioduszewski [213] showed the existence of a liquid-gas coexistence curve, as well as a novel amyloid-glass phase of polyglutamine chains at room temperature and at low temperature, respectively [214].

Pellarin and Caflish introduced a two-state model of ten-bead amphipathic peptide (4 beads for the protein back-bone and the remaining 6 for its side chain). The peptide can rotate around its internal dihedral and trigger the conversion between amyloid-competent and amyloid-protected states. A higher conversion rate implies a higher amyloidogenicity of the peptide [215]. Application of the model has been focused on considering how the fibril-prone propensity of peptides influences their self-assembly kinetics as well as aggregate morphologies [216] under different conditions such as various concentrations [215,217], the presence of membrane [218], crowders [123] or surfactants [219]. Shea et al. developed a middle resolution protein model in which each amino acid consists of one-bead side chain and two other beads representing two interaction centers along the backbone. They divided side chains into 4 types: hydrophobic, polar, positively and negatively charged. Similar to the Pellarin model, Shea's model has been used to solve many aggregation problems, for example fibril formation kinetics in bulk [220,221], on surface [222], on lipid bilayer membrane [134].

***On-lattice coarse-grained models***

Lattice models are highly simplified coarse-grained models that greatly improve sampling and reduce simulation time (Figure 5). However, in such models, all molecules are limited in their movement on the lattice network, which means that they can only be suitable for studying the general properties of the protein aggregation process. One of the simplest lattice models developed by Irback et al., called the stick model, where the monomer has the form of a stick located at a lattice site. When performing MC simulations for 105 sticks, it was reported that the stick model reflects the sigmoid kinetics of the fibril formation process and the interaction between the lateral and longitudinal growth of fibril-like structures during their formation [223]. The peptide can be considered as a cuboidal unit cells in the lattice model of Zhang and Muthukumar, which showed that the self-assembly kinetic of cuboidal monomers follows a nucleation-dependent mechanism [224].

The most complex lattice model is the multi-bead lattice model developed by Frenkel et al. In this model, each residue consists of one bead and a side chain vector, and the surrounding water molecules are assumed to be vacant lattice sites. The integrated MC algorithm allows peptides to move and controls their self-assembly [225]. The model has been used to study the interplay between peptide folding and aggregation [226]. Recently, Tran et al. implemented the OPEP force field in this lattice model and applied it to determine the critical nucleus of self-assembly of truncated Aβ42 peptide [227]. Li et al. developed a model in which each chain contains 8 beads and applied it to study many problems such as evaluating the correlation between fibril formation time $\tau_{fib}$ and charge, hydrophobicity as well as the population of fibril prone state N* of monomer [8]. This model has been also employed to investigate the role of a preformed template [228] and crowding environment [78] in protein aggregation. It has been useful in developing a new method to determine size of the critical nucleus [229], as well as in revealing the relationship between the mechanical stability and the fibril formation rate. CABS model [230] was used to predict fibril-prone fragments of proteins [231].

Because the model developed by Li et al [7] is widely used in works presented in this thesis, we will refer to as Li-Klimov-Straub-Thirumalai model and describe it in detail in the Methods.

# Chapter 3: Computational Methods

## 3.1 Monte Carlo simulation

Monte Carlo simulation (MC simulation) [232] , uses repeated random sampling to explore the phase space and calculate physical quantities of interest. To move from one configuration to another configuration of a polypeptide chain, stochastic random walks , which include 3 local moves (corner flip, tail rotations and crankshaft) (Figure 6 [7]) are trialed. To speed up aggregation we have also implemented global moves, which allow translating or rotating the entire chain. The acceptance of a MC move is decided by using the Metropolis algorithm [232].

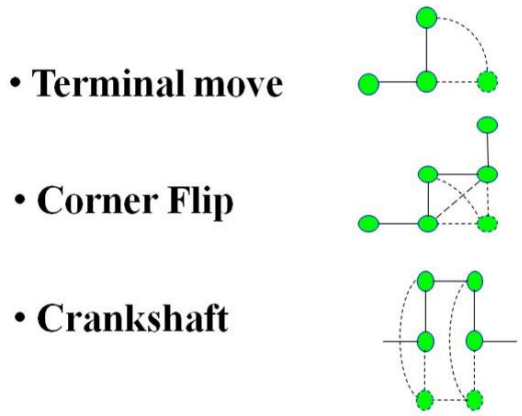


**Figure 7**: 3 types of local moves in our lattice model.

***Metropolis algorithm***

Suppose the local energy of the old conformation is $E_{\text{old}}$ and the local energy of the new conformation obtained after application of a MC move is $E_{\text{new}}$. Then, according to the Metropolis algorithm, which is also named as Metropolis–Hastings algorithm [232], the acceptance rate for the MC move is

$$k_{accept} = \begin{cases} 1, & E_{new} \leq E_{old} \\ e^{\frac{-(E_{old}-E_{new})}{k_B T}}, & E_{new} > E_{old} \end{cases} \quad (4)$$

Note that the Metropolis algorithm holds for a system in the canonical ensemble (NVT) with energy obeying the Boltzmann distribution.

## 3.2 Li-Klimov-Straub-Thirumalai lattice model for protein aggregation:

Li et al. were built a simple lattice model [7] for studying aggregation of polypeptide chains. In this model a chain has 8 beads denoted by +HHPPHH- where +,-, H, P (Figure 8) stand for positive, negative, hydrophobic and hydrophilic amino acids. Chain movement is enabled by 3 local MC moves including tail rotation, corner flip and crankshaft rotation and two global moves (translational and rotational moves). The translational move allows a peptide to be translated by a lattice spacing *a* in random direction while in the rotational move, the peptide is rotated by 90 degrees around a random chosen axis. Polypeptide chains perform random moves in a simulation box with periodic boundary conditions applied. The energy of N peptides is given by the following Equation:

$$E = \sum_{l=1}^{N}\sum_{i<j}^{M} e_{sl(i)sl(j)}\delta(r_{ij} - a) + \sum_{\mathrm{m}<l}^{\mathrm{N}}\sum_{\mathrm{i,j}}^{\mathrm{M}} e_{sl(i)sl(j)}\delta(r_{ij} - a) \quad , (5)$$

Where $r_{ij}$ is the distance between residues *i* and *j*, *a* is a lattice spacing, *sm*(*i*) indicates the type of residue *i* from *m-th* peptide, and $\delta(0) = 1$ and zero, otherwise. The first and second terms in Eq. 5 represent intra-peptide and inter-peptide interactions, respectively. A pair of beads interacts only if they form a contact, i.e. the distance between them $r_{ij}$ is equal to the lattice spacing *a* and $|i\text{-}j| \geq 3$. Our toy force field (Table 1) with interaction energies between different pairs of amino acids is roughly based on the statistical potentials obtained by Betancourt and Thirumalai [233]. The native state of the monomer is compact (Figure 8), while the fibril-like structure has the form of anti-parallel structure.

| **Beads** | **H** | **P** | **+** | **-** |
|---|---|---|---|---|
| **H** | $\varepsilon_{HH}$ | 0.2 | 0.2 | 0.2 |
| **P** | 0.2 | -0.2 | -0.2 | -0.2 |
| **+** | 0.2 | -0.2 | $\varepsilon_{++}$ | $\varepsilon_{+-}$ |
| **-** | 0.2 | -0.2 | $\varepsilon_{+-}$ | $\varepsilon_{--}$ |

**Table 1:** Energy of interaction between beads in the lattice model. H, P, +, - stand for hydrophobic, hydrophilic, positively charged and negatively charged beads, respectively. $\varepsilon_{HH}$, $\varepsilon_{++}$, $\varepsilon_{--}$; $\varepsilon_{+-}$ are the interaction energies between hydrophobic, positively charged, negatively charged and positively-negatively charged pairs, respectively

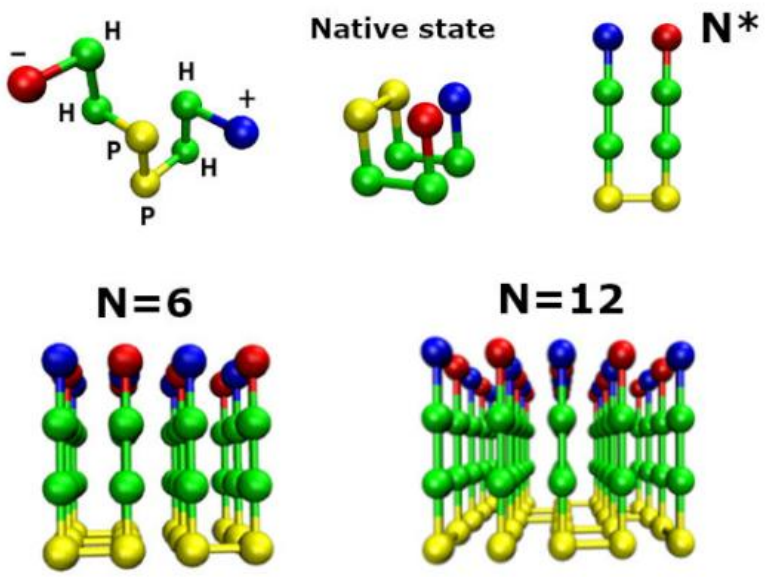


**Figure 8**: First row, from left to right: a random configuration of monomer constituted by the -HHPPHH+ sequence, monomer native state and fibril prone state N*. Second row: the fibril structures of N=6 and N=12 chains.

***Fibril and fibril-like structures***

MC simulation starts from initial random configurations of peptides to more ordered structures including the fibrillary and fibril-like structures. Figure 8 shows the fibril structures of N=6 and N=12 chains in which the monomers are arranged in anti-parallel motif and achieve the lowest energy. Inter- and intra-chain contacts in the fibril state are called fibril contacts. We defined an order cluster as a fibril-like structure if each monomer in the cluster has at least one inter-chain contact and the total number of fibril contacts exceeds 80% of the fibril contacts of the fibril structure.

***Lattice model for smooth and rough surface***

To investigate the effect of foreign surfaces on protein self-assembly, we introduced surfaces into our lattice model. A smooth surface is defined as a square flat surface perpendicular to the z-axis at the origin. Single balls, double balls, or both single and double balls (the numbers of single balls and double balls are the same) are randomly distributed on a smooth surface, which creates a rough S-surface, D-surface or DS-surface, respectively (Figure 9) [11].

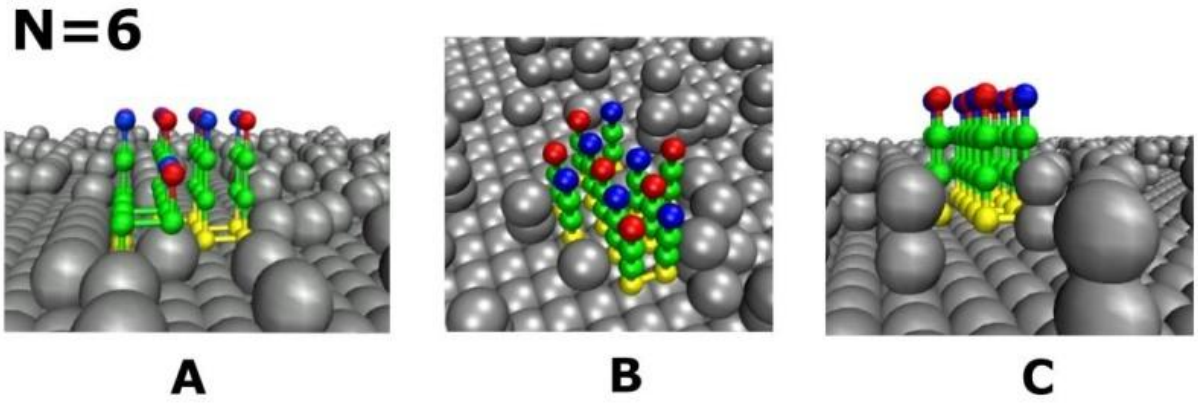


**Figure 9**: Aggregation of 6 peptides system on (A) S-surface (B) DS-surface (C) D-surface

***Fibril formation time and time of formation of the fibril-like structure***

Fibril formation time ($\tau_{fib}$) and time of formation of the fibril-like structure ($\tau_{agg}$) are measured in the number of Monte Carlo steps (MCS). They are defined as the first passage times needed to reach the fibril and fibril-like structure. Note that $\tau_{agg}$ has been used to study aggregation on a rough surface, when the acquisition of the fibril structure is prohibited.

## 3.3 Molecular dynamics

MD simulation is a computational method for studying molecular systems using computer [234]. In MD, trajectories of atoms are obtained from the numerical solution of the Langevin equation (Eq.5) with a given force field and water model.

***Langevin equation***

Stochastic differential Langevin equation is a Newton equation but the friction and noise terms are added:

$$m\frac{d^2\vec{r}}{dt^2} = \overrightarrow{F_c} - \gamma\frac{d\vec{r}}{dt} + \vec{\Gamma} \equiv \vec{F}, \quad (5)$$

$m$ the mass of atom, γ the friction coefficient, and $\vec{F_c} = \nabla U$ , where potential $U$ is given by Eq. 3. Random force $\Gamma$ related to random interactions between atoms of the biomolecule and environment is a white noise

$$< \Gamma(t) >= 0,$$

$$< \Gamma(t)\Gamma(t') >= 2\gamma k_B T\delta(t - t') \quad (6)$$

Where $k_B$ is a Boltzmann's constant, $T$ temperature and $\delta(t - t')$ the Dirac delta function.

The motion Equation 5 was solved using the leap-frog [235] algorithm with a time step $\Delta t$=2 fs. The length of all bonds associated with hydrogen atoms was constrained by the SHAKE algorithm [236]. The temperature was maintained through the Langevin thermostat [237] with a collision frequency of 2 $ps^{-1}$. A cutoff of 1.4 nm was chosen for the calculation of the vdW force, and the particle mesh Ewald method [238] was used to compute the long-range electrostatic interactions. The simulations boxes were chosen large enough to avoid interaction with the periodic images and size effects were minimized by applying periodic boundary conditions. Counter ions were added to neutralize the system.

## 3.4 Steered molecular dynamics

Steer molecular dynamic (SMD) [239] is a simulation method designed to capture single-molecule force spectroscopy experiments including AFM [240], laser optical tweezers [241] and magnetic tweezers [242]. These single-molecule force techniques shed light on many biomolecular phenomena ranging from the folding, unfolding [243] to aggregation [244]of proteins. In SMD simulations [239,245,246] an external force is applied to a dummy moving with constant speed $v$ in pulling direction (Figure 10). This dummy atom is connected with the pulled atom of the studied system through a spring with a spring constant $k$**.** If we define $x$ as the displacement of the pulled atoms from its initial position, then the force experienced by the system $F$ is determined by formula: $F=k(vt-x)$. A typical force-displacement/time has the maximum or rupture force $F_{max}$ (Figure 10), which can be used to characterize the mechanical stability of the complex.

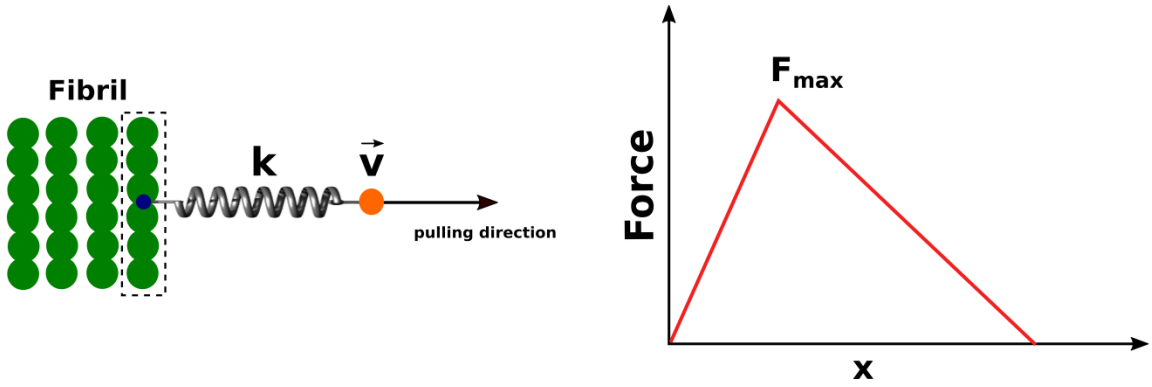


**Figure 10**: (Left) SMD set up for pulling the monomer from the fibril; $k$ and $v$ are the spring stiffness and pulling speed, respectively; the orange circle refers to the dummy atom. (Right) force profile plots the pulling force $F$ as a function of the displacement $x$ of the monomer from its original position; the maximum pulling force $F_{max}$, which can also be called a rupture force since the rupture event occurs at that point.

## 3.5 Analysis tools

***Free energy landscape***

Free energy landscape depending on the reaction coordinate V is determined by the following formula:

$$F(V) = -k_B T ln P(V) \text{ , } (7)$$

*P*(*V*) is the probability distribution extracted from the simulated data.

***Contacts***

In the lattice model, a contact between two unbonded beads is established if the distance between them is equal to the lattice spacing, which was often chosen to be 1. Intra-chain and inter-chain contacts refer to contacts between two beads in the same peptide and different peptides, respectively. In full-atomic models, if the distance between the centers of mass of the side chains of two non-bonded amino acids is less than 6.5 Å, then a contact is formed between them. A fibril contact is a contact that occurs in the fibril structure.

***Secondary structures***

Secondary structure were calculated using the STRIDE algorithm [247]

***Software***

We used VMD [246] to visualize the simulated systems, Grace [248] and Inkscape [249] to make plots.

# Chapter 4: Summary of Publications

## 4.1 Effect of surface roughness on aggregation of polypeptide chains: a Monte Carlo study

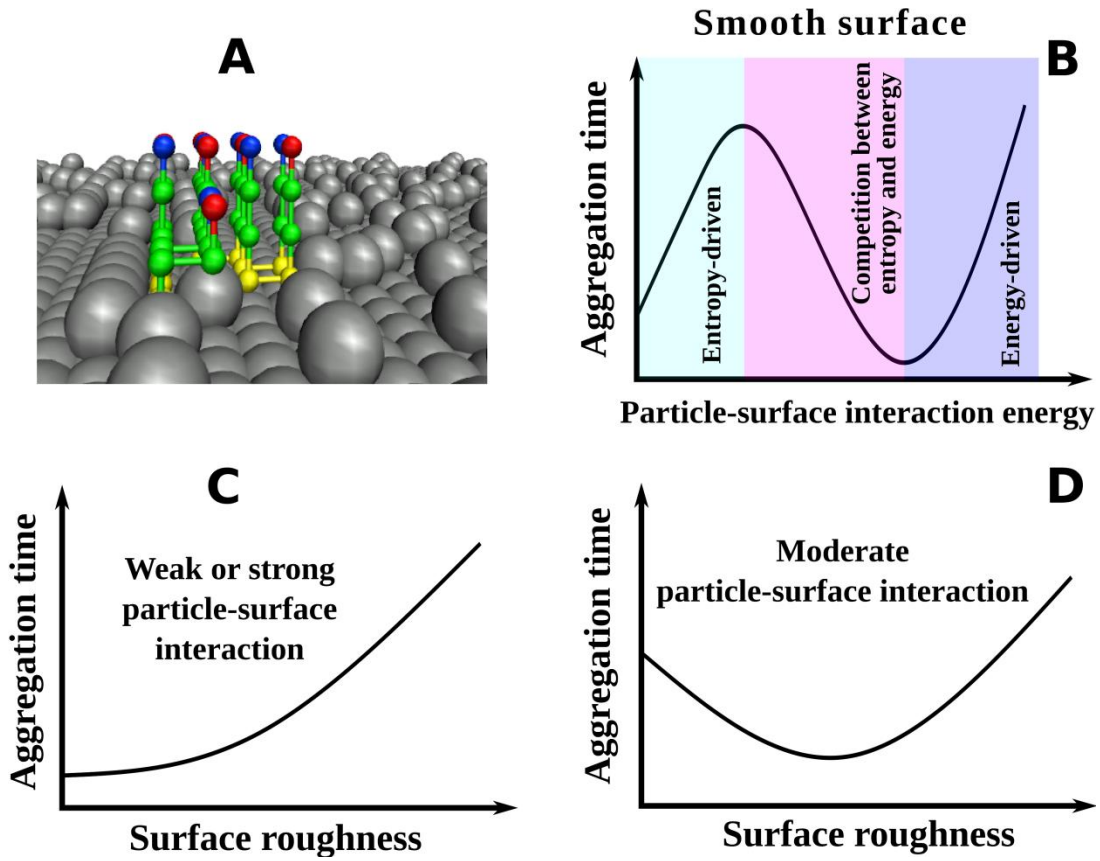


**Figure 11**: A snapshot of the aggregate of six peptides on the S-surface (A), dependence of the aggregation time on the interaction energy between protein and the smooth surfaces (B), correlation between aggregation time and surface roughness in the case of weak or strong particle-surface interaction (C) and of moderate particle-surface interaction (D).

Foreign surfaces such as lipid membranes, etc. in the environment have a strong influence on the mechanism of protein aggregation [130,131]. Different types of surfaces can have different effects including acceleration [250-252], slowdown [253,254], or even a change in the morphology of product aggregates [255,256]. The studies in this article examined the effect of rough surfaces on the self-assembly kinetics of polypeptide chains using an upgraded lattice model because the calculation of the fibril formation time is impractical in off-lattice models.

To create a rough surface, we randomly place balls on a smooth surface consisting of balls regularly located at the nodes of a two-dimensional lattice perpendicular to the z axis (Figure 10 A). We considered hydrophobic and hydrophilic surfaces and controlled their hydrophobicity and hydrophilicity by adjusting parameters characterizing the interaction between protein and surfaces. The particle-surface interaction energy is denoted by ε. Applying the lattice model, we performed simulations for systems consisting of N=6 and N=12 chains in the presence of the different smooth surfaces. We found that dependence of the aggregation time $\tau_{agg}$ on ε followed different scenarios. Weakly absorbing surfaces (small values of ε) reduce the concentration of proteins in bulk but cannot serve as a good template to catalyze the association of peptides. Therefore, they retarded the aggregation process with $\tau_{agg}$ proportional to $\varepsilon$ (Figure 10B). This regime is driven by entropy as it dominates the weak particle-surface interaction. Medium absorbing surfaces (medium values of $\varepsilon$) can trap peptides and restrict the protein conformational space by effectively reducing 3 dimensions in bulk to 2 dimensions on the surface. So, the chains have a higher probability to associate leading to acceleration of the fibrillization, i.e. $\tau_{agg}$ decreases with $\varepsilon$. The decrease in the aggregation time with the protein-surface interaction occurs due to a trade-off between energy and entropy (Figure 10B). For strongly absorbing surfaces (big values of ε), increasing $\varepsilon$ resulted in the retardation of the aggregation process (increasing $\tau_{agg}$*)* because very strong interaction between peptides and the surface restricts peptides diffusion and limits their association (energy-driven regime, Figure 10B). Noteworthy, all the above scenarios holds not only for the systems of N=6 and N=12 chains but also for both hydrophobic and hydrophilic surfaces. The results agreed well with simulations and experimental work of Vacha et.al. [132] .

Random distribution of hydrophobic and hydrophilic balls on the smooth surfaces creates rough hydrophobic and rough hydrophilic surfaces, respectively. Two types of balls including single ball (S-ball) and double ball (D-ball) have been used to construct the rough surfaces (Figure 10 A). Rough S-surface and D-surface consisting of only S-balls and D-balls, respectively represent homogeneous rough surfaces, while the combination of S-balls and D-balls forms SD-surface considered as inhomogeneous rough surface. Roughness degrees Θ and the percent of distributed balls Ω are defined as follows:

$$\Theta = \sqrt{\frac{1}{N_s}\sum_{i=1}^{N_s}\left(h_i - \bar{h}\right)} \quad (10)$$

$$\Omega = \frac{N_b}{N_s} \quad (11)$$

Simulations of the dependence of $\tau_{agg}$ on roughness degree Θ for system N=6 and N=12 chains interacting with hydrophobic and hydrophilic surfaces of S, D and SD types showed different scenarios that can be qualitatively explained by the compromise between the energy and entropy of the system. In the case of weakly absorbing surfaces, the high surface roughness reduces the

phase space of monomers resulting in the decrease of the aggregation rate. Since the surface-protein interaction is weak this process is entropy-driven (Figure 10C). Combination of the strong surface-protein interaction and the surface roughness creates a lot of kinetics traps which are energetically more favorable for monomers than the aggregate state. Therefore, strongly absorbing rough surfaces reduce the mobility of monomers leading to rapid increase in $\tau_{agg}$ and even blocking the process at the high roughness (Figure 10C). This energy-driven process is in line with the study of Shezad et.al [9]. The most interesting result was obtained for the case of medium absorbing surfaces (Figure 10D). For weak roughness, the surface becomes effectively wider than the smooth surface or the template for assembly becomes larger, which promotes protein association instead of hindering them. For a medium attractive surface, a slight surface roughness enhances the monomer adhesion to the surface, and this can not only increase the like hood of critical nucleus but also tend to narrow the peptide phase space to two dimensions. Furthermore, low enough roughness and medium attractive particle-surface interaction still allow the peptides to diffuse and form a fibril-like structure. However, the higher roughness can remarkably reduce the peptides flexibility, which slows the self-assembly process. Thus, for the medium particle-surface interaction, the dependence of $\tau_{agg}$ on $\Theta$ displayed a U-shape form (Figure 10D). It would be interesting to experimentally test this U-shape behavior.

**Publication for this section**: *Effect of Surface Roughness on Aggregation of Polypeptide Chains: A Monte Carlo Study*

Nguyen Truong Co, Mai Suan Li

Biomolecules 2021, 11(4), 596

## Abstract

The self-assembly of amyloidogenic peptides and proteins into fibrillar structures has been intensively studied for several decades, because it seems to be associated with a number of neurodegenerative diseases, such as Alzheimer's and Parkinson's disease. Therefore, understanding the molecular mechanisms of this phenomenon is important for identifying an effective therapy for the corresponding diseases. Protein aggregation in living organisms very often takes place on surfaces like membranes and the impact of a surface on this process depends not only on the surface chemistry but also on its topology. Our goal was to develop a simple lattice model for studying the role of surface roughness in the aggregation kinetics of polypeptide chains and the morphology of aggregates. We showed that, consistent with the experiment, an increase in roughness slows down the fibril formation, and this process becomes inhibited at a very highly level of roughness. We predicted a subtle catalytic effect that a slightly rough surface promotes the self-assembly of polypeptide chains but does not delay it. This effect occurs when the interaction between the surface and polypeptide chains is moderate and can be explained by taking into account the competition between energy and entropy factors.

doi.org/10.3390/biom11040596

Publication source: https://www.mdpi.com/2218-273X/11/4/596#abstractc

## Author contribution statements

Nguyen Truong Co
Division of Theoretical Physics
Institute of physics, Polish of Academia of Sciences
Al. Lotników 32/46
PL-02-668 Warsaw, Poland

**STATEMENT**

I declare that I am the co-author of the publication:

> Nguyen Truong Co, Mai Suan Li. Effect of Surface Roughness on Aggregation of Polypeptide Chains: A Monte Carlo Study. Biomolecules 11, 596 (2021), https://doi.org/10.3390/biom11040596
>
> My contribution was designing the research, developing the upgraded lattice model, conducting the simulation, analyzing, exhibiting the results, and writing the manuscript. My contribution is around 85%.

Warsaw, 30 March 2022

Nguyen Truong Co

Prof. dr hab. Mai Suan Li
Department of Theoretical Physics
Institute of Physics, Polish Academy of Sciences
Al. Lotnikow 32/46
02-668 Warsaw, Poalnd

## STATEMENT

I declare that I am the co-author of the following publications:

> Nguyen Truong Co, **Mai Suan Li**, *Effect of Surface Roughness on Aggregation of Polypeptide Chains: A Monte Carlo Study*, Biomolecules 11, 596 (2021),
> https://doi.org/10.3390/biom11040596
> My contribution was about 15%: Directing the research, data analysis and manuscript writing.

Warsaw, 18 April 2022

Mai Suan Li

biomolecules

MDPI

*Article*

# Effect of Surface Roughness on Aggregation of Polypeptide Chains: A Monte Carlo Study

**Nguyen Truong Co [1] and Mai Suan Li [1,2,*]**

[1] Institute of Physics, Polish Academy of Sciences, Al. Lotnikow 32/46, 02-668 Warsaw, Poland; ntco@ifpan.edu.pl
[2] Institute for Computational Science and Technology, SBI Building, Quang Trung Software City, Tan Chanh Hiep Ward, District 12, Ho Chi Minh City 700000, Vietnam
* Correspondence: masli@ifpan.edu.pl

**Abstract:** The self-assembly of amyloidogenic peptides and proteins into fibrillar structures has been intensively studied for several decades, because it seems to be associated with a number of neurodegenerative diseases, such as Alzheimer's and Parkinson's disease. Therefore, understanding the molecular mechanisms of this phenomenon is important for identifying an effective therapy for the corresponding diseases. Protein aggregation in living organisms very often takes place on surfaces like membranes and the impact of a surface on this process depends not only on the surface chemistry but also on its topology. Our goal was to develop a simple lattice model for studying the role of surface roughness in the aggregation kinetics of polypeptide chains and the morphology of aggregates. We showed that, consistent with the experiment, an increase in roughness slows down the fibril formation, and this process becomes inhibited at a very highly level of roughness. We predicted a subtle catalytic effect that a slightly rough surface promotes the self-assembly of polypeptide chains but does not delay it. This effect occurs when the interaction between the surface and polypeptide chains is moderate and can be explained by taking into account the competition between energy and entropy factors.

**Keywords:** protein aggregation; aggregation of polypeptide chains; fibril formation; neurodegenerative diseases; surface roughness; lattice model



**Citation:** Co, N.T.; Li, M.S. Effect of Surface Roughness on Aggregation of Polypeptide Chains: A Monte Carlo Study. *Biomolecules* **2021**, *11*, 596. https://doi.org/10.3390/biom11040596

Academic Editor: Olga Corti

Received: 3 March 2021
Accepted: 15 April 2021
Published: 18 April 2021



## 1. Introduction

The self-assembly of proteins into aggregates of various morphologies is probably one of the main causes of chronic neurodegenerative diseases such as Alzheimer's, Parkinson's and Huntington's disease [1–3]. Therefore, understanding the mechanisms of protein aggregation plays an important role in discovering effective therapies to treat these diseases. Protein aggregation can occur in solution as well as in complex environments, including various surrounding objects such as cell membranes, DNA, sugars, other biological compounds and industrial artificial surfaces which require the careful study of the effect of different surfaces on the process [4–8]. In general, the impact of foreign surfaces on the protein aggregation process displays complicated behaviors which depend on the type of surfaces, proteins and experiment conditions [9–12]. Lipid membranes were reported to play the role of a template to accelerate the aggregation of different amyloidogenic peptides [13–16]. Mica and glass facilitated the fibril formation of the fragment $A\beta_{18-22}$ [17] and α-synuclein [18] on their surfaces, respectively. However, the surfaces of polymeric nanoparticles slow the self-assembly of IAPP [19], while the protein-coated surfaces of graphene oxide showed a strong inhibition effect for the fibrillogenesis of peptide $A\beta_{42}$ [20]. Carbon nanotubes [21,22] and nanoparticles [23,24] can either accelerate or slow down aggregation depending on the experimental conditions and aggregation agents. Furthermore, the fibril structure of amyloid peptide GAV-9 favors a "stand up" motif on the hydrophilic mica surface, but greatly prefers the "lie down" position on a hydrophobic

HOPG (highly oriented pyrolytic graphite) plain [25,26]. Surfaces can also control the peptide aggregation kinetics as well as their morphologies through surface topologies [27,28] or surface roughness [29,30]. Furthermore, many computational investigations have been conducted to explore the role of smooth surfaces and membrane on protein aggregation using coarse-grained [31,32] and all-atom models [33].

Combining a two-state peptide model [34] and experiment on the self-assembly of $A\beta_{42}$ and $\alpha$-synuclein in the presence of different types of surfaces, Vacha et al. [35] have shown that weakly absorbing surfaces retard proteins aggregation, while strongly absorbing surfaces enhance the process. This implies that the aggregation is modulated by interactions between polypeptide chains and foreign surfaces. When proteins are absorbed on the surface, their movement becomes more limited compared to the three-dimensional case, and this can lead to an increase or decrease in the fibril formation rate depending on the experimental conditions [36]. A weakly absorbing surface reduces the concentration of proteins in the bulk, which reduces the probability of the formation of critical nuclei there [35]. On the other hand, the interactions between surface and polypeptide chains are not strong enough to maintain a sufficient number of chains on the surface to accelerate the aggregation process. Competition between these factors leads to a decrease in the overall rate of protein aggregation on weakly absorbing surfaces [37]. For highly absorbent surfaces, a large amount of proteins is absorbed on the surface, catalyzing the formation of critical nuclei, which accelerates the fibril formation [17]. However, very strong absorption will impede the process due to the hindrance of diffusion and sampling of peptides on the plain [36].

Combining polymer coating, argon plasma treatment and thermal annealing techniques, Shezad et al. [29] were successful in the production of polystyrene surfaces with roughness of varying degrees. They showed that the aggregation rate of Aβ42 (beta amyloid peptide of 42 residues) decreases with increasing surface roughness, and very rough surfaces even block fibril growth. Using various experimental methods, it was shown that a the rough surface restricts the two-dimensional diffusion of peptides, which slows down the surface-mediated formation of fibrillar species [29].

To our best knowledge, theoretical studies of the impact of surface roughness on protein aggregation have not been conducted. In this paper, we develop simple lattice models in which rough surfaces were created by randomly distributed balls on smooth planes and performed Monte Carlo simulations to explain the experimentally observed phenomena. More importantly, we predicted that for moderate particle–surface interactions, slightly rough surfaces can accelerate the fibril formation rather than slow it down.

## 2. Materials and Methods

### *2.1. Lattice Models in Bulk*

Since the fibril formation time of proteins varies from hours to months, its assessment using all-atom or even off-lattice coarse-grained models is not possible within the existing computational capabilities. The problem becomes harder in the presence of rough surfaces that slow down this process. Therefore, we developed simple lattice models that allowed us to estimate the fibril formation rate with a reasonable amount of computational time (our models are simpler than other coarse-grained models [38–41]). These models are an extension of lattice models that were successfully used by our group to simulate the kinetics of fibril formation of polypeptide chains in the absence of surfaces [42]. Despite their simplicity the lattice models correctly captured the dependence of fibril formation time on the hydrophobicity, charge and population of the so called fibril prone state N* in monomeric state [19]. They were also useful in studying the mechanism of heat-induced amyloid fibril degradation [43], the role of crowders in fibrillation [6] and assessing the size of critical nuclei [44].

In our model, polypeptide chains, which are confined to a discrete cubic lattice, consist of $M = 8$ beads, designated as + HHPPHH−, respectively (Figure 1, left), where +, − represent positively and negatively charged residues, and H and P stand for hydrophobic

and polar residues, respectively. Interactions include interactions of beads in the same chain (intra-contact) and interactions of beads from different chains (inter-contact). The intra-chain interaction between two beads is counted if they are not successive in sequence and the distance between them is equal to the lattice spacing $a$. We take into account only the nearest neighbor inter-chain interaction, which occurs when the distance between two interacting beads is equal to $a$. Then, the total energy of the system consisting of $N$ polypeptide chains, $E$, is determined by the first two terms of the following expression:

$$E = \sum_{l=1}^{N}\sum_{i<j}^{M} e_{sl(i)sl(j)}\delta(r_{ij}-a) + \sum_{m<l}^{N}\sum_{i,j}^{M} e_{sl(i)sm(j)}\delta(r_{ij}-a) + \sum_{m=}^{N}\sum_{i=1}^{M}\sum_{k=1}^{Ns} e^{vs}{}_{k,sm(i)}\delta(r_{ik}-a) \quad . \tag{1}$$

where $r_{ij}$ is the distance between amino acids $i$ and $j$, in simulations $a$ is assigned Equal (1), *sm (i)* denotes the amino acid $i^{\text{th}}$ in the $m^{\text{th}}$ peptide chain. The delta-function $\delta$(x) is 1 at x = 0 and 0 otherwise. The first and second terms in Equation (1) describe the intra- and inter-chain interactions, respectively. The pair interactions between beads (or "force field") $e_{ij}$ are given in Table 1. The third term describes the interaction between polypeptide chains and surface (see below). In our models, 20 amino acids were divided into hydrophobic, hydrophilic, negatively charged and positively charged groups. As in our previous works [42,45], their interaction energies shown in Tables 1 and 2 were basically selected based on the statistical potentials that were obtained by Betancourt and Thirumalai [46].

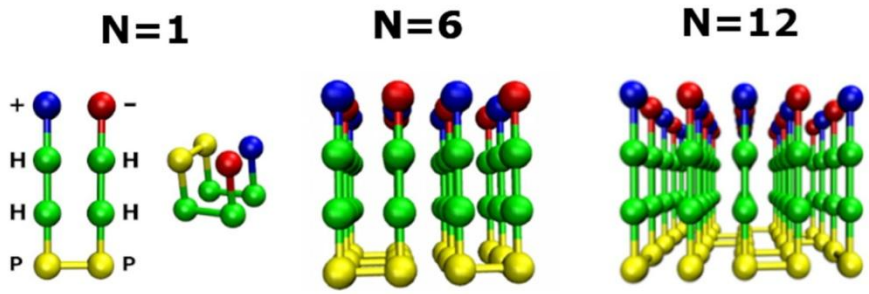


**Figure 1.** (Left) Single peptide of 8 beads that are **+HHPPHH-** in **N*** conformation. Red, green, yellow and blue refer to amino acids **—, H, P, +**, respectively. Native structure of 1 peptide chain is showed next to N*. Fibril structure of the systems of N = 6 and N = 12 chains in the lattice model.

**Table 1.** Interaction energies between two beads of polypeptide chains $e_{ij}$ in the lattice model. The energy is measured in $\varepsilon_H$, where $\varepsilon_H$ is the hydrogen bond energy.

| Beads | H | P | + | − |
|---|---|---|---|---|
| **H** | −1.0 | 0.2 | 0.2 | 0.2 |
| **P** | 0.2 | −0.2 | −0.2 | −0.2 |
| + | 0.2 | −0.2 | 0.35 | −0.7 |
| − | 0.2 | −0.2 | −0.7 | 0.35 |

**Table 2.** Interaction energies between the polypeptide chain (H, P, +, and −) and beads of hydrophilic (Ps) and hydrophobic (Hs) surfaces. $\varepsilon^{ps}$ and $\varepsilon^{hs}$ can be tuned in simulation.

| Beads/Balls | H | P | + | − |
|---|---|---|---|---|
| Ps | 0.2 | $-\varepsilon^{ps}$ | −0.2 | −0.2 |
| Hs | $-\varepsilon^{hs}$ | 0.2 | 0.2 | 0.2 |

By Monte Carlo simulations [19,42] (see also below) we obtained the fibril structures for the systems with N = 6 and 12 peptides (Figure 1).

### *2.2. Lattice Models with Surfaces*

#### 2.2.1. Smooth Surface

We modeled a smooth surface as a systems of beads regularly located at points of a two-dimensional square lattice. The lattice spacing of the surface is the same as in bulk. The surface beads are kept fixed during the simulation, and the interaction between them is not taken into account. The chemical properties of surfaces are characterized by their interaction with polypeptide chains. We examined two types of surfaces: hydrophilic and hydrophobic surfaces, which consist of hydrophobic and hydrophilic beads, respectively. Surface beads are designated as Ps and Hs for the hydrophilic and hydrophobic surfaces, respectively.

Denoting the interaction energy between the bead $i$ of a polypeptide chain and the surface bead $j$ as $e^{\nu s}{}_{i,j}$ (ν can be p for hydrophilic surface and h for hydrophobic surface), the interaction energy between the polypeptide chains and the surface is given by the third term in Equation (1). Here, $N$s is the total number of sites of the surface area. The $e^{\nu s}{}_{i,j}$ values are shown in Table 2. Here, we chose the interaction between surface beads and polypeptide beads to be the same as the interaction between the beads of polypeptide chains. However, in order to explore the dependence of fibril formation kinetics on the strength of interaction with surfaces, we varied the interaction between the hydrophobic beads of the polypeptide chains and the surface $\varepsilon^{hs}$ and the interaction between hydrophilic beads of polypeptide chains and surface $\varepsilon^{ps}$.

Depending on the surface, fibrils may have different morphologies. In our model, for N = 6 and 12 chains, the fibril structure on the hydrophilic surface has the same shape (Figure 2C,F) as in bulk (Figure 2A,D), but on the hydrophobic surface all the chains adopt the monomer native structure (Figure 1) in the fibril state due to strong hydrophobic interactions between the chains and the surface and the short peptides in our model (Figure 2B,E). In other words, the fibril-prone conformation N* coincides with the compact native conformation. Thus, even in the simple model, we showed that the surface can change the morphology of fibrils.

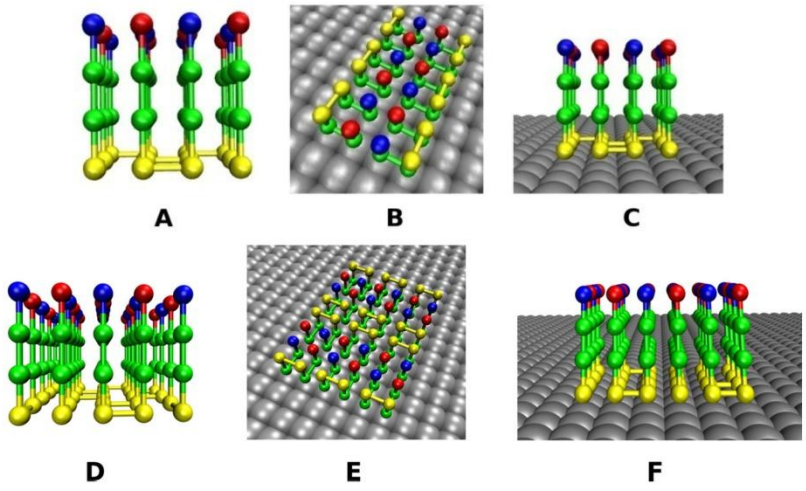


**Figure 2.** Fibril structure of six polypeptide chains in bulk (**A**), on hydrophobic surface (**B**) and hydrophilic surface (**C**). Fibril structure of 12 polypeptide chains in bulk (**D**), on hydrophobic surface (**E**) and hydrophilic surface (**F**).

2.2.2. Rough Surfaces

To build a rough surface, we randomly placed identical balls on a smooth surface. These balls should be hydrophobic and hydrophilic for rough hydrophobic and hydrophilic surfaces, respectively. Each ball has the same size and occupies one lattice site similar as the chain's beads; however, in order to facilitate the visualization, we exhibited them in larger size (Figures 2 and 3). The roughness depends not only on the concentration of randomly distributed balls, but also on how they are arranged. In this paper, we considered 3 types of arrangement: single balls (S-point), double balls (D-point) and the equal mix of S-point and D-point called DS-point (Figure 3); therefore, we have S-surface, D-surface and DS-surface. In the first case, at each position, only one ball was positioned at $a$ distance of the grid pitch $a$ from the surface (Figure 3A). In the case of a D-surface, two rigidly connected balls were placed perpendicular to the surface and the distance between the higher ball and the surface is equal to $2a$ (Figure 3C). Finally, the DS-surface comprises an equal number of S-ball and D-ball randomly distributed on a smooth surface (Figure 3B).

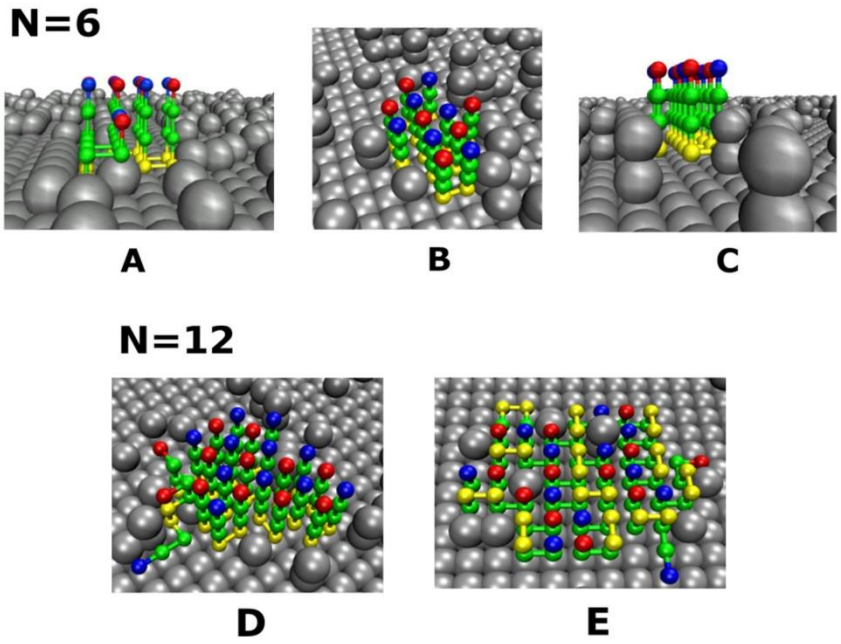


**Figure 3.** Typical fibril-like structures for the system of N = 6 chains on rough hydrophilic surfaces with single balls (S-surface) (**A**), the combination of single and double balls (DS-surface) (**B**), and double balls (D-surface) (**C**). The fibril-like configuration of 12 chains on the hydrophilic DS- surface (**D**), and hydrophobic DS-surface (**E**).

*2.3. Definition of Surface Roughness*

We define the distance (or height) from the ball $i$ to the surface as $h_i$. Then, $h_i$ takes the values 1, 2 and both values for the S-, D- and DS-surface, respectively. For surface point $j$, without ball, $h_j = 0$. The average distance between the surface and randomly distributed balls, $\overline{h}$, is determined by the following formula:

$$\overline{h} = \frac{\sum_{i=1}^{N_s} h_i}{N_s}, \quad (2)$$

where $N_s$ is the number of points of the surface. Then, the degree of surface roughness (or roughness) is the standard deviation of $h$ and is defined as follows:

$$\Theta = \sqrt{\frac{1}{N_s}\sum_{i=1}^{N_s}\left(h_i - \bar{h}\right)^2}. \quad (3)$$

Defining $\Omega$ as the percentage of points at which single and double balls are placed to create surface roughness, we have:

$$\Omega = \frac{N_b}{N_s} \quad (4)$$

where $N_b$ is the number of points with balls.

### 2.4. Monte Carlo Simulation

The concentration of chains that were enclosed in a cubic simulation box was brought to about 6 μM (about 10 times higher than the experimental concentration) for all simulated systems. Although the lattice model is simple, calculating the aggregation time of many polypeptide chains requires an enormous amount of computational resources, especially in the presence of rough surfaces. Therefore, we used a high concentration of peptides to accelerate the aggregation process. We applied the periodic boundary conditions to minimize finite size effects. The Monte Carlo (MC) algorithm was utilized to determine the dynamics of peptide chains. MC moves involved local and global moves. The local move may be tail rotation, corner flip, or crankshaft. The global move is either the rotation of a peptide at a 90-degree angle around a randomly selected coordinate axis, or the translation of a peptide on $a$ in a random direction [19,42]. The probability ratio between global and local moves was chosen as 1:9. The combination of the local move and global move is the Monte Carlo step (MCS), which is a time unit in the lattice model. Although the equivalence between real time and MCS remains controversial, lattice models have been helpful in understanding the mechanisms of protein aggregation in the bulk [19,43,45] and crowded environment [6]. Note that the fibril structures with the lowest energy obtained using MC simulations are shown in Figures 1–3.

It should be noted that we used our homemade programs written to study the self-assembly of polypeptide chains in lattice models. They have been used and developed for different problems since 2008 [42]. We use Fortran 90 and Monte Carlo dynamics. Our code is not parallel and it took about 48 h of CPU on an Intel Xeon E5-2680v3 2.50 GHz, for example, to simulate a trajectory of 12 chains that aggregate on a surface with a roughness of $\Theta = 0.1$. For each data point, we have to average over 150 MC trajectories, which takes a lot of computational time. Therefore, we have to run on the supercomputer TASK located in Gdansk, Poland.

### 2.5. Aggregation Time $\tau_{agg}$ and Fibril Formation Time $\tau_{fib}$

The fibril formation time $\tau_{\mathrm{fib}}$ is the number of MCS required to reach the fibril structure from random initial configurations of the peptide chains. In a simulation with many MC trajectories, $\tau_{\mathrm{fib}}$ is defined as the average value of the first passage times. In the case of smooth surfaces, where the fibril formation is relatively fast, we can estimate $\tau_{\mathrm{fib}}$ from many MC trajectories. However, for rough surfaces, the fibril formation is so slow that even in simple lattice models, it is not feasible to obtain $\tau_{\mathrm{fib}}$ within a reasonable amount of time. Therefore, instead of $\tau_{\mathrm{fib}}$, we introduced the aggregation $\tau_{\mathrm{agg}}$, which is the first passage time for acquiring a structure that has 80% fibril contacts. For each roughness degree, we generated 10–15 random surface profiles and conducted 15–20 MC runs per profile. Thus, for a given roughness, $\tau_{\mathrm{agg}}$ was obtained by averaging over 150 ($10 \times 15$) trajectories.

**3. Results and Discussion**

*3.1. Effect of Smooth Surface on Aggregation Time $\tau_{agg}$*

3.1.1. Hydrophilic Surfaces

We first examined the effect of smooth surfaces on the aggregation process of system N = 6 polypeptide chains at various temperatures. To estimate $\tau_{agg}$, MC simulations were conducted for systems of N = 6, initially random peptides in the cubic box. The number of MC steps to achieve a structure that has 80% fibril contacts was defined as the first passage time. For each parameter set, 100 MC runs were performed and $\tau_{agg}$ was the average value of the 100 first passage times.

For a hydrophilic smooth surface of simulation, we varied the interaction between hydrophilic beads of peptides and the surface $\varepsilon^{ps}$ in the range (0–2.4). The dependence of $\tau_{agg}$ on $\varepsilon^{ps}$ is not monotonic (Figure 4A). At T = 0.54, in the weak peptide–surface interaction regime with $\varepsilon^{ps}$ varying from 0.1 to 1.0, aggregation is slowed by the surface. This is due to the fact that a weakly adsorbing surface cannot serve as a good template for the initiation of aggregation, and interplay between the formation of an aggregate in the bulk and on the surface slows down self-assembly. As the peptide–surface interaction increases ($1.0 < \varepsilon^{ps} \leq 1.4$), the surface becomes a good catalytic center for nucleation, which accelerates aggregation (Figure 4A). Our results are consistent with Vacha et al. [35] who reported that weakly absorbing surfaces increase the aggregation time, while strongly absorbing surfaces catalyze the process.

A further increase in the peptide–surface interaction ($\varepsilon^{ps} > 1.4$) again slows down aggregation again ($\ln\tau_{agg}$ increases from 14.74 to 16.16), but the process remains faster than in the bulk. This increase was not studied by other groups previously and this can be explained by the fact that a strong binding to the interface reduces conformational entropy, which complicates the fibril formation. In other words, strong absorption significantly restricts the mobility monomers on the surface leading to retarded aggregation. As evident from Figure 4A, smooth hydrophilic surfaces have obstacle aggregation for $\varepsilon^{ps} \geq 1.4$. However, with a very strong peptide–surface interaction, aggregation occurs more slowly than in bulk, as we can see in Figure 4C for T = 0.49 and T = 0.52.

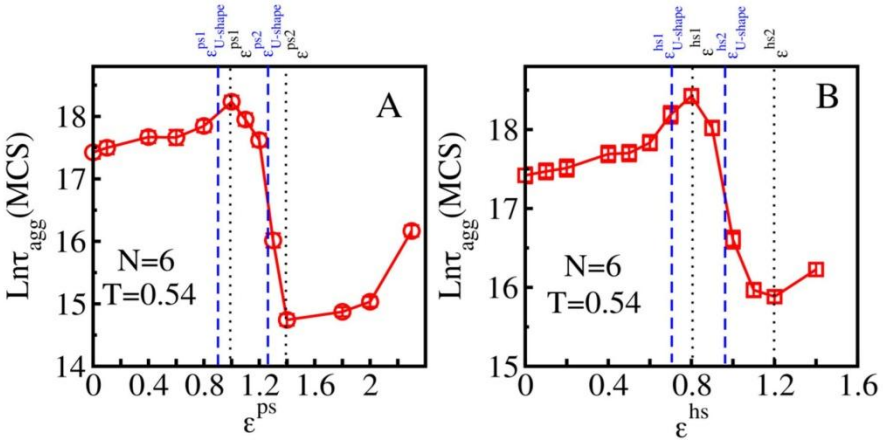


**Figure 4.** *Cont.*

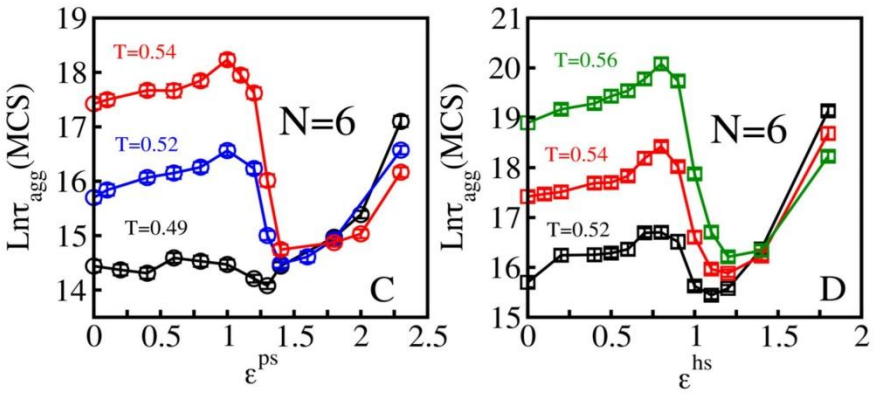


**Figure 4.** Dependence of $\ln\tau_{agg}$ on the interaction of the systems consisting of N = 6 polypeptide chains for hydrophilic (**A**,**C**) and hydrophobic (**B**,**D**) smooth surfaces. The upper row exhibits the simulation at T = 0.54, the values $\varepsilon^{ps1}$ = 1.0, $\varepsilon^{ps2}$ = 1.4, $\varepsilon^{hs1}$ = 0.8 and $\varepsilon^{hs2}$ = 1.2 (black dashed lines) separate the three interaction regions corresponding to the three types of surfaces. Between $\varepsilon^{ps1}_{U-shape}$ = 0.9 and $\varepsilon^{ps2}_{U-shape}$ = 1.25 (blue dashed lines), we observed the U-shape dependence of $\ln\tau_{agg}$ on the roughness degrees Θ for an S-point hydrophilic surface. A similar behavior occurs for a hydrophobic surface between $\varepsilon^{hs1}_{U-shape}$ = 0.7 and $\varepsilon^{hs2}_{U-shape}$ = 0.95 (blue dashed lines). The notations "ps" and "hs" refers to a hydrophilic and hydrophobic surface, respectively. The bottom row also shows correlation of $\ln\tau_{agg}$ and interaction parameters $\varepsilon^{ps}$ of hydrophilic (**C**) and $\varepsilon^{hs}$ hydrophobic (**D**) smooth surfaces for various temperatures and wider ranges of the interaction values. The bottom row shows the dependence of $\ln\tau_{agg}$ on the interaction parameter $\varepsilon^{ps}$ of hydrophilic (**C**) and $\varepsilon^{hs}$ of hydrophobic (**D**) smooth surfaces for various temperatures. Error bars are lower than data symbols.

Higher temperatures enhance the flexibility of peptides, leading to a slower self-assembly in the bulk and on the surface (Figure 4C). On the other hand, they can prevent trapping of polypeptide chains on a strongly absorbing surface, which explains why at $\varepsilon^{ps} \geq 1.8$ aggregation is accelerated at higher temperatures (Figure 4C). A similar effect was seen for hydrophobic surfaces with $\varepsilon^{hs} \geq 1.4$ (Figure 4D).

3.1.2. Hydrophobic Surfaces

For T = 0.54, a similar dependence of the aggregation time on the interaction of polypeptide chains with a smooth hydrophobic interface was obtained for $\varepsilon^{hs}$, which varies in (0; 1.4) interval (Figure 4B). On a weakly absorbing hydrophobic surface ($0.1 < \varepsilon^{hs} < 0.8$), peptide self-assembly was attenuated with $\ln\tau_{agg}$ increasing from 17.42 to 18.43. For $\varepsilon^{hs}$ in the [0.8;1.2] range, aggregation became enhanced with an increase in the peptide–surface interaction and $\ln\tau_{agg}$ decreased from 18.43 to 15.88. Finally, $\ln\tau_{agg}$ leveled from 15.88 to 16.22 as $\varepsilon^{hs}$ changed from 1.2 to 1.4.

As in the case of hydrophilic surfaces, the dependence of the aggregation rate on $\varepsilon^{hs}$ can be rationalized by the interplay between the peptide–surface interaction and the entropy loss due to the reduction in spatial dimensionality from 3 in bulk to 2 on surface. For a weakly absorbing surface, aggregation takes place mainly in bulk, whereas in the opposite case, self-assembly predominately occurs on the surface. Extended calculations for different temperatures and a wider range of $\varepsilon^{hs}$ have been shown in Figure 4D. Higher temperatures can support the aggregation process on very strongly absorbing surfaces ($\varepsilon^{hs} > 1.4$) by promoting peptides' mobility (Figure 4D). Overall, the three modes of dependence of $\ln\tau_{agg}$ on $\varepsilon^{hs}$ remain unchanged for other temperatures including T = 0.52 and T = 0.56.

Aggregation in the presence of weakly absorbing surfaces happen dominantly in bulk, therefore the variation of $\ln\tau_{agg}$ in the simulation time was revealed to be rather similar for both hydrophilic ($\ln\tau_{agg}$ change from 17.49 to 18.23) and hydrophobic cases ($\ln\tau_{agg}$ varies in range of [18.47 to 18.42]). For stronger attractive surfaces, the catalyzing

($\varepsilon^{hs} > 0.8$) and retardation effects ($\varepsilon^{hs} > 1.2$) of hydrophobic surfaces happened earlier compared with hydrophilic surfaces ($\varepsilon^{ps} > 1$ and $\varepsilon^{hs} > 1.4$ for catalyzing and retardation effects, respectively). It is not clear whether this observation is always true or sequence dependent. One of the possible reasons for the difference is that the studied sequence has four hydrophobic residues, while the number of polar residues is two.

#### 3.1.3. Three Classes of Surfaces

Based on the aggregation time and the peptide–surface interaction characterized by either the parameter $\varepsilon^{ps}$ or $\varepsilon^{hs}$, we divided the surfaces into three classes: weakly, medium and strongly absorbing surfaces. The weakly absorbing surface should have $\varepsilon^{ps} < \varepsilon^{ps1}$ or $\varepsilon^{hs} < \varepsilon^{hs1}$, where $\varepsilon^{ps1}$and $\varepsilon^{hs1}$ are the values below which the aggregation time increases with the increasing peptide–surface interaction (Figure 4A,B). For medium absorbing interfaces, $\varepsilon^{ps1} < \varepsilon^{ps} < \varepsilon^{ps2}$ for hydrophilic surfaces and $\varepsilon^{hs1} < \varepsilon^{hs} < \varepsilon^{hs2}$ for hydrophobic surfaces, where $\varepsilon^{ps2}$ and $\varepsilon^{hs2}$ correspond to the minimum in Figure 4A,B. If the interaction exceeds the minimum values, $\varepsilon^{ps2}$ and $\varepsilon^{hs2}$, the corresponding surfaces are classified as strongly absorbing surfaces. In the weakly absorbing surface case, the peptide–surface interaction is weak and the aggregation kinetics is, therefore, driven by entropy. In the opposite case of strongly absorbing surfaces, the self-assembly is an energy-driven process.

The values of $\varepsilon^{ps1,2}$ and $\varepsilon^{hs1,2}$ that divide the surfaces into three classes depend not only the on chemical properties of surfaces, but also on sequences and the number of polypeptide chains. For N = 6, $\varepsilon^{ps1} = 0.8$ and $\varepsilon^{ps2} = 1.4$ for the hydrophilic surfaces and $\varepsilon^{hs1} = 0.8$ and $\varepsilon^{hs2} = 1.2$ for the hydrophobic surfaces (Figure 4).

In our model, the interaction between absorbing particles and the surface is controlled by the parameters $\varepsilon^{ps}$ and $\varepsilon^{hs}$ for hydrophilic and hydrophobic surfaces, respectively. In general, by varying these parameters, we can qualitatively capture aggregation on different surfaces including membrane surfaces with different lipid compositions and carbon nanotubes (see also Introduction). Namely, depending on $\varepsilon^{ps}$ and $\varepsilon^{hs}$, aggregation can be either accelerated or slowed down as has been observed experimentally for various systems. For example, Cabaleiro-Lago et al. reported that hydrophobic single-walled carbon nanotubes slow down the fibril formation of Aβ40 peptide [23], which is consistent with all-atom simulations for the truncated variant $A\beta_{16-22}$ [47]. This experimental observation also agrees with our results obtained for $\varepsilon^{hs} < \varepsilon^{hs1}$ and $\varepsilon^{hs} > \varepsilon^{hs2}$, where the interaction with the surface retards the aggregation.

### *3.2. Effect of Surface Roughness on Fibril Formation: S-Surface*

As mentioned above, the chemical properties of surfaces control the fibrillar growth of polypeptide chains in various scenarios. Therefore, in order to understand the role of surface roughness in protein self-assembly, we must systematically study this process in the presence of foreign surfaces not only of varying degrees of roughness but also of different peptide–surface interactions.

#### 3.2.1. Weakly Absorbing Surfaces: Monotonic Dependence of the Aggregation Time on the Surface Roughness

After generating random particles with a given chemical property on a smooth surface, we obtained tunable rough surfaces corresponding to the chosen chemical properties. For weakly attractive surfaces, we chose $\varepsilon^{ps} = 0.8$ and $\varepsilon^{hs} = 0.6$ (Figure 5A,D). Clearly, the higher the degree of roughness, the slower the peptide aggregation process. As can be seen from Figure 5A, where the value of $\varepsilon^{ps}$ was set to 0.8 which corresponds to weakly attractive smooth hydrophilic surfaces, as the roughness degrees $\Theta_S$ changes from 0 to 0.432, $\ln\tau_{agg}$ increases from 17.75 to 18.87.

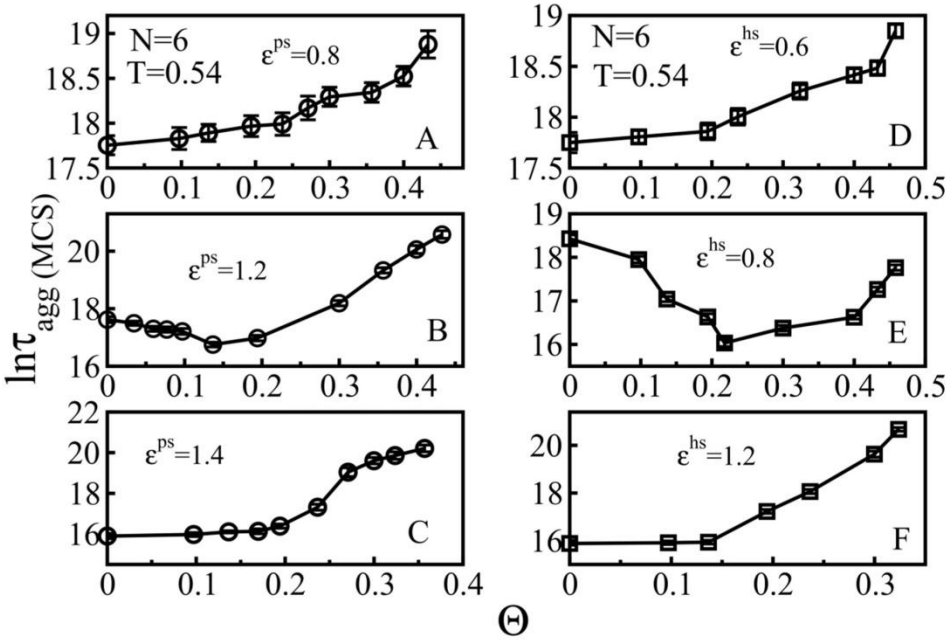


**Figure 5.** Impact of S-surface roughness on the aggregation of N = 6 peptides at temperature T = 0.54. All graphs on the left column (circular data points) display the dependence of the aggregation time $\ln\tau_{agg}$ on the rough degree of different hydrophilic surfaces at various values of $\varepsilon^{ps}$ = 0.8 (**A**), $\varepsilon^{ps}$ = 1.2 (**C**) and $\varepsilon^{ps}$ = 1.4 (**E**). Similarly, the dependence of $\tau_{agg}$ on $\Theta_S$ for various hydrophobic surfaces is shown on the right graphs (square data points), $\varepsilon^{hs}$ = 0.6 (**B**), $\varepsilon^{hs}$ = 0.8 (**D**), and $\varepsilon^{hs}$ = 1.2 (**F**).

A similar result was obtained for a hydrophobic surface (Figure 5D), where $\varepsilon^{hs}$ = 0.6, an increase in $\Theta_S$ from 0 to 0.458 led to an increase in $\ln\tau_{agg}$ from 17.80 to 18.84.

In the corresponding peptide–surface interaction ranges, the kinetics of aggregation on the rough hydrophilic surfaces is similar to the kinetics on the hydrophobic surfaces (Figures 4 and 5), hinting that there are some emphasized physical principles that govern these phenomena. For weakly attractive surfaces, there is interplay between the peptide assembly in the bulk and on the surface; an increase in roughness improves the ability of the peptides to adhere to the surface, increasing the phase space of the peptides in the bulk, which leads to a decreased aggregation rate (Figure 5A,D). We can call this regime entropy driven. We found that the monotonic increase in $\tau_{agg}$ with roughness was observed for $\varepsilon^{ps} < \varepsilon^{ps1}_{U-shape} = 0.9$ and $\varepsilon^{hs} < \varepsilon^{hs1}_{U-shape} = 0.7$ (blue dashed lines in Figure 4A,B)

3.2.2. Medium Absorbing Surfaces: U-Shape Behavior

In order to study the medium absorbing surfaces, we set $\varepsilon^{ps}$ = 1.2 and $\varepsilon^{hs}$ = 0.8 and observed a U-shape dependence, namely, that a slightly rough surface accelerates the fibril formation, while a higher roughness degree slows down the peptide self-association (Figure 5B,E). With a sufficiently low roughness, the roughness increases the probability of monomers aggregating on the surface and the attractive force still allows the proteins to diffuse and associate on the surface, forming fibrillar species, which correspond to the acceleration phase in the U-shape effect. However, as the surface roughness exceeds a threshold point at which the combination of the roughness and absorption restricts the mobility of polypeptide chains, a retardation phase of self-assembly occurs. Thus, the U-shape comes

from the competition between energy and entropy. We found that this behavior occurred for $\varepsilon^{ps1}_{U-shape} < \varepsilon^{ps} < \varepsilon^{ps2}_{U-shape} = 1.25$ and $\varepsilon^{hs1}_{U-shape} < \varepsilon^{hs} < \varepsilon^{hs2}_{U-shape} = 0.95$ (blue dashed lines in Figure 4A,B), for the hydrophilic and hydrophobic surfaces, respectively.

#### 3.2.3. Strongly Absorbing Surfaces: Monotonic Dependence of the Aggregation Time on the Surface Roughness

To investigate this case, we calculated the dependence of the aggregation on the roughness for the parameters $\varepsilon^{ps} = 1.4$ and $\varepsilon^{hs} = 1.2$, which can characterize strongly absorbing hydrophilic and hydrophobic surfaces (Figure 4). In this case, the surface tends to confine the movement of polypeptide chains in two-dimensional space, reducing their mobility. As a result, on very attractive surfaces, there was no acceleration phase at low roughness and the aggregation time rapidly increased with the increasing roughness (Figure 5C,F). The fibril formation becomes practically inhibited for roughness $\Theta_S > 0.356$ and 0.323 for hydrophilic (Figure 5C) and hydrophobic (Figure 5F) surfaces, respectively. This result is in qualitative agreement with the experimental result of Shezal et al. [29] for a highly attractive rough surface, as their experiment was conducted at a protein concentration lower than CMC in order to prevent protein aggregation only in bulk.

We can show that the monotonic increase in Figure 5C,F is possible for $\varepsilon^{ps} > \varepsilon^{ps2}_{U-shape} = 1.25$ and $\varepsilon^{hs} > \varepsilon^{hs2}_{U-shape} = 0.95$ (blue dashed lines in Figure 4A,B), for the hydrophilic and hydrophobic surfaces, respectively. This behavior appears in the energy-driven regime due to the strong peptide–surface interaction.

### *3.3. Effect of Surface Roughness on Fibril Formation: D-Surface and DS-Surface Do Not Qualitatively Change the Results Obtained for S-Surfaces*

Thus far, we considered S-surfaces with a single ball roughness (Figure 3A). In this section, we explore two other cases: a D-surface, where a rough surface is created by randomly placed double balls on a smooth surface (Figure 3C); and a DS-surface, which consists of randomly distributed S-balls and D-balls (Figure 3B). For simplicity, it is assumed that the numbers of S and D balls on the DS-surface are the same.

As we can see in Figure 6, the dependence of $\ln\tau_{agg}$ on roughness $\Theta$ for weakly, moderately, strongly absorbing hydrophilic and hydrophobic of S-surfaces remain the same for DS- and D-surfaces. This result implied that despite the difference in roughness nature, the dependence of the aggregation time on the roughness is driven a general principle, which depends on the interplay between energetic and entropic factors. For weakly (entropy driven, Figure 6A,D) and strongly (energy driven, Figure 6C,F) absorbing surfaces, the dependence of $\tau_{agg}$ on $\Theta$ is monotonic, while for the medium case (Figure 6B,E) the U-shape dependence occurs due to the competition between these two factors. Overall, our results agree with the experiment [29], which showed that at a high enough roughness, a surface can block the self-assemble process.

### *3.4. Size Effects*

#### 3.4.1. Smooth Surfaces

To examine the size effect, we extended simulations to a system of N = 12 peptides (Figure 7). For smooth surfaces, the dependence of the aggregation rate on the protein–surface interaction is similar to the N = 6 case (Figure 4). At T = 0.58 (Figure 7A), for attractive hydrophilic surfaces, no clear effect was seen for $\varepsilon^{ps} < \varepsilon^{ps1} = 1.3$, however, the moderately absorbing surface ($1.3 < \varepsilon^{ps} < 2.0$) remarkably accelerates the aggregation process, as $\ln\tau_{agg}$ decreases from 20.5 to 15.65. The retardation by strongly attractive hydrophilic surfaces appears at $\varepsilon^{ps} > 2.0$. The same scenarios occur for hydrophobic smooth surfaces (Figure 7B), however, at T = 0.56, weakly attractive hydrophobic smooth surfaces ($\varepsilon^{hs} < \varepsilon^{hs1} = 1.1$) noticeably decreased the peptide self-assembly while the catalyzing effect of a medium absorbing smooth surface happened for $1.1 \leq \varepsilon^{hs} \leq 1.5$. The strongly attractive surfaces with $\varepsilon^{hs} > \varepsilon^{hs2} = 1.5$ restricted the formation of fibril-like structure of peptides.

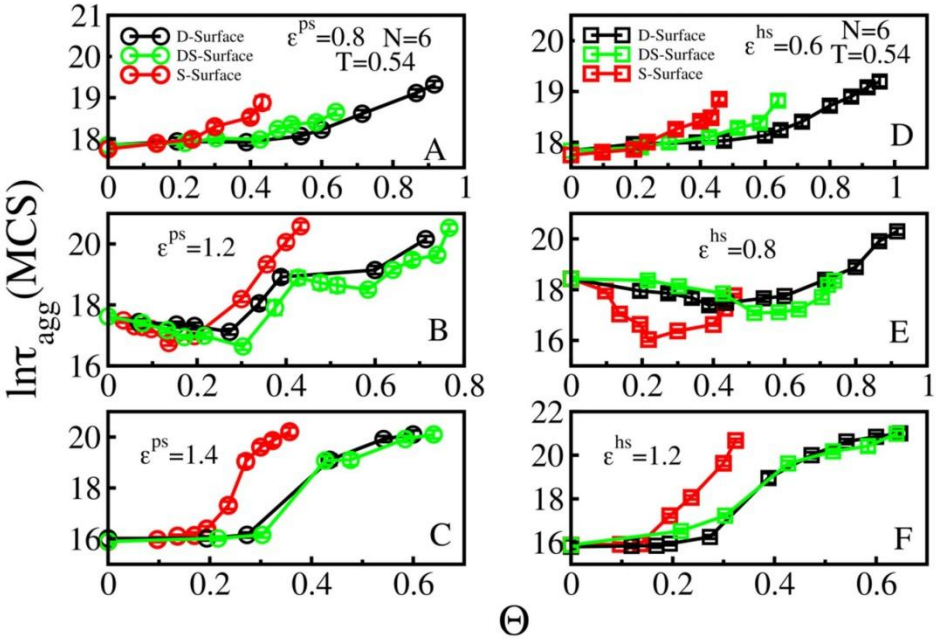


**Figure 6.** Dependence of $\ln\tau_{agg}$ on Θ for N = 6 chains at T = 0.54. Red, green and black circles refer to the S-, DS-, D-surfaces, respectively. Results are shown for the weakly $\varepsilon^{ps} = 0.8$ (**A**), medium $\varepsilon^{ps} = 1.2$ (**B**), strongly $\varepsilon^{ps} = 1.4$ (**C**) absorbing hydrophilic surfaces, as well as for weak $\varepsilon^{hs} = 0.6$ (**D**), medium $\varepsilon^{hs} = 0.8$ (**E**) and strong $\varepsilon^{hs} = 1.2$. (**F**) regimes of attractive hydrophobic surfaces. Error bars are lower than data symbols.

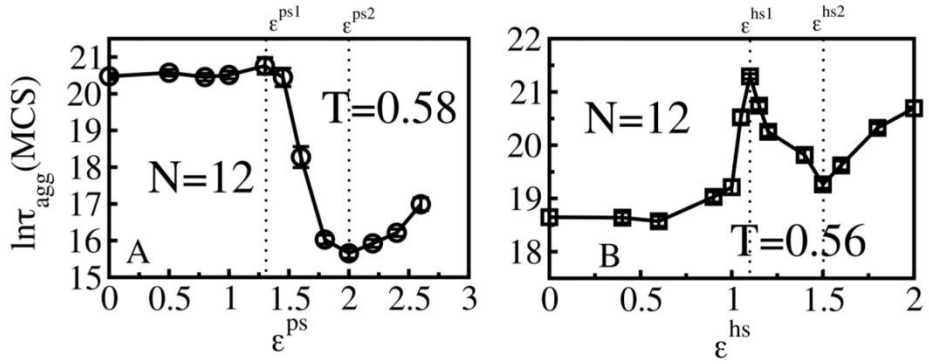


**Figure 7.** Effect of various surfaces on the aggregation time of N = 12 polypeptide chains at T = 0.58 for smooth hydrophilic surfaces (**A**) and at T = 0.56 for hydrophobic surfaces (**B**). The dash lines at values $\varepsilon^{ps1} = 1.3$, $\varepsilon^{ps2} = 2.0$, $\varepsilon^{hs1} = 1.1$ and $\varepsilon^{hs2} = 1.5$ separate the different interaction ranges corresponding to different types of classified surfaces.

#### 3.4.2. Rough Surfaces

As in the smooth surface case, for N = 12 peptides, we also systematically investigated the effect of roughness on the aggregation time in the weak, medium and strong peptide–surface interaction regimes for both hydrophilic and hydrophobic surfaces. Qualitatively, the results are similar to the N = 6 case (compare Figures 6 and 8). However, for $\varepsilon^{ps} = 1$

(Figure 8A) the Θ dependence is rather weak and this is probably because the aggregation mainly occurs in the bulk due to the weak interaction between polypeptide chains and the hydrophilic surface. The surface effect is more pronounced in the case of hydrophobic surface with $\varepsilon^{hs} = 0.8$, as the aggregation time increases with increasing Θ (Figure 8D). The U-shape appears in the medium regime (Figure 8B,E), and this effect is stronger in the presence of D- and DS- surfaces. The highly attractive rough surfaces significantly increased the aggregation time and can even inhibit the process at Θ > 0.42 (Figure 8C) and Θ > 0.38 (Figure 8F) for the hydrophilic and hydrophobic cases, respectively.

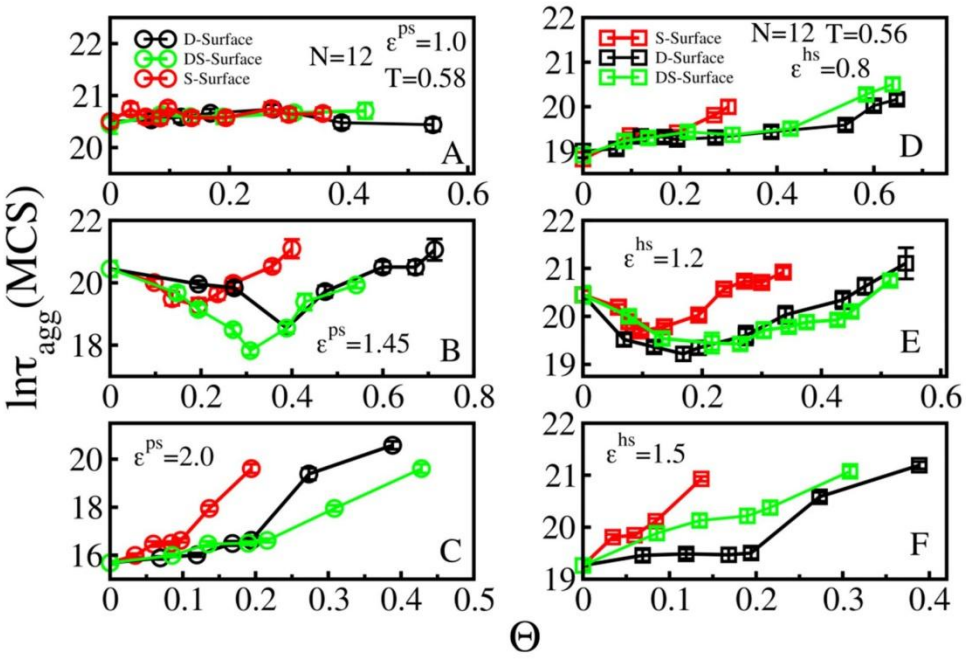


**Figure 8.** Dependence of $\ln\tau_{agg}$ on Θ of N = 12 peptides at T = 0.58 and 0.56 for hydrophilic (**left column**) and hydrophobic surfaces (**right column**). For hydrophilic surfaces, we considered $\varepsilon^{ps}$ = 1.0 (weak regime, **A**), 1.45 (medium, **B**), and 2.0 (strong, **C**). For hydrophobic surfaces the corresponding values $\varepsilon^{hs}$ = 0.8 (**D**), 1.2 (**E**), and 1.5 (**F**).

Thus, the similar behavior of the N = 6 and N = 12 systems with smooth and rough surfaces of various types indicates that our results should be valid for larger systems.

## 4. Conclusions

Since protein aggregation, which is associated with neurodegenerative diseases, occurs in vivo, understanding the influence of various surfaces on this process plays a crucial role in developing new effective therapies. Furthermore, knowledge of the self-assembly mechanism on surfaces is also useful for developing novel materials of fibrillar structure. We constructed a simple lattice model that enabled us to theoretically access the effect of surface roughness on the aggregation kinetics of polypeptide chains. Our model is reliable as it can capture the experimental results of Robert Vacha et al. [35] obtained for both hydrophobic and hydrophilic smooth surfaces that the dependence of the aggregation time on the protein–surface interaction is nontrivial. In addition, our model can explain the experiment of Shezal et al. [29], showing that a rough surface retards the fibril formation and even block it at a high roughness level [48].

By a systematic investigation of the dependence of fibril formation time on the roughness of different surfaces, for the first time, we predicted the U-shape behavior, claiming that a rough surface can not only slow down the aggregation process, but can also accelerate it at a suitable degree of roughness. This can occur in a regime where the entropic factor competes with the energetic factor. Our results were obtained using simple models, but they should be applied to more complex systems, because their validity is guaranteed by general principles, but not by some details. This conclusion is partially supported by the fact that our modeling captures the slowing down or acceleration of aggregation on different surfaces such as lipid membranes [13–16], mica and glass [17,18], carbon nanotubes [21,22], nanoparticles [23,24], HOPG plane [25,26], etc. From this point of view, more advanced off-lattice models should not qualitatively change these results.

Our study also pointed out that the dependence of aggregation time on surface characteristics is complicated, not only by roughness, but also by the geometry of objects that make the surface non-smooth. It would be interesting to experimentally verify our prediction of the U-shaped dependence of aggregation time on roughness.

For the same sequence, the polypeptide chains form different fibrillary structures on the hydrophobic and hydrophilic surfaces (Figure 2). In particular, on a hydrophobic surface, the fibril-prone structure N* has the same structure as the native monomeric structure, which suggests that the hydrophobic surface alters the morphology of fibrils to a greater extent than the hydrophilic surface. This conclusion could be verified by other more advanced theoretical models and experiments.

**Author Contributions:** Conceptualization, N.T.C. and M.S.L.; methodology, N.T.C. and M.S.L.; simulation, N.T.C.; data analysis, N.T.C. and M.S.L.; writing—review and editing, N.T.C. and M.S.L.; supervision, M.S.L. All authors have read and agreed to the published version of the manuscript.

**Funding:** This research was funded by the National Science Centre, Poland, grant number 2015/19/P/ST3/03541, the Department of Science and Technology, Ho Chi Minh city, grant number 02/2018/Đ2/HĐ-KHCNTT and Ministry of Education and Training, project B2019.SPD.03, Vietnam.

**Institutional Review Board Statement:** Not applicable.

**Informed Consent Statement:** Not applicable.

**Data Availability Statement:** Our homemade code for MC simulations and the data that support the findings of this study are available from the corresponding author upon reasonable request.

**Acknowledgments:** We highly appreciate the supercomputer centre TASK in Gdansk, and PLGrid infrastructure, Poland for providing us with computational resources.

**Conflicts of Interest:** The authors declare no conflict of interest.

## References

1. Chiti, F.; Dobson, C.M. Protein Misfolding, Functional Amyloid, and Human Disease. *Annu. Rev. Biochem.* **2006**, *75*, 333–366. [CrossRef]
2. Nasica-Labouze, J.; Nguyen, P.H.; Sterpone, F.; Berthoumieu, O.; Buchete, N.-V.; Coté, S.; De Simone, A.; Doig, A.J.; Faller, P.; Garcia, A.; et al. Amyloid β Protein and Alzheimer's Disease: When Computer Simulations Complement Experimental Studies. *Chem. Rev.* **2015**, *115*, 3518–3563. [CrossRef]
3. Nguyen, P.H.; Ramamoorthy, A.; Sahoo, B.R.; Zheng, J.; Faller, P.; Straub, J.E.; Dominguez, L.; Shea, J.-E.; Dokholyan, N.V.; De Simone, A.; et al. Amyloid Oligomers: A Joint Experimental/Computational Perspective on Alzheimer's Disease, Parkinson's Disease, Type II Diabetes, and Amyotrophic Lateral Sclerosis. *Chem. Rev.* **2021**, *121*, 2545–2647. [CrossRef] [PubMed]
4. Ellis, R. Macromolecular crowding: Obvious but underappreciated. *Trends Biochem. Sci.* **2001**, *26*, 597–604. [CrossRef]
5. O'Brien, E.P.; Straub, J.E.; Brooks, B.R.; Thirumalai, D. Influence of Nanoparticle Size and Shape on Oligomer Formation of an Amyloidogenic Peptide. *J. Phys. Chem. Lett.* **2011**, *2*, 1171–1177. [CrossRef]
6. Co, N.T.; Hu, C.-K.; Li, M.S. Dual effect of crowders on fibrillation kinetics of polypeptide chains revealed by lattice models. *J. Chem. Phys.* **2013**, *138*, 185101. [CrossRef]
7. Musiani, F.; Giorgetti, A. Chapter Two—Protein Aggregation and Molecular Crowding: Perspectives From Multiscale Simulations. In *International Review of Cell and Molecular Biology*; Sandal, M., Ed.; Academic Press: Cambridge, MA, USA, 2017; Volume 329, pp. 49–77.

8. Li, C.; Mezzenga, R. The interplay between carbon nanomaterials and amyloid fibrils in bio-nanotechnology. *Nanoscale* **2013**, *5*, 6207–6218. [CrossRef]
9. Yang, B.; Adams, D.J.; Marlow, M.; Zelzer, M. Surface-Mediated Supramolecular Self-Assembly of Protein, Peptide, and Nucleoside Derivatives: From Surface Design to the Underlying Mechanism and Tailored Functions. *Langmuir* **2018**, *34*, 15109–15125. [CrossRef]
10. Pan, Y.; Banerjee, S.; Zagorski, K.; Shlyakhtenko, L.S.; Kolomeisky, A.B.; Lyubchenko, Y.L. Molecular Model for the Surface-Catalyzed Protein Self-Assembly. *J. Phys. Chem. B* **2020**, *124*, 366–372. [CrossRef]
11. Cholko, T.; Barnum, J.; Chang, C.A. Amyloid-Beta (Abeta42) Peptide Aggregation Rate and Mechanism on Surfaces with Widely Varied Properties: Insights from Brownian Dynamics Simulations. *J. Phys. Chem. B* **2020**, *123*, 5549–5558. [CrossRef]
12. Keller, A.; Grundmeier, G. Amyloid aggregation at solid-liquid interfaces: Perspectives of studies using model surfaces. *Appl. Surf. Sci.* **2020**, *506*, 144991. [CrossRef]
13. Galvagnion, C.; Buell, A.K.; Meisl, G.; Michaels, T.C.; Vendruscolo, M.; Knowles, T.P.; Dobson, C.M. Lipid vesicles trigger α-synuclein aggregation by stimulating primary nucleation. *Nat. Chem. Biol.* **2015**, *11*, 229–234. [CrossRef] [PubMed]
14. Lindberg, D.J.; Wesén, E.; Björkeroth, J.; Rocha, S.; Esbjörner, E.K. Lipid membranes catalyse the fibril formation of the amyloid-β (1–42) peptide through lipid-fibril interactions that reinforce secondary pathways. *Biochim. Biophys. Acta (BBA) Biomembr.* **2017**, *1859*, 1921–1929. [CrossRef] [PubMed]
15. Morriss-Andrews, A.; Brown, F.L.H.; Shea, J.-E. A Coarse-Grained Model for Peptide Aggregation on a Membrane Surface. *J. Phys. Chem. B* **2014**, *118*, 8420–8432. [CrossRef] [PubMed]
16. Butterfield, S.M.; Lashuel, H.A. Amyloidogenic Protein-Membrane Interactions: Mechanistic Insight from Model Systems. *Angew. Chem. Int. Ed.* **2010**, *49*, 5628–5654. [CrossRef] [PubMed]
17. Lin, Y.-C.; Li, C.; Fakhraai, Z. Kinetics of Surface-Mediated Fibrillization of Amyloid-β (12–28) Peptides. *Langmuir* **2018**, *34*, 4665–4672. [CrossRef]
18. Rabe, M.; Soragni, A.; Reynolds, N.P.; Verdes, D.; Liverani, E.; Riek, R.; Seeger, S. On-Surface Aggregation of α-Synuclein at Nanomolar Concentrations Results in Two Distinct Growth Mechanisms. *ACS Chem. Neurosci.* **2013**, *4*, 408–417. [CrossRef]
19. Cabaleiro-Lago, C.; Lynch, I.; Dawson, K.A.; Linse, S. Inhibition of IAPP and IAPP(20−29)Fibrillation by Polymeric Nanoparticles. *Langmuir* **2010**, *26*, 3453–3461. [CrossRef] [PubMed]
20. Mahmoudi, M.; Akhavan, O.; Ghavami, M.; Rezaee, F.; Ghiasi, S.M.A. Graphene oxide strongly inhibits amyloid beta fibrillation. *Nanoscale* **2012**, *4*, 7322–7325. [CrossRef] [PubMed]
21. Ghule, A.V.; Kathir, K.M.; Suresh Kumar, T.K.; Tzing, S.-H.; Chang, J.-Y.; Yu, C.; Ling, Y.-C. Carbon nanotubes prevent 2,2,2 trifluoroethanol induced aggregation of protein. *Carbon* **2007**, *45*, 1586–1589. [CrossRef]
22. Linse, S.; Cabaleiro-Lago, C.; Xue, W.-F.; Lynch, I.; Lindman, S.; Thulin, E.; Radford, S.E.; Dawson, K.A. Nucleation of protein fibrillation by nanoparticles. *Proc. Natl. Acad. Sci. USA* **2007**, *104*, 8691–8696. [CrossRef] [PubMed]
23. Cabaleiro-Lago, C.; Quinlan-Pluck, F.; Lynch, I.; Lindman, S.; Minogue, A.M.; Thulin, E.; Walsh, D.M.; Dawson, K.A.; Linse, S. Inhibition of Amyloid β Protein Fibrillation by Polymeric Nanoparticles. *J. Am. Chem. Soc.* **2008**, *130*, 15437–15443. [CrossRef]
24. Saraiva, A.M.; Cardoso, I.; Pereira, M.C.; Coelho, M.A.N.; Saraiva, M.J.; Möhwald, H.; Brezesinski, G. Controlling Amyloid-β Peptide(1-42) Oligomerization and Toxicity by Fluorinated Nanoparticles. *ChemBioChem* **2010**, *11*, 1905–1913. [CrossRef] [PubMed]
25. Kang, S.-G.; Huynh, T.; Xia, Z.; Zhang, Y.; Fang, H.; Wei, G.; Zhou, R. Hydrophobic Interaction Drives Surface-Assisted Epitaxial Assembly of Amyloid-like Peptides. *J. Am. Chem. Soc.* **2013**, *135*, 3150–3157. [CrossRef] [PubMed]
26. Zhang, F.; Du, H.-N.; Zhang, Z.-X.; Ji, L.-N.; Li, H.-T.; Tang, L.; Wang, H.-B.; Fan, C.-H.; Xu, H.-J.; Zhang, Y.; et al. Epitaxial Growth of Peptide Nanofilaments on Inorganic Surfaces: Effects of Interfacial Hydrophobicity/Hydrophilicity. *Angew. Chem. Int. Ed.* **2006**, *45*, 3611–3613. [CrossRef]
27. Huang, R.; Su, R.; Qi, W.; Zhao, J.; He, Z. Hierarchical, interface-induced self-assembly of diphenylalanine: Formation of peptide nanofibers and microvesicles. *Nanotechnology* **2011**, *22*, 245609. [CrossRef]
28. Morriss-Andrews, A.; Shea, J.-E. Kinetic pathways to peptide aggregation on surfaces: The effects of ?-sheet propensity and surface attraction. *J. Chem. Phys.* **2012**, *136*, 65103. [CrossRef]
29. Shezad, K.; Zhang, K.; Hussain, M.; Dong, H.; He, C.; Gong, X.; Xie, X.; Zhu, J.; Shen, L. Surface Roughness Modulates Diffusion and Fibrillation of Amyloid-β Peptide. *Langmuir* **2016**, *32*, 8238–8244. [CrossRef]
30. Nayak, A.; Dutta, A.K.; Belfort, G. Surface-enhanced nucleation of insulin amyloid fibrillation. *Biochem. Biophys. Res. Commun.* **2008**, *369*, 303–307. [CrossRef]
31. Morriss-Andrews, A.; Bellesia, G.; Shea, J.-E. Effects of surface interactions on peptide aggregate morphology. *J. Chem. Phys.* **2011**, *135*, 85102. [CrossRef]
32. Friedman, R.; Pellarin, R.; Caflisch, A. Amyloid Aggregation on Lipid Bilayers and Its Impact on Membrane Permeability. *J. Mol. Biol.* **2009**, *387*, 407–415. [CrossRef] [PubMed]
33. Press-Sandler, O.; Miller, Y. Molecular mechanisms of membrane-associated amyloid aggregation: Computational perspective and challenges. *Biochim. Biophys. Acta (BBA) Biomembr.* **2018**, *1860*, 1889–1905. [CrossRef] [PubMed]
34. Vácha, R.; Frenkel, D. Relation between Molecular Shape and the Morphology of Self-Assembling Aggregates: A Simulation Study. *Biophys. J.* **2011**, *101*, 1432–1439. [CrossRef] [PubMed]
35. Vácha, R.; Linse, S.; Lund, M. Surface Effects on Aggregation Kinetics of Amyloidogenic Peptides. *J. Am. Chem. Soc.* **2014**, *136*, 11776–11782. [CrossRef] [PubMed]

36. Cabaleiro-Lago, C.; Szczepankiewicz, O.; Linse, S. The Effect of Nanoparticles on Amyloid Aggregation Depends on the Protein Stability and Intrinsic Aggregation Rate. *Langmuir* **2012**, *28*, 1852–1857. [CrossRef] [PubMed]
37. Cabaleiro-Lago, C.; Quinlan-Pluck, F.; Lynch, I.; Dawson, K.A.; Linse, S. Dual Effect of Amino Modified Polystyrene Nanoparticles on Amyloid β Protein Fibrillation. *ACS Chem. Neurosci.* **2010**, *1*, 279–287. [CrossRef]
38. Abeln, S.; Vendruscolo, M.; Dobson, C.M.; Frenkel, D. A Simple Lattice Model That Captures Protein Folding, Aggregation and Amyloid Formation. *PLoS ONE* **2014**, *9*, e85185. [CrossRef] [PubMed]
39. Gupta, P.; Hall, C.K.; Voegler, A.C. Effect of denaturant and protein concentrations upon protein refolding and aggregation: A simple lattice model. *Protein Sci.* **1998**, *7*, 2642–2652. [CrossRef]
40. Tran, T.T.; Nguyen, P.H.; Derreumaux, P. Lattice model for amyloid peptides: OPEP force field parametrization and applications to the nucleus size of Alzheimer's peptides. *J. Chem. Phys.* **2016**, *144*, 205103. [CrossRef]
41. Sterpone, F.; Doutreligne, S.; Tran, T.T.; Melchionna, S.; Baaden, M.; Nguyen, P.H.; Derreumaux, P. Multi-scale simulations of biological systems using the OPEP coarse-grained model. *Biochem. Biophys. Res. Commun.* **2018**, *498*, 296–304. [CrossRef]
42. Li, M.S.; Klimov, D.K.; Straub, J.E.; Thirumalai, D. Probing the mechanisms of fibril formation using lattice models. *J. Chem. Phys.* **2008**, *129*, 175101. [CrossRef]
43. Co, N.T.; Lan, P.D.; Quoc Huy, P.D.; Li, M.S. Heat-induced degradation of fibrils: Exponential vs logistic kinetics. *J. Chem. Phys.* **2020**, *152*, 115101. [CrossRef] [PubMed]
44. Co, N.T.; Li, M.S. New method for determining size of critical nucleus of fibril formation of polypeptide chains. *J. Chem. Phys.* **2012**, *137*, 095101. [CrossRef] [PubMed]
45. Li, M.S.; Co, N.T.; Reddy, G.; Hu, C.-K.; Straub, J.E.; Thirumalai, D. Factors Governing Fibrillogenesis of Polypeptide Chains Revealed by Lattice Models. *Phys. Rev. Lett.* **2010**, *105*, 218101. [CrossRef] [PubMed]
46. Betancourt, M.R.; Thirumalai, D. Pair potentials for protein folding: Choice of reference states and sensitivity of predicted native states to variations in the interaction schemes. *Protein Sci.* **2008**, *8*, 361–369. [CrossRef] [PubMed]
47. Li, H.; Luo, Y.; Derreumaux, P.; Wei, G. Carbon Nanotube Inhibits the Formation of β-Sheet-Rich Oligomers of the Alzheimer's Amyloid-β(16-22) Peptide. *Biophys. J.* **2011**, *101*, 2267–2276. [CrossRef]
48. Shen, L.; Adachi, T.; Vanden Bout, D.; Zhu, X.-Y. A Mobile Precursor Determines Amyloid-β Peptide Fibril Formation at Interfaces. *J. Am. Chem. Soc.* **2012**, *134*, 14172–14178. [CrossRef]

## 4.2 Aggregation rate of amyloid beta peptide is controlled by beta-content in monomeric state

The association between protein aggregation and many neurodegenerative diseases has stimulated a large number of studies on the kinetics of protein self-assembly [1,2,30]. In addition to external factors such as temperature, ionic strength, peptide concentration, pH, etc., the fibrillation process is strongly influenced by internal factors (hydrophobicity, secondary structure, total charge, etc.) [4,257]. Using a simple lattice model [7], we proved that aggregation rate depends exponentially on the population of the fibril-prone conformation of the N* monomer [8]. Although the N* state is to some extent related to monomer beta content, there is no conclusive evidence for a relationship between monomer beta content and protein self-assembly rate. The main goal of this work is to quantify the correlation between fibril formation time and monomer β content using full atom molecular dynamics modeling and experimental data obtained for the Aβ42 peptide and its mutations.

First, all-atom replica exchange molecular dynamics (REMD) simulation with the optimized potentials for liquid (OPLS) and implicit solvent have been perform to determine the secondary structures (percent of β-sheet or β-content, α-helix, coil and turn) of the wild type (WT) and 19 mutants of Aβ42 monomer, then the correlation between experimental aggregation rates $\kappa$ and the secondary structures have been investigated.

We showed that the relative aggregation rate $\kappa$ defined as ratio of $\kappa_{\text{mut}}/\ \kappa_{\text{wt}}$ can be described by a linear (Eq. 12) or exponential dependence on the β-content (Eq. 13) ($\kappa_{\text{mut}}$, $\kappa_{\text{wt}}$ stand for the aggregation rates of the mutations and WT, respectively. R is the correlation coefficient), which implied that the richer the β-content the faster aggregation. Besides, the results also showed that κ is not associated with helix, coil propensity and exhibits a relatively poor correlation with the turn.

$$\kappa = \kappa_{\text{mut}}/\kappa_{\text{wt}} = -0.29 + 0.0635\beta, R = 0.85 \quad (12)$$

$$\kappa = \kappa_0 \exp(\text{c}\beta)\,, \text{c} = 0.071, R = 0.8 \quad (13)$$

The change in the free energy for conversion from α-helical to β-sheet, $\Delta\Delta G$, was estimated as a sum of the free energy change from coil to β-state ($\Delta\Delta G_{\beta\text{-coil}}$) and the free energy change from coil to α-helix ( $\Delta\Delta G_{\text{coil-}\alpha}$). Our calculation using 27 sequences from Chiti and Dobson's dataset [258] showed that if the effect of net charge is included, $\kappa$ displays a poor correlation with $\Delta\Delta G$ ($R$=0.4) , which is consistent with Chiti and Dobson experiment ($R$=0.41).

Our study also reported the modest correlation between $\kappa$ and the change in hydrophobicity ($\Delta Hydr$) ($R$=0.661) and the net charge change ($\Delta Charge$) ($R$=0.683) due to mutation, which is consistent with Chiti and Dobson [258].

Finally, using equation (14), the variation of relative aggregation rates κ caused by the mutations was studied. From linear fit of $\ln(\kappa_{mut}/\kappa_{wt})$ and $\Delta Hydr$, $\Delta\Delta G$ and $\Delta Charge$ , we extracted the corresponding slopes $A$, $B$, $C$ . Contradict to the case of only $\Delta\Delta G$, $\kappa$ revealed significant correlation with the change of combination of hydrophobic, $\Delta\Delta G$ and charge ($R$=0.863). More interesting, the predicted rates almost concise to the experimental work because their correlation coefficient R approximately equals to 1.

Following Chiti and Dobson [258] we tried to predict the mutation induced change in the aggregation rate using the following equation

$$\ln(\kappa_{\mathrm{mut}}/\kappa_{wt}) = A.\Delta Hydr + B.\Delta\Delta G + C.\Delta Charge\ . \quad (14)$$

Here $A$ = -0.081, $B$ = 0.063 and $C$ = -0.304 are the slopes from the linear fit of $\ln(\kappa_{mut}/\kappa_{wt})$ with $\Delta Hydr$, $\Delta\Delta G$ and $\Delta Charge$. We showed that the predicted rate (Eq. 14) is highly correlated with the experiment as $R$=0.83.

Since the computation of the aggregation rate using all-atom models is prohibited in modern computing power, our result is important as it allows estimating κ based only on the knowledge of the beta content (Eqs 12, 13) which can be obtained from simulations of monomer.

**Publication for this section**: *Aggregation rate of amyloid beta peptide is controlled by beta-content in monomeric state*

Tran Thi Minh Thu, Nguyen Truong Co, Ly Anh Tu, Mai Suan Li

J. Chem. Phys. **150**, 225101 (2019); doi: 10.1063/1.5096379

## Abstract

Understanding the key factors that govern the rate of protein aggregation is of immense interest since protein aggregation is associated with a number of neurodegenerative diseases. Previous experimental and theoretical studies have revealed that the hydrophobicity, charge, and population of the fibril-prone monomeric state control the fibril formation rate. Because the fibril structures consist of cross beta sheets, it is widely believed that those sequences that have high beta content (β) in the monomeric state should have high aggregation rates as the monomer can serve as a template for fibril growth. However, this important fact has never been explicitly proven, motivating us to carry out this study. Using replica exchange molecular dynamics simulation with implicit water, we have computed β of 19 mutations of amyloid beta peptide of 42 residues (Aβ42) for which the aggregation rate $\kappa$ has been measured experimentally. We have found that $\kappa$ depends on β in such a way that the higher the propensity to aggregation, the higher the beta content in the monomeric state. Thus, we have solved a long-standing problem of the dependence of fibril formation time of the β-structure on a quantitative level.

doi.org/10.1063/1.5096379

Publication sources: **https://aip.scitation.org/doi/abs/10.1063/1.5096379**

## Author contribution statements

Nguyen Truong Co
Division of Theoretical Physics
Institute of physics, Polish of Academia of Sciences
Al. Lotnikow 32/46
PL-02-668 Warsaw, Poland

**STATEMENT**

I declare that I am the co-author of the publication

Tran Thi Minh Thu, Nguyen Truong Co, Ly Anh Tu, and Mai Suan Li, **Aggregation rate of amyloid beta peptide is controlled by beta-content in monomeric state** J. Chem. Phys. **150**, 225101 (2019); https://doi.org/10.1063/1.5096379

My contribution was conducting molecular dynamic simulation, analyzing data and exhibiting results in the manuscript. My contribution is around 35%.

Warsaw, 30 March 2022

Nguyen Truong Co

Tran Thi Minh Thu
International Centre for Research on Innovative Bio-based Materials
Lodz University of Technology
116 Zeromskiego St.
90-924 Lodz, Poland

## STATEMENT

I declare that I am the co-author of the publication :

Tran Thi Minh Thu, Nguyen Truong Co, Ly Anh Tu, and Mai Suan Li, **Aggregation rate of amyloid beta peptide is controlled by beta-content in monomeric state** J. Chem. Phys. **150**, 225101 (2019); https://doi.org/10.1063/1.5096379

My contribution was conducting molecular dynamic simulation, analyzing data, exhibiting results and writing the manuscript. My contribution is 45%.

Lodz, 30th March 2022

Tran Thi Minh Thu

Dr. Ly Anh Tu
Department of Applied Physics
Ho Chi Minh City University of Technology
268 Ly Thuong Kiet St., ward 14, Dist.10, Ho Chi Minh City, Vietnam

## STATEMENT

I declare that I am the co-author of the publication

> Tran Thi Minh Thu, Nguyen Truong Co, Ly Anh Tu, and Mai Suan Li, **Aggregation rate of amyloid beta peptide is controlled by beta-content in monomeric state** J. Chem. Phys. **150**, 225101 (2019); https://doi.org/10.1063/1.5096379
>
> I took part in discussing and correcting the manuscript. My contribution is around 5%.

Ho Chi Minh, 31st March, 2022

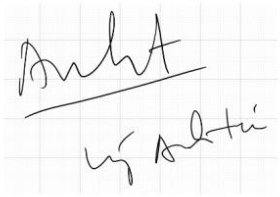

Prof. dr hab. Mai Suan Li
Department of Theoretical Physics
Institute of Physics, Polish Academy of Sciences
Al. Lotnikow 32/46
02-668 Warsaw, Poalnd

## STATEMENT

I declare that I am the co-author of the following publications:

1. Tran Thi Minh Thu, Nguyen Truong Co, Ly Anh Tu, and **Mai Suan Li**, *Aggregation rate of amyloid beta peptide is controlled by beta-content in monomeric state,* J. Chem. Phys. 150, 225101 (2019); https://doi.org/10.1063/1.5096379
   My contribution was about 15%: Design of the research, data analysis and manuscript writing.

Warsaw, 18 April 2022

Mai Suan Li

The Journal of Chemical Physics ARTICLE scitation.org/journal/jcp

# Aggregation rate of amyloid beta peptide is controlled by beta-content in monomeric state

**Cite as: J. Chem. Phys. 150, 225101 (2019); doi: 10.1063/1.5096379**
**Submitted: 17 March 2019 • Accepted: 20 May 2019 •**
**Published Online: 10 June 2019**

View Online Export Citation CrossMark

**Tran Thi Minh Thu,[1,2,3] Nguyen Truong Co,[4] Ly Anh Tu,[3] and Mai Suan Li[4,a)]**

**AFFILIATIONS**

[1]Institute for Computational Science and Technology, SBI Building, Quang Trung Software City, Tan Chanh Hiep Ward, District 12, Ho Chi Minh City, Vietnam

[2]Department of Metarials Science and Technology, University of Science-VNUHCM, 227 Nguyen Van Cu, District 5, Ho Chi Minh City, Vietnam

[3]Department of Applied Physics, Faculty of Applied Science, Ho Chi Minh City University of Technology-VNU HCM, 268 Ly Thuong Kiet Street, District 10, Ho Chi Minh City, Vietnam

[4]Institute of Physics, Polish Academy of Sciences, Al. Lotnikow 32/46, 02-668 Warsaw, Poland

[a)]**Email:** masli@ifpan.edu.pl

**ABSTRACT**

Understanding the key factors that govern the rate of protein aggregation is of immense interest since protein aggregation is associated with a number of neurodegenerative diseases. Previous experimental and theoretical studies have revealed that the hydrophobicity, charge, and population of the fibril-prone monomeric state control the fibril formation rate. Because the fibril structures consist of cross beta sheets, it is widely believed that those sequences that have a high beta content ($\beta$) in the monomeric state should have high aggregation rates as the monomer can serve as a template for fibril growth. However, this important fact has never been explicitly proven, motivating us to carry out this study. Using replica exchange molecular dynamics simulation with implicit water, we have computed $\beta$ of 19 mutations of amyloid beta peptide of 42 residues (Aβ42) for which the aggregation rate $\kappa$ has been measured experimentally. We have found that $\kappa$ depends on $\beta$ in such a way that the higher the propensity to aggregation, the higher the beta content in the monomeric state. Thus, we have solved a long-standing problem of the dependence of fibril formation time of the β-structure on a quantitative level.



## I. INTRODUCTION

A number of neurodegenerative diseases are believed to be associated with the aggregation of amyloid proteins. For example, according to the amyloid cascade hypothesis, Alzheimer's disease (AD) is caused by the fibrillation of amyloid beta (Aβ) peptides forming amyloid plaques.[1,2] Aβ peptides, which are cleaved from amyloid precursor protein (APP) by $\beta$- and $\gamma$-secretases, have 36–43 residues, but Aβ40 (40 amino acids) and Aβ42 (42 amino acids) are most abundant. As the main component of amyloid plaques in the human brain, Aβ42 is more neurotoxic than Aβ40 due to faster self-assembly.[3] Because understanding key factors driving protein aggregation is important not only for basic research but also for designing efficient drugs for many diseases, this problem has attracted a lot of attention of researchers in recent decades.

Accumulated experimental and theoretical data indicate that in addition to external factors (pH, T, ionic strength, and protein concentration),[4] there are intrinsic factors such as the hydrophobicity, net charge, secondary structure,[4–7] and chain-length polydispersity[8] and the so-called population of fibril-prone state in monomeric state $\mathbf{N}^*$[7,9] which play a key role in the aggregation propensity. Locking the monomer in a strandlike state by constraining the Asp23-Lys28 salt bridge accelerates the aggregation of amyloid beta peptides considerably.[10,11] As shown by NMR dispersion experiments[12] and simulation,[13] $\mathrm{N}^*$ of Fyn SH3 is a nativelike folding intermediate that is prone to aggregation. A high population of fibril-prone state $\mathbf{N}^*$

The Journal of Chemical Physics ARTICLE scitation.org/journal/jcp

promotes the formation of template for the protein accumulation leading to an exponential dependence of fibril formation time on the population of this conformation.[7]

The regions enriched by hydrophobic residues promote aggregation[14–17] as evident from the high correlation between the hydration free energy and the aggregation rate of proteins Aβ42, HypF-N, and AcP.[6] Charged residues strongly influence protein aggregation not only because they are involved in specific salt bridges but also because a nonzero net charge prevents self-assembly through repulsion between chains.[18,19]

Chiti and Dobson have demonstrated[5] that the variation in the aggregation rate upon mutation depends on the free energy change in conversion from the α-helix to β-sheet conformation, $\Delta\Delta G = \Delta\Delta G_{\text{coil-}\alpha} + \Delta\Delta G_{\beta\text{-coil}}$. Here, $\Delta\Delta G_{\text{coil-}\alpha}$ and $\Delta\Delta G_{\beta\text{-coil}}$ refer to free energy changes in coil-helix and beta-coil transformations, respectively. However, these quantities were estimated using α-helix and β-sheet propensities of individual wildtype (WT) and mutant residues,[5] leaving the question of the dependence of the fibril formation rate on the monomer β-content open.

In order to clarify the impact of secondary structures on the propensity to aggregation, one has to compute them consistently taking into account the contribution of all residues. To do so, in this paper, we have performed the all-atom replica exchange molecular dynamics (REMD) simulation using the optimized potentials for liquid simulations (OPLS) force field and implicit solvent for the wildtype (WT) and 19 mutants of Aβ42. We showed that the experimentally determined aggregation rate is strongly correlated with the β-content of the monomer, while no correlation with the α-content was observed.

So far, it is believed that the higher the β-content in the monomeric state, the faster the formation of fibrils, but there is no convincing evidence. Here, based on the results obtained for a large dataset, for the first time, we strongly supported this widespread opinion.

## II. CHOICE OF SEQUENCES

It is well known that the sequence of a protein controls not only its folding ability but also the propensity to self-assembly.[20,21] Mutation is used to change the sequence resulting in a variation of the aggregation rate.[5] Because the turn region[21–23] of Aβ42, for example, plays a key role in the fibril formation, some mutations, such as Flemish (A21G), Osaka (E22D), Italian (E22K), Arctic (E22G), and Iowa (D23N), have been intensively studied.[18,22,23] Table S1 of the supplementary material lists 19 Aβ42 mutants, for which the aggregation rate has been measured experimentally.[22–24] We will perform a REMD simulation for this set of mutants. Note that by performing 100 ns all-atom conventional MD simulation in explicit water, Chong and Ham showed that the experimentally determined self-assembly rates of these mutants strongly correlate with hydrophobicity in such a way that the higher the hydrophobicity, the faster the aggregation[6] implying the important role of hydration.

## III. MOLECULAR DYNAMICS SIMULATION

We have calculated secondary structures of WT and 19 mutants (Table S1 of the supplementary material) in the monomeric state using the OPLS force field[25] and the generalized Born (GB) model for an implicit solvent.[26] The OPLS-AA force field was chosen because for the Aβ monomer it provided conformations consistent with the NMR data.[27] In addition, using this force field in combination with the GB model for water, we previously obtained a reliable estimation of the secondary structures not only of WT but also of mutations of Aβ.[28,29] To improve sampling, REMD was employed with 12 replicas in the temperature range from 290.16 to 490.16 K (see the supplementary material for more details), and for each replica, 500 ns MD simulation was performed. One of the representative structures, obtained in our previous work for the monomer,[28] was chosen as the initial structure for all replicas in WT simulation, while for the mutants we used the same structure but the corresponding mutation was made using the Raptor X web server[30] (Fig. S1 of the supplementary material). Because we used the REMD method, the results should not depend on the starting configuration.

## IV. EQUILIBRATION

### A. Effectiveness of REMD simulation

To show the effectiveness of REMD simulation, we monitored the evolution of each replica in the replica space. For illustration, we plot the time dependence of exchanges of the second replica with the remaining partners [Fig. S2 (upper panel) of the supplementary material]. Clearly, this replica was exchanged with everyone else, including the farthest 12th, implying that the replica exchange method worked well for our system. This is also confirmed by a strong overlap between adjacent distributions of potential energy of 12 replicas [Fig. S2 (lower panel) of the supplementary material]. For contiguous temperatures, the probability of exchanges is about 20%–30% and this is consistent with the overlap of the potential energy distributions.

### B. Time dependence of RMSD, total energy, and beta content

We monitored the time dependence of the root mean square displacement (RMSD), which was calculated using the initial structure as a reference structure and the coordinates of Cα-atoms. We assumed that the system has reached equilibrium when RMSD gets saturation. As evident from Fig. S3 (upper panel) of the supplementary material, the equilibration time is about 210 ns for WT and mutants. This conclusion is further supported by the time dependence of the total energy and beta content of three sequences (Fig. S3 of the supplementary material).

### C. Heat capacity in two time windows

To ensure that 210 ns is enough for equilibration, we have computed the specific heat for time windows [210–400] and [210–500] ns using the formula $Cv = (\langle E^2\rangle - \langle E\rangle^2)/(k_B T^2)$, where $E$ is the potential energy and $\langle \ldots \rangle$ denotes the thermodynamics average. The heat capacity, obtained in two time windows at 300 K, for WT, A21G, and E22K, is shown in Fig. S5 of the supplementary material. Since $C_V$ is almost the same for two windows, we conclude that the data were equilibrated. Note that together with WT, we select A21G and E22K as representatives for displaying data because the former is

The Journal of Chemical Physics ARTICLE scitation.org/journal/jcp

among the sequences with low β-content, while the latter has the highest β-content (see below). Our result obtained for WT (Fig. S4 of the supplementary material) is consistent with the data reported by Hicks[31] that *Cv* slightly increases with the temperature in the range of 300–350 K.

### D. Secondary structure in two time windows

We have also calculated the secondary structures for the [210–400] and [210–500] ns time windows using the STRIDE algorithm.[32] Since within error the obtained results are identical for these windows (Fig. S5 of the supplementary material), the Aβ42 variants are at equilibrium after 210 ns (see also our previous works for WT[28,29]). The secondary structures obtained in the [210–500] ns window will be used for data analysis. Although the MD simulation has been performed for 12 temperatures, we will consider $T = 300$ K where experimental data were collected. Details of MD simulation are provided in the supplementary material.

## V. AGGREGATION RATE DEPENDS ON β-CONTENT

The free energy surface was constructed for Aβ42-WT and two selected mutants A21G and E22K (Fig. S6 of the supplementary material) by using the dihedral angle principle component analysis (dPCA) method in which only the first two important components $V1$ and $V2$ were kept (see the supplementary material for more details). Structures (S) representing major basins clearly show that the mutations alter secondary structures. This is also evident from the per-residue distributions and the most important structures of three sequences shown in Fig. 1. For WT, these distributions were discussed in detail in our previous works.[28,29] For E22K, the β-propensity at the C-terminal levels up compared with WT, while the reduction occurs in this region for A21G. The β-content is compatible in the 18–23 fragment for WT and E22K. Overall, E22K increases the β-content from 21% (WT) to 29%, but A21G reduces it to 13.7% (Table I). This is consistent with the experiments showing that E22K speeds up aggregation, while Flemish A21G slows it down.[6,23]

### A. Linear and exponential dependence

Figure 2 shows that the experimentally measured aggregation rate linearly depends on β-content

$$\kappa_{\mathrm{mut}}/\kappa_{\mathrm{wt}} = -0.29 + 0.0635\,\beta, \tag{1}$$

where β is measured in percentage. The correlation level is high as $R = 0.85$. Thus, for the first time, we explicitly showed that the β-content of the monomer controls the aggregation propensity for Aβ peptides and this is expected to be true for other proteins.

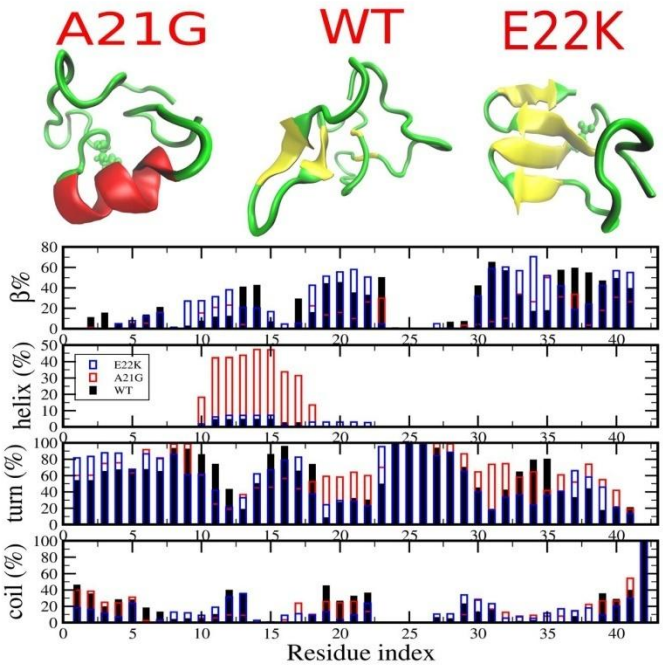


**FIG. 1.** (Upper) Most representative structures obtained by the clustering method at equilibrium (see structures S1 in Fig. S3 of the supplementary material) for WT, A21G, and E22K. The mutated residue is in the all-atom presentation. (Lower) Per-residue distributions of secondary structures of Aβ42-WT, A21G, and E22K at 300 K. Results were obtained at equilibrium.

J. Chem. Phys. **150**, 225101 (2019); doi: 10.1063/1.5096379

The Journal of Chemical Physics ARTICLE scitation.org/journal/jcp

**TABLE I**. The relative computational β-content and observed aggregation propensities of all mutations. The simulation result was obtained at 300 K, the aggregation rate was taken from experiment, and reference is at the last column.

| | Simulation | | Experiment | |
|---|---|---|---|---|
| Mutations | β-content (%) | α-content (%) | log ($\kappa_{mut}/\kappa_{wt}$) | Reference |
| Aβ42 | 20.94 ± 1.91 | 0.07 ± 1.70 | 0 | |
| I41D-A42Q | 12.92 ± 2.37 | 1.98 ± 0.47 | −0.964 | 6 and 24 |
| I41D-A42S | 12.15 ± 1.93 | 0.58 ± 0.15 | −0.913 | |
| I41H-A42D | 11.99 ± 2.38 | 3.32 ± 0.87 | −0.708 | |
| I41E-A42L | 13.83 ± 2.32 | 8.00 ± 2.16 | −0.445 | |
| I41H-A42N | 15.06 ± 2.85 | 2.37 ± 0.75 | −0.837 | |
| A21G | 13.7 ± 2.02 | 7.63 ± 2.43 | −0.671 | 6 and 23 |
| I41T-A42N | 11.82 ± 1.74 | 0.73 ± 0.21 | −0.605 | 6 and 24 |
| I41T-A42Q | 13.31 ± 1.82 | 0.69 ± 0.30 | −0.590 | |
| I41L-A42N | 14.61 ± 2.66 | 0.60 ± 0.14 | −0.561 | |
| I41Q- A42L | 19.79 ± 3.17 | 1.35 ± 0.42 | −0.295 | |
| I41T-A42M | 12.78 ± 1.8 | 4.72 ± 1.63 | −0.292 | |
| I41T- A42I | 13.72 ± 1.96 | 0.26 ± 0.06 | −0.075 | |
| I41K | 19.00 ± 4.12 | 0 | −0.518 | |
| I41K-A42L | 18.56 ± 3.46 | 3.05 ± 0.72 | −0.379 | |
| I41R-A42R | 16.54 ± 2.07 | 3.97 ± 1.39 | −0.324 | |
| A42R | 15.49 ± 1.9 | 4.92 ± 1.54 | −0.034 | |
| E22G | 20.52 ± 2.43 | 0.67 ± 0.22 | 0.209 | 6 and 23 |
| D23N | 23.91 ± 2.39 | 0.80 ± 0.14 | 0.238 | 22 |
| E22K | 29.06 ± 3.53 | 1.28 ± 0.36 | 0.545 | 6 and 23 |

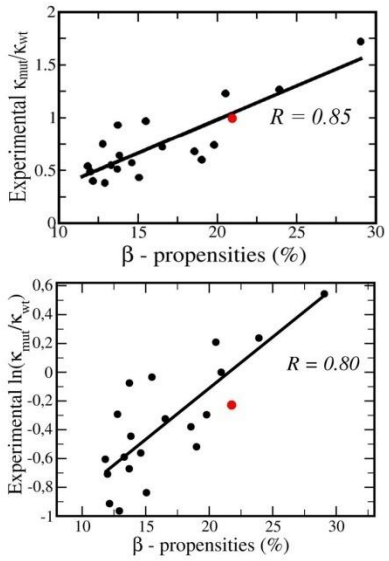


**FIG. 2**. Dependence of the relative aggregation rate (upper panel) and the logarithm of the relative aggregation rate on the β-content (lower panel). The red circle refers to WT. Linear fits are $y = -0.29 + 0.0635 \times (R = 0.85)$ and $y = -1.534 + 0.071 \times (R = 0.80)$.

Although linear fit [Fig. 2 and Eq. (1)] works well, we can show that the exponential fit is also possible. As evident from Fig. 2, there is also a high correlation ($R = 0.8$) between $\ln(\kappa_{mut}/\kappa_{wt})$ and β-content and their relationship can be described by an exponential function

$$\kappa = \kappa_0 \exp(c\beta), \quad c = 0.071, \tag{2}$$

where $\kappa_0$ is a fitting constant and $\beta$ is measured in percentage. A mutation that levels up self-aggregation enhances the β-propensity in the monomeric state and slows it down otherwise. One can expect that the exponential dependence is valid for other systems as the α-β conversion is a barrier crossing event but constant $c$ may be not universal.

Using lattice models, Li *et al.* have observed the exponential dependence of $\kappa$ on the population of fibril-prone state $\mathbf{N}^*$.[7] On the other hand, the $\mathbf{N}^*$ conformation is rich in β-sheets implying that the exponential behavior [Eq. (2)] is in the line with this work. From this point of view, exponential fit is more favorable than linear, despite the fact that the correlation of the linear fit is higher. One of the reasons why it is difficult to distinguish two dependences is that the β-content varies in a narrow interval. We have to study a larger dataset to solve this problem.

### B. Aggregation rate does not correlate with helix-, turn-, and coil-propensity

At 300 K, the helix-content of Aβ42-WT is practically zero, and the mutations E22K and A21G increase it to 1.28% and 7.63%, respectively (Fig. 1). The enhancement occurs mainly in the 10–18 region. With the exception of I41K, all mutations increase the propensity to helix formation, varying from 0.26 (I41T-A42I) to 8% (I41E-A42L) (Table I). A small change in this quantity as a result of mutations leads to a poor correlation between the self-assembly rate and the α-content (Fig. S7 of the supplementary material, $R = 0.16$). This is also consistent with the experiment showing that Aβ42-WT is much more aggregation prone than Aβ40-WT[33] although they have almost the same helix content.[28]

The turn is highly populated at the C-terminal and in the 22–29 region (Fig. 1). In A21G, it increases mainly at residues 9, 19–21 and 31–34, while a notable reduction occurs at positions 11, 12, and 15–18, which leads to a slight increase from 61.17% (WT) to 63.47% (A21G). Upon E22K replacement, the turn propensity increases at residues 1–3 and 23, but decreases at positions 11–15 and 29–31, resulting in a decline by about 5%. Compared to the α-content, the turn propensity varies over a wider range from 31.81 (D23N) to 73.54 (I41T-A42N) leading to a higher correlation with experiments ($R = 0.46$, Fig. S8 of the supplementary material). The rationale for this observation is that the formation of fibril contacts, such as the Asp23-Lys28 salt bridge, in the turn segment plays a key role in the fibril growth.[10,11] Nevertheless, it cannot be concluded that the turn-propensity controls the aggregation rate as the correlation coefficient remains below 0.5 (Fig. S8 of the supplementary material).

J. Chem. Phys. **150**, 225101 (2019); doi: 10.1063/1.5096379

The Journal of Chemical Physics ARTICLE scitation.org/journal/jcp

In WT, the coil structure is about 16% (Table S3 of the supplementary material) and it is predominantly populated at several first and last residues (Fig. 1). After mutation, the per-residue distribution changes (Fig. 1), but the total amount slightly changes remaining in the interval of 13%–21% (Table S3 of the supplementary material). Consequently, as in the case of α-content, the coil propensity poorly correlates with the aggregation rate, having R = 0.15 (Fig. S9 of the supplementary material). One of the possible causes of poor correlation with the α- and coil-content is that these structures are poorly populated in the $\mathbf{N}^*$ state.[34]

## VI. EFFECT OF CHARGE, HYDROPHOBICITY, AND PROPENSITY TO CONVERSION FROM AN α-HELICAL TO A β-SHEET CONFORMATION

### A. Aggregation rate poorly correlates with the free energy for conversion from an α-helical to a β-sheet conformation ΔΔG

The change in free energy from the coil to the β-state, $\Delta\Delta G_{\beta\text{-coil}}$, was calculated using the formula $\Delta\Delta G_{\beta\text{-coil}} = 13.64(P_\beta^{wt} - P_\beta^{mut})$, where $P_\beta^{wt}$ and $P_\beta^{mut}$ are the β sheet propensities of the wildtype and mutant residues, respectively, and 13.64 is the conversion constant from the normalized scale to the unit kJ/mol, and $\Delta\Delta G_{\beta\text{-coil}}$ is measured in kJ/mol. Using $P_\beta$ for the 20 amino acids provided in the supplementary material of Chiti and Dobson[5] and in Table I of Street and Mayo,[35] we obtained $\Delta\Delta G_{\beta\text{-coil}}$ for all sequences studied (Table S4 of the supplementary material).

The change in free energy from α-helix to the coil, $\Delta\Delta G_{coil\text{-}\alpha}$, was estimated using the equation $\Delta\Delta G_{coil\text{-}\alpha} = RT\ \ln(P_\alpha^{wt}/P_\alpha^{mut})$, where $P_\alpha^{wt}$ and $P_\alpha^{mut}$ are α-helical propensities of the wildtype and mutated sequences at the mutation site, respectively, and gas constant R = 0.008 314 kJ mol$^{-1}$ K$^{-1}$. The helix percentage was calculated using the AGADIR algorithm (www.http://agadir.crg.es/), and the results are shown in Table S3 of the supplementary material. The free energy of conversion from an α-helical to a β-sheet conformation, $\Delta\Delta G$, is defined as $\Delta\Delta G = \Delta\Delta G_{\beta\text{-coil}} + \Delta\Delta G_{coil\text{-}\alpha}$ and its values are also given in Table S3 of the supplementary material.

As shown in Fig. 3(a), the correlation between the experimental aggregation rates and $\Delta\Delta G$ is quite low ($R = 0.40$), suggesting that the β-content of the monomeric state is a better indicator for the self-assembly propensity compared to the propensity to conversion from the α-helix to the β-sheet conformation. By confining to mutations that do not change the net charge, Chiti and Dobson showed[5] that for a set of 15 sequences, the correlation level between $\kappa$ and $\Delta\Delta G$ is noticeably higher ($R = 0.71$) than ours. This result seems to contradict our result, but using the entire set of 27 sequences,[5] we obtained $R = 0.41$ (Fig. S10 of the supplementary material) which is close to our value 0.40. From this prospect, our result is consistent with that of Chiti and Dobson.[5] Nevertheless, further study is needed to clarify the correlation with $\Delta\Delta G$.

### B. Aggregation rate correlates with the change in the hydrophobicity (ΔHydr) and overall charge (ΔCharge) due to mutation

Following Dobson *et al.*,[5] we calculated the change in hydrophobicity ΔHydr = $\text{Hydr}_{wt} - \text{Hydr}_{mut}$, where $\text{Hydr}_{wt}$ and $\text{Hydr}_{mut}$ are the hydrophobicity of the wildtype and mutant sequences, respectively. Similarly, a change in the net charge is

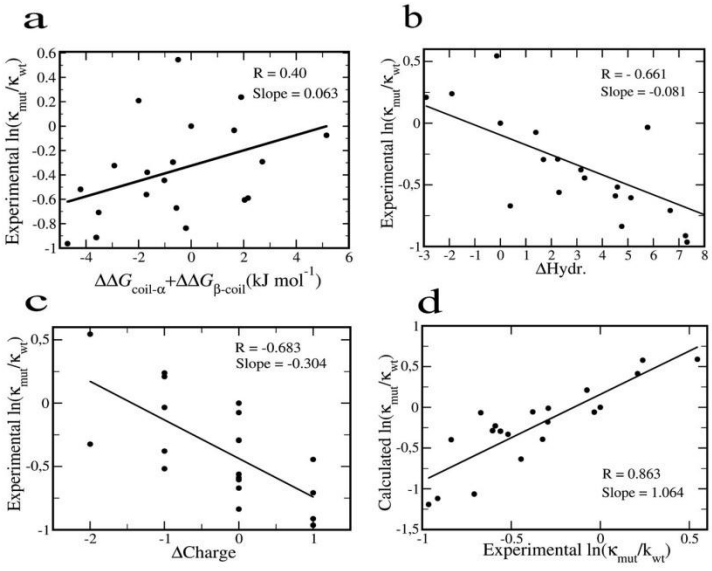


**FIG. 3**. Dependence of the logarithm of the relative aggregation rate on the predicted change in propensity to convert from an α-helical to a β-sheet conformation (a), hydrophobicity (b), charge (c), and the calculated aggregation rate obtained by Eq. (3) (d). The correlation level and the slope are also shown.

The Journal of Chemical Physics ARTICLE scitation.org/journal/jcp

defined as $\Delta$Charge = |Charge$_{mut}$| − |Charge$_{wt}$|, where Charge$_{mut}$ and Charge$_{wt}$ are the charge of the mutation and the wildtype, respectively. We calculated $\Delta$Hydr and $\Delta$Charge for all studied sequences (Table S4 of the supplementary material) using the values of hydrophobicity and charge for 20 amino acids provided in the supplementary material of Dobson *et al.*[5]

The level of correlation between the experimental aggregation rate and $\Delta$Hydr and $\Delta$Charge is $R$ = 0.661 and 0.683, respectively [Figs. 3(b) and 3(c)]. These values are compatible with 0.545 and 0.721 reported by Dobson *et al.*,[5] but they are noticeably lower than the correlation level between the aggregation rate and the beta content.

We have calculated the change in the aggregation rate due to mutation, using the following equation:[5]

$$\ln(\kappa_{mut}/\kappa_{wt}) = A \cdot \Delta\text{Hydr} + B \cdot \Delta\Delta G + C \cdot \Delta\text{Charge}. \quad (3)$$

Here, A, B, and C are the slopes obtained from the linear fit between $\ln(\kappa_{mut}/\kappa_{wt})$ and $\Delta$Hydr, $\Delta\Delta G$, and $\Delta$Charge, respectively, as follows from Figs. 3(a)–3(c) are −0.081, 0.063 and −0.304, respectively. The predicted aggregation rates, obtained by using Eq. (3), are shown in column 7 of Table S4 of the supplementary material. Despite the poor correlation with $\Delta\Delta G$, its combination with hydrophobicity and charge significantly improves the correlation between the predicted and experimental aggregation rates as we have R = 0.863 [Fig. 3(d)]. This correlation level is as high as that for correlation with the beta content. Interestingly, because the slope in Fig. 3(d) is 1.064 (close to 1), the predicted and experimentally measured rates are almost the same.

## VII. CONCLUSION

We have carried out the all-atom REMD simulation in implicit water for various mutations of Aβ42. The correlation between the secondary structures obtained in the monomeric state and the experimentally determined aggregation rates has been thoroughly analyzed. We have found that there is no correspondence between the experimental rate and the helix and coil propensities, while the fit with the turn is relatively poor. Using the data set of 27 sequences from Chiti and Dobson,[5] we demonstrated that if the change in net charge was taken into account, then the experimental $\kappa$ does not correlate with the propensity to conversion from α-helical to β-sheet conformation free energy $\Delta\Delta G$ as $R$ is below 0.5. One of the possible reasons is that $\Delta\Delta G_{\beta\text{-coil}}$ and $\Delta\Delta G_{\text{coil-}\alpha}$ were determined by the empirical propensities $P_\beta$ and $P_\alpha$.[5] A direct estimate of $\Delta\Delta G$ from the all-atom simulation may improve the correlation but this requires for a long simulation that is beyond the scope of this paper. Another possible scenario is that the poor correlation between $\kappa$ and $\Delta\Delta G$ is due to a small dataset. To clarify this problem, we need more experimental as well as simulation data that are more convincing rather than the existing ones.

We have found a strong correlation between the experimental aggregation rate and β-propensity in the monomer. The dependence of $\kappa$ on $\beta$ is expressed by an exponential function in such a way that the higher the β-propensity, the faster the formation of fibril [Eq. (2)]. But linear dependence [Eq. (1)] is not excluded, probably due to the fact that the dataset is not large enough. Nevertheless, our result sheds light on our understanding of major principles that regulate the self-aggregation propensity of proteins, in particular, intrinsically disordered proteins.

Since an estimation of the aggregation rate of long polypeptide chains is beyond existing computational facilities, Eq. (2) [or maybe Eq. (1)] is very useful because it would allow us to predict the aggregation rate based on the β-content, which can be easily obtained by REMD simulation.

## SUPPLEMENTARY MATERIAL

See supplementary material for "Material and Method"; initial structure for MD simulation of WT; plots showing the performance of the RE method; time dependence of RMSD, total energy, and beta-content of the three representative sequences; temperature dependence of the heat capacity, per-residue distributions of the beta-content, and free energy surfaces of WT, A21G, and E22K; dependence of the aggregation rate on $\Delta\Delta G$, helix, turn, and coil propensity; tables showing sequences of Aβ42-WT and mutations, characteristics of structures representing major basins on the free energy surface of WT, A21G, and E22K, turn and coil propensities, $\Delta\Delta G_{\beta\text{-coil}}$ and $\Delta\Delta G_{\text{coil-}\alpha}$, estimated for 20 sequences through the β- and α-propensities of amino acids, and $\Delta$Hydr and $\Delta$Charge.

## ACKNOWLEDGMENTS

This work was supported by Narodowe Centrum Nauki in Poland (Grant No. 2015/19/B/ST4/02721) and Department of Science and Technology at Ho Chi Minh City, Vietnam (Grant No. 19/2017/HĐ-KHCNTT). Allocation of CPU time at the supercomputer center TASK in Gdansk (Poland) is highly appreciated. This research was also supported in part by PLGrid Infrastructure in Poland.

## REFERENCES

[1] D. J. Selkoe, Science **275**, 630 (1997).
[2] J. Hardy and G. Higgins, Science **256**, 184 (1992).
[3] D. J. Selkoe, Physiol. Rev. **81**, 741 (2001).
[4] M. Belli, M. Ramazzotti, and F. Chiti, EMBO Rep. **12**, 657 (2011).
[5] F. Chiti, M. Stefani, N. Taddei, G. Ramponi, and C. M. Dobson, Nature **424**, 805 (2003).
[6] S. H. Chong and S. Ham, Angew. Chem. **126**, 4042 (2014).
[7] M. S. Li, N. T. Co, G. Reddy, C. K. Hu, J. E. Straub, and D. Thirumalai, Phys. Rev. Lett. **105**, 218101 (2010).
[8] A. Hernik-Magon, W. Pulawski, B. Fedorczyk, D. Tymecka, A. Misicka, P. Szymczak, and W. Dzwolak, Biomacromolecules **17**, 1376 (2016).
[9] B. Tarus, J. E. Straub, and D. Thirumalai, J. Am. Chem. Soc. **128**, 16159 (2006).
[10] G. Reddy, J. E. Straub, and D. Thirumalai, J. Phys. Chem. B **113**, 1162 (2009).
[11] K. L. Sciarretta, D. J. Gordon, A. T. Petkova, R. Tycko, and S. C. Meredith, Biochemistry **44**, 6003 (2005).
[12] P. Neudecker, P. Robustelli, A. Cavalli, P. Walsh, P. Lundstrom, A. Zarrine-Afsar, S. Sharpe, M. Vendruscolo, and L. E. Kay, Science **336**, 362 (2012).
[13] P. I. Zhuravlev, G. Reddy, J. E. Straub, and D. Thirumalai, J. Mol. Biol. **426**, 2653 (2014).
[14] C. Tanford, Science **200**, 1012 (1978).
[15] K. A. Dill, Biochemistry **29**, 7133 (1990).
[16] A. Ben-Naim, *Hydrophobic Interactions* (Springer Science & Business Media, 2012).
[17] W. Kim and M. H. Hecht, Proc. Natl. Acad. Sci. U. S. A. **103**, 15824 (2006).

[18]F. Chiti, M. Calamai, N. Taddei, M. Stefani, G. Ramponi, and C. M. Dobson, Proc. Natl. Acad. Sci. U. S. A. **99**, 16419 (2002).
[19]A. T. Petkova, Y. Ishii, J. J. Balbach, O. N. Antzutkin, R. D. Leapman, F. Delaglio, and R. Tycko, Proc. Natl. Acad. Sci. U. S. A. **99**, 16742 (2002).
[20]F. Chiti and C. M. Dobson, Annu. Rev. Biochem. **75**, 333 (2006).
[21]J. Nasica-Labouze *et al.*, Chem. Rev. **115**, 3518 (2015).
[22]K. Murakami, K. Irie, A. Morimoto, H. Ohigashi, M. Shindo, M. Nagao, T. Shimizu, and T. Shirasawa, J. Biol. Chem. **278**, 46179 (2003).
[23]C. Nilsberth *et al.*, Nat. Neurosci. **4**, 887 (2001).
[24]W. Kim and M. H. Hecht, J. Biol. Chem. **280**, 35069 (2005).
[25]G. A. Kaminski, R. A. Friesner, J. Tirado-Rives, and W. L. Jorgensen, J. Phys. Chem. B **105**, 6474 (2001).
[26]V. Tsui and D. A. Case, Biopolymers **56**, 275 (2000).
[27]N. G. Sgourakis, Y. Yan, S. A. McCallum, C. Wang, and A. E. Garcia, J. Mol. Biol. **368**, 1448 (2007).
[28]H. L. Nguyen, T. T. M. Thu, P. M. Truong, P. D. Lan, V. H. Man, P. H. Nguyen, L. A. Tu, Y.-C. Chen, and M. S. Li, J. Phys. Chem. B **120**, 7371 (2016).
[29]N. H. Linh, T. T. M. Thu, L. Tu, C.-K. Hu, and M. S. Li, J. Phys. Chem. B **121**, 4341 (2017).
[30]S. Wang, W. Li, S. Liu, and J. Xu, Nucleic Acids Res. **44**, W430 (2016).
[31]D. E. Hicks, "Thermophysical properties of the amyloid beta protein from differential scanning calorimetry," Ph.D. thesis (University of Tennessee, 2005).
[32]M. Heinig and D. Frishman, Nucleic Acids Res. **32**, W500 (2004).
[33]S. W. Snyder, U. S. Ladror, W. S. Wade, G. T. Wang, L. W. Barrett, E. D. Matayoshi, H. J. Huffaker, G. A. Krafft, and T. F. Holzman, Biophys. J. **67**, 1216 (1994).
[34]M. A. Wälti, F. Ravotti, H. Arai, C. G. Glabe, J. S. Wall, A. Böckmann, P. Güntert, B. H. Meier, and R. Riek, Proc. Natl. Acad. Sci. U. S. A. **113**, E4976 (2016).
[35]A. G. Street and S. L. Mayo, Proc. Natl. Acad. Sci. U. S. A. **96**, 9074 (1999).

J. Chem. Phys. **150**, 225101 (2019); doi: 10.1063/1.5096379

## 4.3 Heat-induced degradation of fibrils: Exponential vs. logistic kinetics

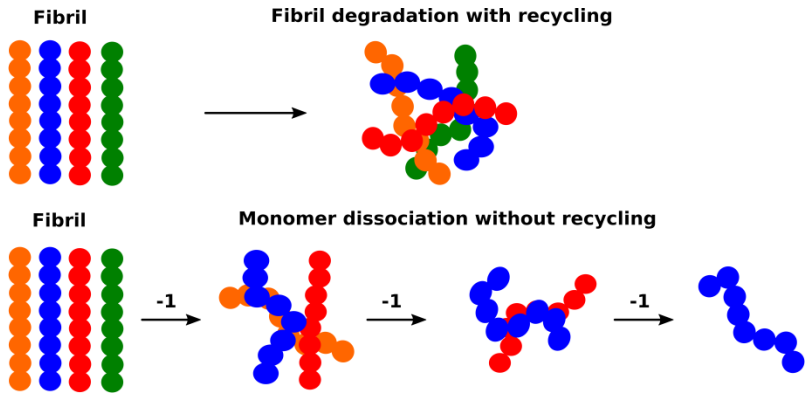


**Figure 12**: Heat-induced degradation schemes. Upper panel: heat-induced degradation of β structure with recycling of monomers; Lower panel: monomer dissociation from the fibril structure without recycling, where the protein capture

Self-assembly of proteins has been proposed to be associated with many neurodegenerative diseases [3]. Many studies have recently shown that oligomers are much toxic than mature fibrils [259]. Therefore, in addition to knowing the kinetics of peptide formation into the amyloid fibril structure, understanding the stability of fibrils and their degradation kinetics is also critical due to the potential toxicity of the intermediately dissociated agents [260].

The research in this paper [13] aimed to theoretically characterize the difference between the experiment on heat-induced fibril degradation by Goto's group [10] and the monomers dissociation experiment carried by Gruning et al using the protein capture technique [261]. The former used Thioflavin fluorescence to monitor the degradation of fibril content ($\Omega$) and reported that the time dependence of $\Omega$ follows a bi-exponential kinetics. The latter estimated the remaining fraction of associated monomers $\Theta$ using a Trytophan fluorescence assay in which engineered protein called *ZA*β3 was used to prevent $A\beta_{42}$ monomers from oligomerization or recycling back to their mother pieces. By this way, Gruning et al. observed a mono-exponential dependence of $\Theta$ on time [261]. The difference between these two experiments/assays is sketched in Figure 11. The upper panel showed the heat-induced degradation fibril which leads to the reduction of β structures. The lower panel represents the dissociation of monomers from protofibrils by using the monomer capture technique.

It has been already known that the time dependence of $\Omega(t)$ can be described by a bi-exponential function experiment [10]. However, an analytical formula for the time dependence of $\Theta(t)$, which can be measured by Trytophan fluorescence, remains unknown. Therefore, we have developed a phenomenological theory showing that $\Theta(t)$ obeys the logistics function:

$$\Theta(t) = \frac{\Theta_0}{\tau b\Theta_0 + (1 - \tau b\Theta)e^{\frac{t}{\tau}}} + C_{eq} \qquad (15)$$

Here $\tau$, $b$ and $\Theta_0$ are phenomenological parameters; $C_{eq}$ is non-zero in the case of allowing free peptides reunite and 0 when free peptides are excluded from the system. A typical dependence of $\Theta(t)$ on $t$ is shown in Figure 12 for the case with recycling (red) and without recycling (blue) of monomers.

Our simulation with lattice models [262] for the systems of N=10, 16, 28 chains and all-atom models [263] for the Aβ17-42 (2BEG) (5 chains) and Aβ37-42 (10 chains) fibrils proved that $\Omega$ in heat-induced fibril degradation follows a bi-exponential function (Figure 12: purple curve). Our results agreed well with experiment by Goto et al. [10].
In lattice model, $\Theta$ has been estimated as the difference of the total number of monomers and the number of free monomers. In order to mimic the protein capture technique which prevents free monomers from recycling back to their original aggregate, a newly produced free monomer is excluded from the lattice system during simulation.

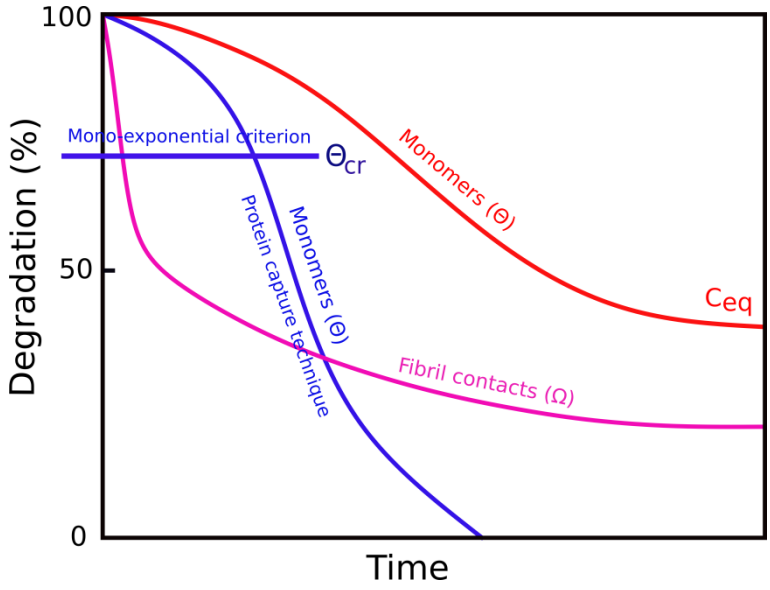


**Figure 12**: Schemes of different heat-induced degradation kinetics of fibril. Bi-exponential purple curve shows the time-dependent degradation of percent of β structure ($\Omega$) represented by number of fibril contact. Percent of bounded chains ($\Theta$) during the dissociation process of monomers from fibril were exhibited by red and blue logistical curves for applying and non-applying monomer capture technique, respectively. The horizontal blue line determines the value of $\Theta_{cr}$

Our lattice simulations confirmed the logistics behavior of $\Theta$ (Eq. 15 and Figure 12) for both recycling and non-recycling scenarios.

At long enough time scales the second term in the denominator in Eq. 15 dominates, then we have a mono-exponential dependence $\Theta(t) \sim e^{-t/\tau}$, which was observed experimentally by Gruning et al. [261]. This behavior holds when $\Theta$ exceeds a threshold value $\Theta_{\text{cr}}$ (Figure 15). It would be interesting to experimentally verify our prediction for $\Theta$ below $\Theta_{\text{cr}}$.

**Publication for this section:** *Heat-induced degradation of fibrils: Exponential vs. logistic kinetics*

Nguyen Truong Co, Pham Dang Lan, Pham Dinh Quoc Huy, and Mai Suan Li

J. Chem. Phys. 152, 115101 (2020)

## Abstract

The degradation of fibrils under the influence of thermal fluctuations was studied experimentally by various groups around the world. In the first set of experiments, it was shown that the decay of fibril content, which can be measured by the ThT fluorescence assay, obeys a bi-exponential function. In the second series of experiments, it was demonstrated that when the monomers separated from the aggregate are not recyclable, the time dependence of the number of monomers belonging to the dominant cluster is described by a single-exponential function if the fraction of bound chains becomes less than a certain threshold. Note that the time dependence of the fraction of bound chains can be measured by tryptophan fluorescence. To understand these interesting experimental results, we developed a phenomenological theory and performed molecular simulation. According to our theory and simulations using the lattice and all-atom models, the time dependence of bound chains is described by a logistic function, which slowly decreases at short time scales but becomes a single exponential function at large time scales. The results, obtained by using lattice and all-atom simulations, ascertained that the time dependence of the fibril content can be described by a bi-exponential function that decays faster than the logistic function on short time scales. We have uncovered the molecular mechanism for the distinction between the logistic and bi-exponential behavior. Since the dissociation of the chain from the fibrils requires the breaking of a greater number of inter-chain contacts as compared to the breaking of the beta sheet structure, the decrease in the number of connected chains is slower than the fibril content. Therefore, the time dependence of the aggregate size is logistic, while the two-exponential behavior is preserved for the content of fibrils. Our results are in agreement with the results obtained in both sets of experiments.

doi: 10.1063/1.5144305

Publication source: https://aip.scitation.org/doi/abs/10.1063/1.5144305

## Author contribution statements

Nguyen Truong Co
Division of Theoretical Physics
Institute of Physics, Polish of Academia of Sciences
Al. Lotników 32/46
PL-02-668 Warsaw, Poland

**STATEMENT**

I declare that I am the co-author of the publication

Nguyen Truong Co, Pham Dang Lan, Pham Dinh Quoc Huy, and Mai Suan Li **Heat-induced degradation of fibrils**: **Exponential vs logistic kinetics** J. Chem. Phys. **152**, 115101 (2020); https://doi.org/10.1063/1.5144305

My contribution was conducting simulation with lattice model, molecular dynamic simulation with Amber software, analyzing data, constructing theory, and presenting results in the manuscript. My contribution is around 50%.

Warsaw, 30 March 2022

Nguyen Truong Co

Pham Dang Lan
Life Sciences Lab
Institute for Computational Science and Technology
SBI Building, Quang Trung Software City
Tan Chanh Hiep Ward, District 12, Ho Chi Minh City, Vietnam

## STATEMENT

I declare that I am the co-author of the publication

Nguyen Truong Co, Pham Dang Lan, Pham Dinh Quoc Huy, and Mai Suan Li **Heat-induced degradation of fibrils**: **Exponential vs logistic kinetics** J. Chem. Phys. **152**, 115101 (2020); https://doi.org/10.1063/1.5144305

My contribution was performing all-atom molecular dynamic simulations with Amber software, analyzing data, constructing theory, and presenting results in the manuscript. My contribution is 30%.

Ho Chi Minh, 30 March 2022

Pham Dang Lan

Pham Dinh Quoc Huy
Division of Laboratory of Biological Physics
Institute of Physics, Polish of Academia of Sciences
Al. Lotników 32/46
PL-02-668 Warsaw, Poland

**STATEMENT**

I declare that I am the co-author of the publication

Nguyen Truong Co, Pham Dang Lan, Pham Dinh Quoc Huy, and Mai Suan Li **Heat-induced degradation of fibrils: Exponential vs logistic kinetics** J. Chem. Phys. **152**, 115101 (2020); https://doi.org/10.1063/1.5144305

My contribution was conducting molecular dynamic simulation with Amber software, analyzing data and presenting results in the manuscript. My contribution is around 10%.

Warsaw, 30 March 2022

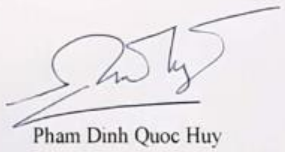

Pham Dinh Quoc Huy

Prof. dr hab. Mai Suan Li
Department of Theoretical Physics
Institute of Physics, Polish Academy of Sciences
Al. Lotnikow 32/46
02-668 Warsaw, Poalnd

## STATEMENT

I declare that I am the co-author of the following publications:

Nguyen Truong Co, Pham Dang Lan, Pham Dinh Quoc Huy, and **Mai Suan Li**, *Heat-induced degradation of fibrils: Exponential vs logistic kinetics*, J. Chem. Phys. 152, 115101 (2020); https://doi.org/10.1063/1.5144305
My contribution was about 10%: Design of the research, data analysis and manuscript writing.

Warsaw, 18 April 2022

Mai Suan Li

The Journal of Chemical Physics ARTICLE scitation.org/journal/jcp

# Heat-induced degradation of fibrils: Exponential vs logistic kinetics

**Cite as: J. Chem. Phys. 152, 115101 (2020); doi: 10.1063/1.5144305**
**Submitted: 5 January 2020 • Accepted: 27 February 2020 •**
**Published Online: 16 March 2020**

View Online Export Citation CrossMark

**Nguyen Truong Co,[1] Pham Dang Lan,[2,3] Pham Dinh Quoc Huy,[1] and Mai Suan Li[1,a)]**

**AFFILIATIONS**

[1]Institute of Physics, Polish Academy of Sciences, Al. Lotnikow 32/46, 02-668 Warsaw, Poland
[2]Institute for Computational Science and Technology, SBI Building, Quang Trung Software City, Tan Chanh Hiep Ward, District 12, Ho Chi Minh City, Vietnam
[3]Faculty of Physics and Engineering Physics, VNUHCM-University of Science, 227, Nguyen Van Cu Street, District 5, Ho Chi Minh City, Vietnam

[a)]**Author to whom correspondence should be addressed:** masli@ifpan.edu.pl

**ABSTRACT**

The degradation of fibrils under the influence of thermal fluctuations was studied experimentally by various groups around the world. In the first set of experiments, it was shown that the decay of fibril content, which can be measured by the ThT fluorescence assay, obeys a bi-exponential function. In the second series of experiments, it was demonstrated that when the monomers separated from the aggregate are not recyclable, the time dependence of the number of monomers belonging to the dominant cluster is described by a single-exponential function if the fraction of bound chains becomes less than a certain threshold. Note that the time dependence of the fraction of bound chains can be measured by tryptophan fluorescence. To understand these interesting experimental results, we developed a phenomenological theory and performed molecular simulation. According to our theory and simulations using the lattice and all-atom models, the time dependence of bound chains is described by a logistic function, which slowly decreases at short time scales but becomes a single exponential function at large time scales. The results, obtained by using lattice and all-atom simulations, ascertained that the time dependence of the fibril content can be described by a bi-exponential function that decays faster than the logistic function on short time scales. We have uncovered the molecular mechanism for the distinction between the logistic and bi-exponential behavior. Since the dissociation of the chain from the fibrils requires the breaking of a greater number of inter-chain contacts as compared to the breaking of the beta sheet structure, the decrease in the number of connected chains is slower than the fibril content. Therefore, the time dependence of the aggregate size is logistic, while the two-exponential behavior is preserved for the content of fibrils. Our results are in agreement with the results obtained in both sets of experiments.



## INTRODUCTION

Protein aggregation is believed to be associated with neurodegenerative diseases. For example, aggregation of α-synuclein protein may be related to Parkinson's disease, while Alzheimer's disease (AD), which is often seen in older people, is presumably caused by formation of extracellular senile plaques consisting of amyloid beta (Aβ) peptides in the patient's brain.[1] Aβ peptides, which are cleaved from amyloid precursor protein (APP) under the influence of β- and γ-secretases,[2] have most abundant isoforms $A\beta_{40}$ (40 amino acids) and $A\beta_{42}$ (42 amino acids). Aβ aggregation occurs by the nucleation mechanism with the lag phase to form mature fibrils with transverse β-strands. Recent experiments have provided evidence that senile plaque levels are weakly correlated with the severity of dementia, but intermediate oligomers are predominantly toxic species.[3,4] Thus, knowledge about the intermediate stages of fibril growth plays a crucial role in determining effective AD therapy. In addition, since finite-sized oligomers and fibrils can decompose into non-toxic monomers, it is important to understand the process of dissociation in detail.

Several experimental studies of the chemical stability[5–10] and dissociation of amyloid fibrils under high pressure[11–14] and laser irradiation[15,16] have been carried out, while only a limited research was conducted to study their thermal stability.[17–24] It was shown[24]

The Journal of Chemical Physics ARTICLE scitation.org/journal/jcp

that due to thermal fluctuations, the dissociation kinetics can be described by a bi-exponential function with two very different time scales or degradation rates.

Recently, Gruning *et al.*[25] have carried out an interesting experiment allowing for the study of the dissociation of Aβ fibrils without re-association. Using the engineered protein ZAβ3W for the sequestration of the Aβ monomer, they were able to control the dissociation by tryptophan fluorescence. The basic idea of their experiment was based on the fact that ZAβ3W inhibits the Aβ aggregation by sequestering the aggregation-prone central and C-terminal regions of the Aβ monomer.[26,27] Therefore, in the experiment of Gruning *et al.*,[25] the concurrent effect of reverse and forward reactions was avoided. More importantly, it was shown that in the absence of monomer recycling, the dissociation of fibrils obeys a single exponential law instead of bi-exponential decay. This interesting result has not been theoretically explained.

Protein aggregation, in particular, the oligomerization of full-length and truncated Aβ peptides, has been studied by many groups around the world using molecular dynamics (MD) simulation.[28–33] However, the degradation of fibrils has not been theoretically considered. On the other hand, since the destruction of insoluble amyloid fibrils is one of the possible ways to treat neurodegenerative diseases, this problem is of great interest not only from the point of view of basic research but also from the point of view of application.

In this paper, combining theory with all-atom MD and lattice-based Monte Carlo simulations, we study the temperature-driven dissociation of fibrils with and without recycling (Fig. 1). In a standard scenario with monomer recycling, the released monomer is allowed to reattach to the mother aggregate, whereas in the case without recirculation, the released monomer is removed from the studied system. We have developed an analytical theory to describe the fibril degradation with and without the capture of monomers, which are detached from the parent aggregate (we use the words aggregate and fibril with the same meaning, but, in general, the aggregate is of less order than the fibril). We showed that the time dependence of the aggregate size is described by the logistic function,

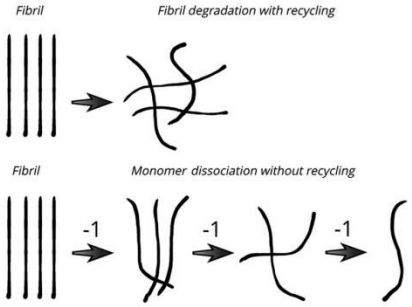


**FIG. 1**. Top panel: schematic plot for the dissociation of fibrils in a standard scenario with recycling, where the freed chain can reunite with the mother aggregate and, therefore, the total number of chains is fixed. Bottom panel: the decomposition of fibrils without monomer recycling, in which the released monomer is removed, not allowing to reattach to the mother unit.

while the behavior of the fibril content (the fibril content is proportional to the ThT fluorescence signal and is measured by the number of fibril contacts or beta content in simulation) is controlled by a bi-exponential function. Then, our theory and the results, obtained by tryptophan and ThT fluorescence techniques, were verified by simulations using lattice and all-atom models.

We expect that the results obtained in this work should be valid for the thermal degradation of not only proteins but also of other systems.

## MATERIALS AND METHODS

### Lattice model

To study the degradation of sufficiently large fibrils, we used a simple lattice model,[34,35] in which each amino acid is represented by a bead and the polypeptide chain has $M = 8$ beads. The sequence of a polypeptide chain was chosen the same as in our previous works,[34,35] i.e., this is +HHPPHH−. Here, H and P refer to hydrophobic and polar residues, respectively, while + and − are charged beads located at the ends.

The potential energy of $N$ chains is as follows:

$$E = \sum_{l=1}^{N}\sum_{i<j}^{M} E_{sl(i)sl(j)}\,\delta(r_{ij}-a) + \sum_{m<l}^{N}\sum_{i,j}^{M} E_{sm(i)sl(j)}\,\delta(r_{ij}-a), \quad (1)$$

where the first and second terms are intra- and inter-chain interactions, respectively. $r_{ij}$ stands for the distance between beads $i$ and $j$, and the lattice spacing is denoted by $a$. $sm(i)$ is the type of residue $i$ in the $m$th peptide, and $\delta(0) = 1$ and zero, otherwise. For intra-chain interaction, we count the interaction energy between two residues $i$ and $j$ that are separated by a lattice spacing but are not successive in sequence. For a cubic lattice, this condition means that $|i-j|$ must be greater or equal to 3. In the case of inter-chain interaction, any pair of two residues from different chains that are separated from each other by distance $a$ should contribute to the interaction energy.

The energy is measured in the unit of the hydrogen bond energy $\varepsilon_{HB}$. We chose the contact energies as $E_{P,\alpha} = -0.2$, where $\alpha$ = P; +; −, and the interaction energy between two hydrophobic residues as $E_{HH} = -1$.[34] To favor the formation of "salt bridge," we assign the sufficiently strong attraction between oppositely charged beads $E_{+-} = -0.6$, while the repulsive interaction was chosen to be weaker with $E_{++} = E_{--} = -E_{+-}/2 = 0.3$. For all other contacts, we have $E_{\alpha\beta} = 0.2$. Note that the lattice model was successfully used to study the formation of critical nucleus[36] and fibril formation in a crowded environment.[37]

### *Monte Carlo moves*

The MC (Monte Carlo) algorithm was used to study degradation of fibrils on a discrete cubic lattice. MC moves include local (corner flip, tail rotation, and crankshaft rotation) and global moves. Global moves involve translating the entire chain along a randomly chosen direction with a step of $a$ and rotating it 90° around a randomly selected one of the three axes. Since global moves are artificial, we tried to maintain their acceptance rate as low as possible. However, if this rate is too low, the degradation process will be so slow that the problem becomes computationally unfeasible. Therefore, as in our previous work,[34] the acceptance rates of local and global moves were set at 0.9 and 0.1, respectively.

J. Chem. Phys. **152**, 115101 (2020); doi: 10.1063/1.5144305

The Journal of Chemical Physics ARTICLE scitation.org/journal/jcp

Simulation was conducted in a hypercube with a periodic boundary condition. Simulation time is measured in units of MCS (MC step), which is a combination of local and global moves.[34] The concentration of chains in each system was chosen to be around 57 $\mu$M, which corresponds to the cubic sizes of 135, 165, and 235$a$ for $N$ = 10, 16, and 28 monomers, respectively, with $a$, lattice spacing, set equal to 1. This concentration has the same order of magnitude as in typical experiments. To obtain reliable results, we performed 100–150 independent MC trajectories for each simulation set.

### *Fibril structures in lattice models*

Fibril-like structures in the lattice model are a set of monomers forming anti-parallel structures with the lowest energy. In order to find such structures, we carried out multiple MC simulations starting from random configurations. Figure 2 shows fibril structures for $N$ = 10, 16, and 28 for the force field described above.

### *Simulation of fibril degradation in lattice models*

To study the kinetics and mechanisms of thermal degradation of fibrils in the lattice model, simulations were conducted starting from a fibril-like structure (Fig. 2) at various temperatures. Inter- and intra-chain contacts that exist in the fibril structure are called fibril contacts. The intra-chain contact between beads $i$ and $j$ is formed if $|i - j| \geq 3$, and the distance between them is equal to the lattice spacing $a$. The inter-chain contact between two beads belonging to two different chains occurs if the distance between them is $a$.

### *Temperature in lattice model*

Since in the lattice model the energy is measured in $\varepsilon_{HB}$, the temperature is measured in $\varepsilon_{HB}/k_B$. In what follows, we use dimensionless temperature but mean that its unit is $\varepsilon_{HB}/k_B$. The folding temperature of the monomer $T_F$ can be obtained either from the maximum of heat capacity[38] or from the condition $\langle Q(T_F)\rangle = 0.5$, where $Q(T_F)$ is the fraction of native contacts at the folding temperature.[34] Since the chain contains only eight beads, these quantities can be calculated exactly. From the temperature dependence of $\langle Q(T)\rangle$, we obtained $T_F \approx 0.39$ (Fig. S1 of the supplementary material). The same value of $T_F$ was obtained from the temperature dependence of the heat capacity (results not shown). The room temperature is set as the folding temperature of the monomer $T_F = 0.39$. The lattice simulations were performed at temperatures above room temperature.

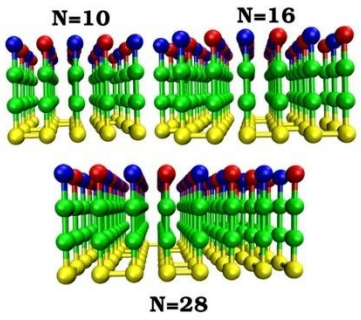


**FIG. 2.** Fibril structures of $N$ = 10, 16, and 28 polypeptide chains in the lattice model. Blue, red, green, and yellow balls represent positive charges, negative charges, hydrophobic amino acids, and hydrophilic amino acids, respectively. The connections between beads are peptide bonds. These structures have 114 (84), 192 (144), and 360 (276) fibril contacts for $N$ = 10, 16, and 28, respectively. The number of inter-chain contacts is shown in brackets.

### All-atom MD simulation

The structure of Aβ fibrils remains controversial. The N-terminus of the peptide is believed to be either disordered or ordered in the fibril stage. Fibril structures of N-terminus truncated peptides were proposed by Lührs *et al.*[39] ($A\beta_{17-42}$), Petkova *et al.* ($A\beta_{9-40}$),[40] and Paravastu *et al.* ($A\beta_{9-40}$)[41] because the first 16 residues of $A\beta_{1-42}$ and the first 8 residues of $A\beta_{1-40}$ were assumed as unstructured. However, recent experiments have shown that the N-terminus might be ordered and involved in the fibril structure.[42–46] In this work, we carried out all-atom MD simulation to study the degradation of the fibril-like structure of 10 truncated peptides $A\beta_{37-42}$ (37GGVVIA42). The cross beta structure (Fig. 7) was resolved by the Eisenberg group using the solid state NMR and has ID 2ONV on the website http://people.mbi.ucla.edu/sawaya/jmol/xtalpept/index.html. We also performed the simulation for the fibril-like structure of five $A\beta_{17-42}$ chains (PDB ID: 2BEG,[39] Fig. 8).

As in the case of lattice models, the contacts formed in a fibril-like structure are called fibril contacts. The contact between two amino acids is formed if the distance between their centers of mass is less than 6.5 Å. For intra-chain contacts, we do not count the contact between successive residues.

We used the Amber11 package[47,48] to perform explicit solvent simulation applying the amber force field 99SB[49] and TIP3P water model.[50] It is worth to mention that the amber force field 99SB and TIP3P model of water is the best combination.[51,52] The motion equation was solved by the leap-frog algorithm[53] with a time step of 2 fs. By the SHAKE algorithm,[54] all bonds with hydrogen atoms were constrained. A Langevin thermostat[55] was applied to maintain the designed temperature with 2 $ps^{-1}$ collision frequency. The vdW interaction at distances longer than 1.4 nm was not taken into account, and the electrostatic interaction was treated by the particle mesh Ewald method.[56]

### Why we have to use lattice and all-atom models?

The best model to use is the all-atom model, but we also studied the lattice model for two reasons: First, due to its simplicity, we can perform simulation with a larger number of chains compared to the all-atom model. Second, in order to capture an experiment without recycling,[25] we must remove the monomer that has just dissociated from the mother aggregate before continuing with the simulation. This can be easily implemented in simple lattice models, but it is not so in an all-atom model, where the removal of one chain requires to re-solvate a simulation box with a reduced number of water molecules. In principle, to avoid this problem, we can use implicit all-atom or off-lattice coarse-grained models, but we

The Journal of Chemical Physics ARTICLE scitation.org/journal/jcp

have chosen lattice models because they allow us to deal with a large number of polypeptide chains.

### Experimental technique for monomer capture and simulation protocol

In order to prevent the released Aβ monomer itself from reuniting with the parent aggregate, experimentally it was removed from the system. For this, the free monomer was marked by the tryptophan fluorescence.[25] Since the Aβ peptide does not contain tryptophan, the ZAβ3W protein, which was obtained from ZAβ3 making a single point Y18W mutation, was used as a tryptophan fluorescence probe for monomer Aβ because it binds to the Aβ monomer but not to the fibril. In detail, when ZAβ3W is bound to the Aβ peptide, the fluorescence intensity increased and led to a blue-shifted emission maximum λmax. Using a special simulation technique, Gruning *et al.* found a correlation between λmax and the fraction of free ZAβ3W, after which they inferred the Aβ fraction, which still remains in fibrils.[25]

In the simulation, we followed exactly the same protocol as in the experiment of Gruning *et al.*[25] that the dissociated peptide was removed from the simulation box. This can be easily implemented in simple lattice models, but it is not so in an all-atom model, where the removal of one chain requires to re-solvate a simulation box with a reduced number of water molecules. Thus, in this work, we only used a lattice model to capture the process without recycling.

### Quantities used for data analysis

#### *Fraction of fibril contacts Ω*

Because the simulation started from the fibril structure (Figs. 1, 4, and 5) at $t = 0$, the number of fibril contacts, $N_{\text{fibril}}(0)$, is the largest one. The fraction of fibril contacts, which measures the $\beta$-structure, is defined as $\Omega(t) = N_{\text{fibril}}(t)/N_{\text{fibril}}(0)$. Experimentally, this quantity can be obtained by the ThT fluorescence technique.

#### *Fraction of bound monomers Θ*

Monomers that have no contact with the rest are called free monomers. The number of bound (non-free) monomers that belong to oligomers or fibrils is the difference between the total number of monomers and the number of free monomers. The concentration of non-free monomers is defined as $\Theta(t) = N_{\text{non-free}}/N$. In experiments, this quantity can be measured by the tryptophan fluorescence.[25] In the capture scenario (without recycling), a monomer detached from the aggregate is removed from the simulation box.

#### *Free energy*

To show the existence of intermediate states, we calculated the free energy as a function of fibril contacts. It is defined as follows:

$$G(N_{\text{fibril}}) = -k_B T \ln(P(N_{\text{fibril}})), \tag{2}$$

where $P(N_{\text{fibril}})$ is the population of states with $N_{\text{fibril}}$ fibril contacts. In simulation, $P(N_{\text{fibril}}) = n(N_{\text{fibril}})/n_{\text{total}}$, where $n(N_{\text{fibril}})$ is the number of times the state with $N_{\text{fibril}}$ fibril contacts occurs and $n_{\text{total}}$ is the total number of sampled conformations.

The calculation of the equilibrium free energies is very time consuming since the degradation and formation of fibrils are irreversible processes. For systems with a finite number of chains, these processes are reversible but building equilibrium free energy landscapes remains computationally difficult. Therefore, we will construct nonequilibrium free energy landscapes, using Eq. (2) and all sampled snapshots including those taken before equilibration.

## RESULTS

### Theory

#### *Dissociation of monomers from fibril without recycling*

*Logistic behavior.* In the first approximation, the decay of the number of bound chains depends linearly on the number of chains, i.e., $d\Theta/dt \sim \Theta$ or $d\Theta/dt = -a\Theta$, where parameter $a > 0$ for decomposition. This equation leads to exponentially fast decay $\Theta \sim \exp(-at)$. However, as can be seen from the simulation results below (Figs. 3, 5, and 7), $\Theta(t)$ decreases much more slowly than exponential behavior at short time scales. To overcome this difficulty, we add a term that is proportional to $\Theta^2$, leading to the following kinetics equation:

$$\frac{d\Theta}{dt} = -a\Theta + b\Theta^2, \tag{3}$$

where fitting parameter $b > 0$. Equation (3) is similar to the equation for population growth, but the sign of the right side is opposite (https://en.wikipedia.org/wiki/Logistic_function).

In our phenomenological theory, temperature is implicitly expressed through adjustable parameters. For example, we do not

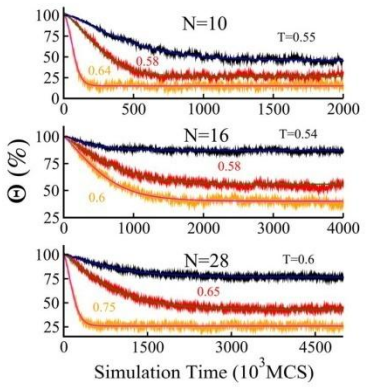


**FIG. 3.** Time dependence of percentage of bound monomers, $\Theta(t)$, with recycling. Color curves represent the logistic fitting [Eq. (7)] for each data set at different temperatures and $N$. For $N = 10$, the sets of fitting parameters ($\Theta_0$, $\Theta_{eq}$, $\tilde{b}$, $\tau$) are (57.21, 45.83, $3.64 \times 10^{-5}$, 294.1), (74.25, 26.75, $9.26 \times 10^{-5}$, 121.95), and (87.61, 15.17, $3.4 \times 10^{-4}$, 29.6) for $T = 0.55$, 0.58, and 0.64, respectively. For $N = 16$, they are (14.76, 87.39, $8.26 \times 10^{-5}$, 502.5), (44.0, 55.82, $3.11 \times 10^{-5}$, 438.6), and (61.109, 40.18, $2.391 \times 10^{-5}$, 378.78) for $T = 0.54$, 0.58, and 0.60, respectively. In the $N = 28$ case, we have (24.21, 76.44, $2.301 \times 10^{-5}$, 791.4), (58.74, 43.20, $1.088 \times 10^{-5}$, 645.2), and (76.13, 25.89, $1.14 \times 10^{-4}$, 89.3) for $T = 0.60$, 0.65, and 0.75, respectively. The characteristic time $\tau$ is measured in $10^3$ MCS and highlighted in blue.

The Journal of Chemical Physics ARTICLE scitation.org/journal/jcp

know exactly the temperature dependence of the parameters $a$ and $b$ in Eq. (3), but we expect $a$ to increase with temperature because degradation accelerates with an increase in temperature. The parameter $b$ may decrease or increase with $T$ depending on the situation (see below). In general, these parameters should be chosen in such a way that the right side of Eq. (3) is negative in order to guarantee a decrease in $\Theta$ with time. Thus, at $t = 0$, we have $b\Theta^2 - a\Theta < 0$ or $b\Theta_0/a < 1$. The larger the system, the more stable the system; hence, the parameters $a$ and $b$ should depend on the system size. This will be confirmed by our simulation.

Equation (3) has the exact solution

$$\Theta(t) = \frac{\Theta_0}{\tau b\Theta_0 + (1 - \tau b\Theta_0)e^{t/\tau}}, \tag{4}$$

implying that, in general, the fraction of bound chains follows logistic kinetics without recycling. Here, the parameter $\tau$ ($\tau = 1/a$) plays the role of "relaxation" time. Since degradation becomes faster with an increase in temperature, $\tau$ should decrease with an increase in $T$.

*Single exponential kinetics.* At large enough time scales, the second term in the denominator in Eq. (4) dominates over the first term and we have

$$\Theta(t) \sim \exp(-t/\tau). \tag{5}$$

We will show that this single exponential kinetics can describe the experiment of fibril degradation without recycling.[25] Namely, using a special technique that does not allow the separated monomers to reunite with the mother oligomer, it was shown that the dissociation of monomer[25] obeys a single exponential kinetics if the fraction of bound proteins becomes less than the crossover value $\Theta_{cr} \sim 90\%$.

### Dissociation of monomers from fibril with recycling

When released monomers are not captured, one has to add to Eq. (3) an additional term that describes the recycling. Because the probability of recycling depends not only on the size of the parent cluster but also on the number of free monomers, this term should be proportional to $\Theta(\Theta_0 - \Theta)$. Then, Eq. (3) becomes

$$\frac{d\Theta}{dt} = -a\Theta + b\Theta^2 + c\Theta(\Theta_0 - \Theta). \tag{6}$$

Because the recycling disfavors degradation, the coefficient $c > 0$. Introducing $\tilde{a} = a - c\Theta_0$ and $\tilde{b} = b - c$, the last equation becomes identical to Eq. (3) but with the renormalized parameters $\tilde{a}$ and $\tilde{b}$ and $\Theta_0 \to \Theta_0 - \Theta_{eq}$. In other words, for the case of recycling, the dissociation of monomers from the aggregate is governed by the following logistic equation:

$$\Theta(t) = \frac{\Theta_0 - \Theta_{eq}}{\tilde{b}(\Theta_0 - \Theta_{eq})\tau + [1 - \tilde{b}(\Theta_0 - \Theta_{eq})\tau]e^{t/\tau}} + \Theta_{eq}, \tag{7}$$

where $\tau = 1/\tilde{a}$. Contrast to the case without recycling, in the $t \to \infty$ limit, the portion of bound chains approaches a nonzero equilibrium value $\Theta_{eq}$. Equation (7) satisfies this condition and the requirement that $\Theta = \Theta_0$ at $t = 0$. Note that the parameter $\Theta_{eq}$ should depend on $a$, $b$, and $c$, but we do not have an analytical dependence. It can be obtained in simulation from the time dependence of $\Theta(t)$ in the limit $t \to \infty$.

### Simulation results and comparison with experiment

#### *Dissociation with recycling*

*Time dependence of the number of bound chains: Lattice models.* Figure 3 shows the time dependence of the fraction of bound chains for $N = 10$, 16, and 28 at different temperatures. Recall that the temperature in the lattice model is implied in the Metropolis algorithm and is dimensionless as $k_BT$ is measured in the characteristic energy $\varepsilon_{HB}$.[34] Simulations were carried out at $T > 0.39$, i.e., above room temperature.

In agreement with our theory, the logistic dependence [Eq. (7)] works well for all cases. As the temperature is lowered, the portion of bound monomers at large time scales becomes larger or $\Theta_{eq}$ increases. For $N = 28$, $\Theta_{eq} = 76.44\%$, 43.20%, and 25.89% for $T = 0.60$, 0.65, and 0.75, respectively. The value of $\Theta_{eq}$ for $N = 10$ and 16 at different temperatures is given in the caption of Fig. 3.

*Time dependence of the fibril contacts: Lattice models.* The fraction of fibril contacts, $\Omega(t)$, can be experimentally measured by the ThT fluorescence array, and it was shown that[24] its time dependence is described by a bi-exponential function,

$$\Omega(t) = \Omega_0 + \Omega_1 \exp(-t/\tau_1) + \Omega_2 \exp(-t/\tau_2). \tag{8}$$

The existence of two time scales $\tau_1$ and $\tau_2$ means that the fibril degradation occurs through an intermediate state. $\tau_1$ and $\tau_2$ describe the decay at short and large time scales, respectively. To demonstrate the existence of an intermediate state, we plot the free energy as a function of the fraction of fibril contacts for $N = 28$ and $T = 0.60$ (Fig. 4) (similar results for other systems and temperatures are not shown). For individual trajectories, we have two local maxima implying that the intermediate state occurs upon fibril dissociation. It is important to note that two local minima disappear if we average over many MC trajectories (bottom panel in Fig. 4) due to the fact that local minima/maxima of separate paths are located at different positions.

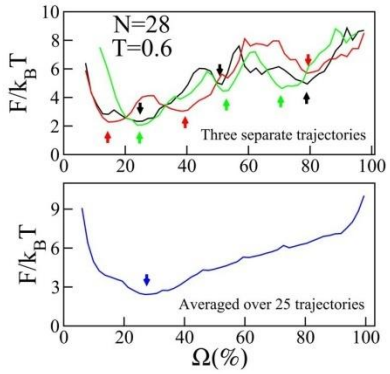


**FIG. 4.** Top panel: free energy as a function of the fraction of fibril contacts, obtained in three MC trajectories, for $N = 28$, $T = 0.60$. Bottom panel: the same as on the top panel, but the results were averaged over 25 trajectories. Arrows show the position of local minima.

The Journal of Chemical Physics ARTICLE scitation.org/journal/jcp

Therefore, care must be taken when interpreting simulation data on a free energy landscape.

As can be seen from Fig. 5, in accordance with the experiment,[24] the fraction of fibril contacts is perfectly fitted to the bi-exponential function. For a given number of chains, characteristic times $\tau_1$ and $\tau_2$ decrease with an increase in temperature (caption of Fig. 5) since with shorter characteristic times, the degradation occurs faster. Depending on the system size and temperature, $\tau_2$ is 1–2 orders of magnitude greater than $\tau_1$. This result is consistent with the experiment on degradation of β2-microglobulin amyloid fibrils,[24] which showed that the off-rate constant of the second term is much greater than the first one.

Figure 6 shows the temperature dependence of the degradation rates $\kappa_{off1} = 1/\tau_1$ and $\kappa_{off12} = 1/\tau_2$. These results suggest that both rates obey the Arrhenius formula as they depend linearly on $1/T$. Using the experimental data (Fig. 3 from the work of Kardos *et al.*[24]), we can show that the degradation kinetics of $\beta 2m$ amyloid fibrils is bi-exponential (Fig. S2). Using the fitting parameters from Fig. S2, we can extract $\kappa_{off1}$ and $\kappa_{off12}$ and show that they also obey the Arrhenius law (Fig. S3). Thus, our simulation results are consistent with the experiment.[24]

*Time dependence of the number of bound chains: All-atom model.* Because the lattice model can produce artificial results due to its discrete nature, we carried out the MD simulation with the use of all-atom models with explicit water. The simulation started from the fibril-like structure of 10 truncated peptides $A\beta_{37-42}$ at $T$ = 350 K, 375 K, and 400 K (Fig. 7). For each temperature, 10 trajectories were performed with different initial velocity fields, and the

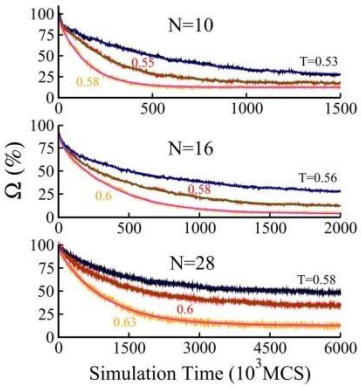


**FIG. 5**. Thermal degradation kinetics of three fibril structures with10, 16, and 28 polypeptide chains at different temperatures. The results were obtained using the lattice model. Smooth curves refer to the bi-exponential fit given by Eq. (8). For $N$ = 10, the set ($\Omega_0$, $\Omega_1$, $\Omega_2$, $\tau_1$, $\tau_2$) is (24.81, 17.65, 64.61, 8.55, 526.32), (17.29, 14.18, 76.8, 4.35,277.78), and (12.45, 13.55, 81.41, 3.73, 147.06) for $T$ = 0.53, 0.55, and 0.58, respectively. For $N$ = 16, we have (24.6, 17.79, 49.67, 55.56, 769.23), (10.24, 16.09, 67.79, 47.62, 588.24), and (3.68, 11.84, 77.47, 17.54, 384.61) for $T$ = 0.56, 0.58, and 0.60, respectively. In the $N$ = 28 case, the fitting sets are (40.95, 33.92, 23.04, 961.54, 4761.90), (30.1, 32.16, 34.85, 751.88, 2564.10), and (12.7, 5.35, 82.08, 32.26, 1000.0) for $T$ = 0.58, 0.60, and 0.63, respectively. Here, $\Omega_0$, $\Omega_1$, and $\Omega_2$ are in % and $\tau_1$ and $\tau_2$ are measured in $10^3$ MCS.

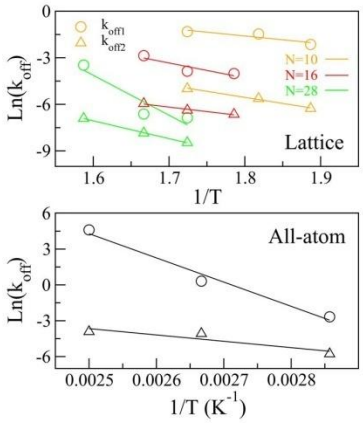


**FIG. 6**. Temperature dependence of the degradation rate $\kappa_{off1}$ and $\kappa_{off2}$, obtained by using the lattice (upper panel) and all-atom simulation (lower panel). $K_{off}$ is measured in $(10^3 \text{ MCS})^{-1}$.

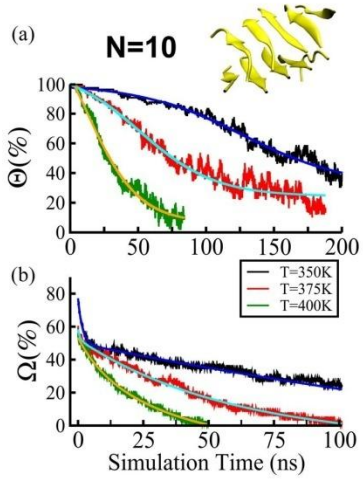


**FIG. 7**. Upper panel: fibril-like structure of 10 truncated peptides $A\beta_{37-42}$. This structure has 113 fibril contacts. (a) Dependence of the percentage of bound monomers $\Theta(t)$ on the simulation time without the capture of released monomers. The results were obtained using the all-atom model. The logistic fitting [Eq. (7)] was conducted for each data set at different temperatures. The sets of fitting parameters ($\Theta_0$, $\Theta_{eq}$, $\tilde{b}$, $\tau$) are (72.43, 26.25, 2.9 × $10^{-4}$, 45.45), (84.87, 18.94, 1.9 × $10^{-4}$, 43.48), and (99.02, 6.34, 3.2 × $10^{-4}$, 19.61) for $T$ = 350 K, 375 K, and 400 K, respectively. The results were averaged over 10 MD trajectories. (b) Time dependence of the fraction of fibril contacts of $N$ = 10 chains, $\Omega(t)$, in the all-atom simulation. Bi-exponential fits are $y = 27.58e^{-t/1.64} + 102.1e^{-t/322.6} - 52.14$ ($T$ = 350 K), $y = 6.13e^{-t/0.73} + 62.35e^{-t/58.8} - 9.95$ ($T$ = 375 K), and $y = 11.31e^{-t/0.01} + 53.93e^{-t/50} - 11.85$ ($T$ = 400 K). Time $t$ is measured in ns.

J. Chem. Phys. **152**, 115101 (2020); doi: 10.1063/1.5144305

The Journal of Chemical Physics ARTICLE scitation.org/journal/jcp

results were averaged over all trajectories. As in the lattice model, the fraction of bound chains $\Theta(t)$ obeys the logistic behavior [Eq. (7)]. We can show that the set of fitting parameters $(\tilde{b}, \tau)$ is equal to $(2.9 \times 10^{-4}, 45.5)$, $(1.9 \times 10^{-4}, 43.5)$, and $(3.3 \times 10^{-4}, 19.6)$ for $T$ = 350 K, 375 K, and 400 K, respectively (caption of Fig. 7). The characteristic time $\tau$, which is measured in ns, is of order of 10 ns and decreases with an increase in $T$ as the temperature increase speeds up the degradation.

From a visual inspection, it seems that multiple exponential fits are also suitable for the time dependence of the number of bound chains. To clarify this issue, we performed exponential fits with different time scales, as shown in Fig. S4. The bi- and tri-exponential fits do not work at $T$ = 350 K because the initial slow decay cannot be captured. This remains valid for a higher-order fit (results not shown). At $T$ = 375, the tri-exponential works better than in the $T$ = 350 K case, but again the initial decrease in $\Theta$ cannot be described. At $T$ = 400 K, both logistic and single exponential fits work well. So, at sufficiently high temperatures, when the degradation is fast, a fit with multiple time scales should work.

*Time dependence of the fibril contacts: All-atom model.* Figure 7 shows that the portion of fibril contacts $\Omega(t)$ of 10 short peptides $A\beta_{37-42}$ is well described by the bi-exponential function, given by Eq. (8). The set of fitting parameters $(\Omega_0, \Omega_1, \Omega_2, \tau_1, \tau_2)$ are (−52.14, 27.58, 102.1, 1.64, 322.6), (−9.95, 6.13, 62.35, 0.73, 58.8), and (−11.85, 11.31, 53.93, 0.01, 50) for $T$ = 350 K, 375 K, and 400 K, respectively (caption of Fig. 7). The characteristic time $\tau_1$ decreases from 1.64 ns to 0.01 ns and $\tau_2$ decreases from 322.6 ns to 50 ns as the temperature increases from 350 K to 400 K, implying that the degradation is very sensitive to temperature. It can be expected that at sufficiently high temperatures, the time dependence of the fibril contacts can be described by a single exponential because the initial stage becomes so short that $\tau_1 \to 0$.

*Fibril contacts decay faster than the number of bound chains: All-atom simulation of $5A\beta_{17-42}$.* From the lattice simulation, it can be seen that with an increase in temperature, $\Omega(t)$ decreases faster than $\Theta(t)$ (Figs. 3 and 5). For $N$ = 10 and at $T$ = 0.55 and $t = 5 * 10^5$ MCS, $\Theta(t) \approx 67\%$, which is higher than $\Omega(t) \approx 29\%$. For $N$ = 16 and $T$ = 0.60, after $t = 1.5 * 10^6$ MCS, we have $\Theta(t) \approx 49\%$, but $\Omega(t)$ drops to 8.5%. This is also true for the all-atom model with $10A\beta_{37-42}$ (Fig. 7), where at $t$ = 25 ns, $\Theta(t) \approx 96.7$, 87.5%, and 52.2%, whereas $\Omega(t) \approx 42.5\%$, 32.1%, and 15.7% for $T$ = 350 K, 375 K, and 400 K, respectively.

However, the simplicity of the lattice model and the shortness of the chains studied in the all-atom model can affect our main conclusion, prompting us to study the degradation of the fibril structure of longer sequences using the all-atom model. We performed the MD simulation starting from the fibril-like structure of five $A\beta_{17-42}$ chains (PDB ID: 2BEG[39]) and using the AMBER force filed 99SB. The 2BEG structure has 184 fibril contacts. Figure 8 shows the time dependence of the fraction of fibril contacts at 300 K. This fraction (or the $\beta$-content) rapidly decreases according to the exponential law. Although both fits work well for simulation data as indicated by the high correlation levels ($R$ = 0.97 and 0.99 for the single and bi-exponential fits, respectively), only the bi-exponential fit captures the initial stage of the decay process. In the bi-exponential fit, the off-rate constant of the first term is about 22 times greater than the

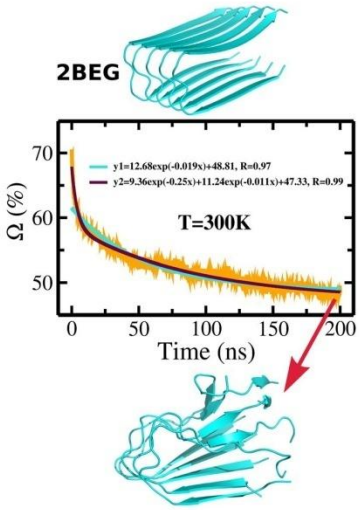


**FIG. 8.** Time dependence of fibril contacts of 2BEG at $T$ = 300 K. The results were averaged over MD 20 trajectories of 200 ns. Shown is the fibril structure 2BEG from PDB (upper panel) and one of the last snapshots in the simulation (lower panel).

second one. This result is in qualitative agreement with the exponential behavior observed in experiments on the dissociation of the $\beta$ 2m amyloid fibril in the elevated temperature region[24] as well as at the ambient temperature.[25]

At $t$ = 200 ns, the fraction of fibril contacts $\Omega(t)$ falls below 50% but $\Theta(t)$ remains equal to 100% as none of the chains was dissociated from the fibril (Fig. 8). This clearly demonstrates that the reduction of $\Omega(t)$ is much faster than $\Theta(t)$ and this behavior cannot be fitted to the logistic function [Eq. (7)]. This is the major difference between two quantities.

### Dissociation without recycling

*Time dependence of the number of bound chains: Lattice models.* To study the degradation without recycling, MC simulation was started with fibril conformations shown in Fig. 2 for $N$ = 10, 16, and 28, but, as in the experiment by Gruning *et al.*,[25] we removed any released chain from the box, not allowing it to rejoin the mother aggregate. To get good statistics, hundreds of MC trajectories were generated using different random seed numbers. The results were averaged over all trajectories.

Figure 9 shows the time dependence of the fraction of bound chains in lattice models with $N$ = 10, 16, and 28 in the capture scenario. For all cases and three temperatures, the curves are perfectly fitted to Eq. (3), implying that the thermal degradation obeys the logistic behavior. Because $\tau$ controls the degradation rate, it decreases as the temperature increases (caption of Fig. 9). For example, in the $N$ = 16 case, we have $\tau = 892.9 \times 10^3$, $396.8 \times 10^3$,

The Journal of Chemical Physics ARTICLE scitation.org/journal/jcp

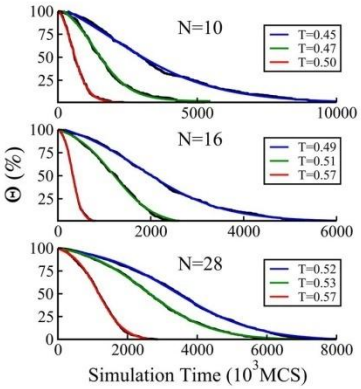


**FIG. 9**. Dependence of the fraction of bound monomers $\Theta$ on the simulation time in the capture scenario for $N$ = 10, 16, and 28 and three temperatures. Black curves refer to the raw data. The color curves refer to the logistics fit [Eq. (3)]. For $N$ = 10, sets of fitting parameters ($\Theta_0$, $b$, $\tau$) are (105.0, 3.83 × $10^{-6}$, 1852.8), (101.7, 1.383 × $10^{-5}$, 632.9), and (101.9, 3.006 × $10^{-5}$, 285.7) for $T$ = 0.45, 0.47, and 0.50, respectively. In the $N$ = 16 case, we obtained (101.98, 9.69 × $10^{-6}$, 892.9), (98.18, 2.45 × $10^{-5}$, 396.8), and (100.78, 9.508 × $10^{-5}$,101.0) for $T$ = 0.49, 0.51, and 0.57, respectively. For $N$ = 28, we have (98.48, 0.924 × $10^{-6}$, 1098.9), (99.69, 1.051 × $10^{-5}$, 909.1), and (98.19, 2.45 × $10^{-5}$, 400.0) for $T$ = 0.52, 0.53, and 0.57, respectively. The characteristic time $\tau$ is measured in $10^3$ MCS and highlighted in blue.

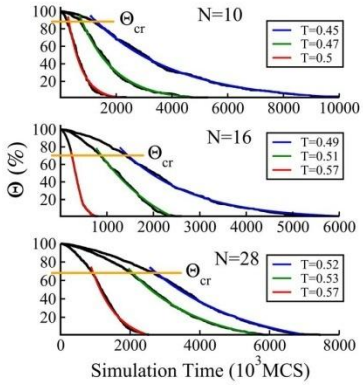


**FIG. 10**. Data are the same as in Fig. 6, but we show the single exponential fit after $\Theta(t)$ reached the crossover value $\Theta_{cr}$, noted by the orange straight line. Here, $\Theta_{cr}$ = 87%, 70%, and 67% for $N$ = 10, 16, and 28, respectively. The blue, dark green, and red curves represent an exponential fit by equation $\Theta = \Theta_0 * \exp(-x/\tau) + \Theta_1$. For $N$ = 10, the parameter set ($\Theta_0$, $\tau$, $\Theta_1$) is (140.54, 2857, −3.01), (170.89, 1220, −2.11), and (166.44, 500, −0.79) for $T$ = 0.45, 0.47, and 0.5, respectively. For $N$ = 16, we have (194.13, 1538, −2.13), (196.58, 1471, −39.67), and (260.85, 208, −6.8) for $T$ = 0.49, 0.51, and 0.57, respectively. For $N$ = 28, we have (230.74, 2778, −17.8), (222.89, 2041, −12.41), and (280.22, 714, −7.66) for $T$ = 0.52, 0.53, and 0.57, respectively. The characteristic time $\tau$ is measured in $10^3$ MCS and highlighted in blue.

and 101 × $10^3$ MCS for $T$ = 0.49, 0.51, and 0.57, respectively. A similar result was obtained for $N$ = 10 and 28.

We can show that in the case when the capture of released chains is allowed, the time dependence of the fibril contacts can be represented using a bi-exponential function [Eq. (8)].

*Crossover from logistic to single-exponential kinetics.* Initially, when the rigidity of the fibril is still high, $\Theta(t)$ slowly decreases (Fig. 10), but after reaching the crossover value $\Theta_{cr}$, the degradation becomes fast and the kinetics can be described by the single exponential function (Fig. 10). $\Theta_{cr}$ depends on the number of chains and temperature, but as a rule, the smaller the $N$ and the higher the $T$, the larger the $\Theta_{cr}$. This is because as the number of chains is increased or the temperature is lowered, it becomes increasingly difficult to fit the data into single exponential function. For all temperatures studied, we obtained $\Theta_{cr}$ = 87%, 70%, and 67% for $N$ = 10, 16, and 28, respectively (Fig. 10). Restricting to data with $\Theta \le \Theta_{cr}$, we get a good single exponential fit for all cases studied. This result agrees with the experiment,[25] which shows that single exponential kinetics works for $\Theta_{cr}$ < 90%. As expected, for a given $N$, the relaxation time $\tau$ [Eq. (4)] decreases with the temperature. For example, in the $N$ = 28 case, $\tau$ = 2778 × $10^3$, 2041 × $10^3$, and 714 × $10^3$ MCS for $T$ = 0.52, 0.53, and 0.57, respectively (Fig. 10).

### *Temperature and size dependence of the parameters of the phenomenological theory*

The fitting parameters $a$, $b$, $\tilde{a}$, $\tilde{b}$, and $\Theta_0$ (parameter $c$ is just intermediate and not involved in the final formula of the theory) in our phenomenological theory [Eqs. (4) and (7)] can be obtained using microscopic theory. However, this issue is beyond the scope of the present paper. Here, we extract their temperature dependence from the lattice and all-atom simulation (Fig. S5). In all cases, $a$ and $\tilde{a}$ increase with $T$ because they are the main factors that control the intensification of dissociation with an increase in temperature. The behavior of $b$ and $\tilde{b}$ is more complicated as they can increase as well as decrease with $T$ (Fig. S5). In the all-atom models with recycling and the lattice models without recycling, the parameter $\Theta_0$ grows with temperature, but in the lattice model with recycling, its temperature dependence is not monotonic.

Since the fibril stability depends on the system size, the fitting parameters should depend on the number of chains (Fig. S5). In the lattice model, for a given temperature, $a$ and $\tilde{a}$ decrease with an increase in $N$. As expected, the dependence of $b$ and $\tilde{b}$ on the system size is not monotonic.

### *Exponential vs logistic kinetics from the free energy perspective*

We have shown that the decay of the number of fibril contacts can be described by a bi-exponential function, while the slower time dependence of the number of dissociated chains is subordinate to the logistic function. Since the kinetic properties are determined by thermodynamics, it is worth understanding the difference between the two kinetics in terms of free energy landscapes.

The bi-exponential kinetics is associated with the existence of one intermediate in the free energy profile plotted as a function of the fraction of fibril contacts (Fig. 4). Because the logistic kinetics is

The Journal of Chemical Physics ARTICLE scitation.org/journal/jcp

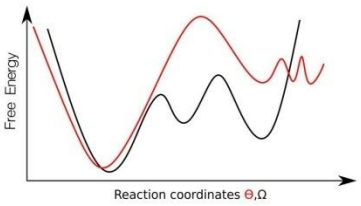


**FIG. 11**. Schematic plots for free energy landscapes plotted as a function of the fraction of fibril contacts $\Omega$ (black) and the fraction of bound chains $\Theta$ (red). Bi-exponential kinetics of $\Omega$ is associated with two maxima (black curve), while logistic behavior of $\Theta$ is due to a pronounced maximum and a rough free energy profile at the initial stage (red curve).

related to the time dependence of the number of bound chains, we plot the free energy as a function the fraction of bound chains $\Theta$ for the lattice model with $N = 28$ at $T = 0.75$ (Fig. S6). For a sufficiently large $\Theta$ (initial stage), the presence of shallow local minima can be considered as a roughness of free energy that led to a slow decay in the logistic behavior. On a large time scale, the logistic kinetics becomes exponential due to the existence of a global maximum of free energy (Fig. S6).

The free energy profiles that are responsible for the difference between two kinetics are depicted in Fig. 11. For bi-exponential kinetics, the corresponding free energy, plotted as a function of the fraction of fibril contacts $\Omega$, has two pronounced maxima separating ordered and disordered states. In the case of logistic behavior, there is only one barrier that controls fast kinetics at sufficiently large time scales, while the initial slow decay of the fraction of coupled chains is related to the roughness of free energy.

## CONCLUSION

We have developed a theory to describe the temperature-induced degradation of protein aggregates. Our theory is phenomenological since the temperature dependence is accounted in accordance with the fitting constants rather than from physical insights. It is shown that the decrease in the number of bound chains, which can be measured by using the tryptophan fluorescence technique, is represented by a logistic function. This contrasts sharply with the bi-exponential kinetics of fibril contacts or beta content, which can be experimentally monitored using the ThT fluorescence array. Logistic kinetics occurs in both cases with and without recycling of released chains. The main difference between the logistic and bi-exponential behavior is that in the first case, the decrease in the corresponding quantity is slower than in the second case. The number of connected chains decreases with time more slowly than the fibril content because to separate a chain from an aggregate, one needs to break more inter-chain contacts than to spoil beta-sheets.

We explored the difference between bi-exponential and logistic kinetics in terms of free energy. It was shown that the bi-exponential behavior is associated with the existence of two maxima in the free energy profile, plotted as a function of the fraction of fibril contacts. If the proportion of bound chains $\Theta$ is used as the reaction coordinate, then the free energy has one global maximum and shallow traps at large values of $\Theta$. Such free energy led to logistic behavior.

Our lattice and all-atom simulations support the bi-exponential kinetics observed in the experiment of Kardos *et al.*, who measured the ThT fluorescence signal characterizing the content of fibrils.[24] Studying the free energy profile, we showed that this behavior is due to the existence of intermediate states. Using the tryptophan fluorescence technique to monitor the fraction of released proteins, it was found[25] that the degradation kinetics is described by a single exponential function if recycling is not allowed. We show that a single exponential behavior occurs if we ignore the slow dynamics when the concentration of bound chains exceeds the crossover value $\Theta_{cr}$. For the entire time interval, logistic kinetics should take place regardless of whether we capture the released polypeptide chains or not. It would be interesting to check our prediction of logistic behavior experimentally.

## SUPPLEMENTARY MATERIAL

See the supplementary material for Fig. S1—temperature dependence of the fraction of fibril contacts $\langle Q(T)\rangle$of the lattice monomer; Fig. S2—experimental data, obtained by Goto's group, for thermal dissociation of β2m amyloid fibrils at different temperatures; Fig. S3—temperature dependence of two experimental degradation rates $k_{off1}$ and $k_{off2}$, extracted from the bi-exponential fits shown in Fig. S2; Fig. S4—dependence of percentage of bound monomers $\Theta(t)$ on the simulation time without the capture of released monomers and multiple exponential fits; Fig. S5—temperature dependence of parameters of the phenomenological theory; and Fig. S6—free energy of the lattice model with $N = 28$ chains plotted as a function the fraction of bound chains $\Theta$ for three trajectories at $T = 0.75$.

## AUTHOR'S CONTRIBUTIONS

N.T.C. and P.D.L. contributed equally to this work.

## ACKNOWLEDGMENT

This work was supported by the Narodowe Centrum Nauki in Poland (Grant No. 2015/19/B/ST4/02721) and the Department of Science and Technology of Ho Chi Minh City, Vietnam. The allocation of CPU time at the supercomputer center TASK in Gdansk and PLGrid infrastructure (Poland) is highly appreciated.

## REFERENCES

[1] J. Hardy and D. J. Selkoe, Science **297**(5580), 353–356 (2002).
[2] J. Kang, H. G. Lemaire, A. Unterbeck, J. M. Salbaum, C. L. Masters, K.-H. Grzeschik, G. Multhaup, K. Beyreuther, and B. J. Muller-Hill, Nature **325**, 733–736 (1987).
[3] C. Haass and D. J. Selkoe, Nat. Rev. Mol. Cell Biol. **8**, 101–112 (2007).
[4] J. Nasica-Labouze, P. H. Nguyen, F. Sterpone, O. Berthoumieu, N. V. Buchete, S. Cote, A. De Simone, A. J. Doig, P. Faller, A. Garcia, A. Laio, M. S. Li, S. Melchionna, N. Mousseau, Y. G. Mu, A. Paravastu, S. Pasquali, D. J. Rosenman, B. Strodel, B. Tarus, J. H. Viles, T. Zhang, C. Y. Wang, and P. Derreumaux, Chem. Rev. **115**(9), 3518–3563 (2015).
[5] J. Brange, L. Andersen, E. D. Laursen, G. Meyn, and E. Rasmussen, J. Pharm. Sci. **86**(5), 517–525 (1997).
[6] D. Hamada and C. M. Dobson, Protein Sci. **11**, 2417–2426 (2002).

[7]N. Hirota-Nakaoka, H. Kazuhiro, N. Hironobu, and G. Yuji, J. Biochem. **134**(1), 159–164 (2003).
[8]J. Murali and R. Jayakumar, J. Struct. Biol. **150**(2), 180–189 (2005).
[9]T. Narimoto, K. Sakurai, A. Okamoto, E. Chatani, M. Hoshino, K. Hasegawa, H. Naiki, and Y. Goto, FEBS Lett. **576**(3), 313–319 (2004).
[10]H. Wille and S. B. Prusiner, Biophys. J. **76**, 1048–1062 (1999).
[11]W. Dzwolak, Biochim. Biophys. Acta **1764**(3), 470–480 (2006).
[12]D. Foguel and J. L. Silva, Biochemistry **43**(36), 11361–11370 (2004).
[13]F. Meersman and C. M. Dobson, Biochim. Biophys. Acta **1764**(3), 452–460 (2006).
[14]J. Torrent, C. Balny, and R. Lange, Protein Pept. Lett. **13**, 271–277 (2006).
[15]T. Kawasaki, J. Fujioka, T. Imai, K. Torigoe, and K. Tsukiyama, Lasers Med. Sci. **29**(5), 1701–1707 (2014).
[16]M. H. Viet, P. Derreumaux, M. S. Li, C. Roland, C. Sagui, and P. H. Nguyen, J. Chem. Phys. **143**(15), 155101 (2015).
[17]A. Arora, C. Ha, and C. B. Park, Protein Sci. **13**(9), 2429–2436 (2004).
[18]U. Baxa, P. D. Ross, R. B. Wickner, and A. C. Steven, J. Mol. Biol. **339**, 259–264 (2004).
[19]L. Bousset, F. Briki, J. Doucet, and R. Melki, J. Struct. Biol. **141**, 132–142 (2003).
[20]J. Dubois, A. A. Ismail, S. L. Chan, and Z. Ali-Khan, Scand. J. Immunol. **49**, 376–380 (1999).
[21]S. V. Litvinovich, S. A. Brew, S. Aota, S. K. Akiyama, C. Haudenschild, and K. C. Ingham, J. Mol. Biol. **280**, 245–258 (1998).
[22]B. Morel, L. Varela, and F. Conejero-Lara, J. Phys. Chem. B **114**, 4010–4019 (2010).
[23]K. Sasahara, H. Naiki, and Y. Goto, J. Mol. Biol. **352**, 700–711 (2005).
[24]J. Kardos, A. Micsonai, H. Pal-Gabor, E. Petrik, L. Gráf, J. Kovács, Y.-H. Lee, H. Naiki, and Y. Goto, Biochemistry **50**(15), 3211–3220 (2011).
[25]C. S. R. Gruning, S. Klinker, M. Wolff, M. Schneider, K. Toksoz, A. N. Klein, L. Nagel-Steger, D. Willbold, and W. Hoyer, J. Biol. Chem. **288**, 37104–37111 (2013).
[26]W. Hoyer, C. Grönwall, A. Jonsson, S. Ståhl, and T. Härd, Proc. Natl. Acad. Sci. U. S. A. **105**, 5099–5104 (2008).
[27]L. M. Luheshi, W. Hoyer, T. P. de Barros, I. van Dijk Hard, A. C. Brorsson, B. Macao, C. Persson, D. C. Crowther, D. A. Lomas, S. Stahl, C. M. Dobson, and T. Hard, PLoS Biol. **8**(3), e1000334 (2010).
[28]D. K. Klimov and D. Thirumalai, Structure **11**(3), 295–307 (2003).
[29]P. H. Nguyen, M. S. Li, G. Stock, J. E. Straub, and D. Thirumalai, Proc. Natl. Acad. Sci. U. S. A. **104**(1), 111–116 (2007).
[30]P. D. Q. Huy, Q. V. Vuong, G. La Penna, P. Faller, and M. S. Li, ACS Chem. Neurosci. **7**(10), 1348–1363 (2016).
[31]S. Mitternacht, I. Staneva, T. Hard, and A. Irback, J. Mol. Biol. **410**(2), 357–367 (2011).
[32]L. Nagel-Steger, M. C. Owen, and B. Strodel, ChemBioChem **17**(8), 657–676 (2016).
[33]W. H. Zheng, M. Y. Tsai, M. C. Chen, and P. G. Wolynes, Proc. Natl. Acad. Sci. U. S. A. **113**(42), 11835–11840 (2016).
[34]M. S. Li, D. K. Klimov, J. E. Straub, and D. Thirumalai, J. Chem. Phys. **129**, 175101 (2008).
[35]M. S. Li, N. T. Co, G. Reddy, C.-K. Hu, J. E. Straub, and D. Thirumalai, Phys. Rev. Lett. **105**, 218101 (2010).
[36]N. T. Co and M. S. Li, J. Chem. Phys. **137**(9), 095101 (2012).
[37]N. T. Co, C. K. Hu, and M. S. Li, J. Chem. Phys. **138**(18), 185101 (2013).
[38]M. S. Li and M. Cieplak, Phys. Rev. E **59**(1), 970–976 (1999).
[39]T. Lührs, C. Ritter, M. Adrian, D. Riek-Loher, B. Bohrmann, H. Doeli, D. Schubert, and R. Riek, Proc. Natl. Acad. Sci. U. S. A. **102**, 17342–17347 (2005).
[40]A. T. Petkova, W.-M. Yau, and R. Tycko, Biochemistry **45**(2), 498–512 (2006).
[41]A. K. Paravastu, R. D. Leapman, W. M. Yau, and R. Tycko, Proc. Natl. Acad. Sci. U. S. A. **105**, 18349–18354 (2008).
[42]I. Bertini, L. Gonnelli, C. Luchinat, J. Mao, and A. Nesi, J. Am. Chem. Soc. **133**(40), 16013–16022 (2011).
[43]H. A. Scheidt, I. Morgado, S. Rothemund, and D. Huster, J. Biol. Chem. **287**, 2017–2021 (2012).
[44]J. X. Lu, W. Qiang, W. M. Yau, C. D. Schwieters, S. C. Meredith, and R. Tycko, Cell **154**, 1257–1268 (2013).
[45]M. A. Walti, F. Ravotti, H. Arai, C. G. Glabe, J. S. Wall, A. Bockmann, P. Guntert, B. H. Meier, and R. Riek, Proc. Natl. Acad. Sci. U. S. A. **113**(34), E4976–E4984 (2016).
[46]L. Gremer, D. Scholzel, C. Schenk, E. Reinartz, J. Labahn, R. B. G. Ravelli, M. Tusche, C. Lopez-Iglesias, W. Hoyer, H. Heise, D. Willbold, and G. F. Schroder, Science **358**(6359), 116 (2017).
[47]D. A. Pearlman, D. A. Case, J. W. Caldwell, W. S. Ross, T. E. Cheatham III, S. DeBolt, D. Ferguson, G. Seibel, and P. Kollman, Comput. Phys. Commun. **91**(1-3), 1–41 (1995).
[48]D. A. Case, T. E. Cheatham, T. Darden, H. Gohlke, R. Luo, K. M. Merz, A. Onufriev, C. Simmerling, B. Wang, and R. J. Woods, J. Comput. Chem. **26**(16), 1668–1688 (2005).
[49]V. Hornak, R. Abel, A. Okur, B. Strockbine, A. Roitberg, and C. Simmerling, Proteins: Struct., Funct., Bioinf. **65**(3), 712–725 (2006).
[50]W. L. Jorgensen, J. Chandrasekhar, J. D. Madura, R. W. Impey, and M. L. Klein, J. Chem. Phys. **79**(2), 926–935 (1983).
[51]W. F. van Gunsteren, S. R. Billeter, A. A. Eising, P. H. Hunenberger, P. Kruger, A. E. Mark, W. R. P. Scott, and I. G. Tironi, *Biomolecular Simulation: The GROMOS96 Manual and User Guide* (Vdf Hochschulverlag AG an der ETH Zurich, Zurich, 1996).
[52]T. T. Nguyen, M. H. Viet, and M. S. Li, Sci. World J. **2014**, 536084.
[53]R. W. Hockney, S. P. Goel, and J. Eastwood, J. Comput. Phys. **14**(2), 148–158 (1974).
[54]J.-P. Ryckaert, G. Ciccotti, and H. J. C. Berendsen, J. Comput. Phys. **23**(3), 327–341 (1977).
[55]X. W. Wu and B. R. Brooks, Chem. Phys. Lett. **381**(3-4), 512–518 (2003).
[56]T. Darden, D. York, and L. Pedersen, J. Chem. Phys. **98**(12), 10089–10092 (1993).

# Chapter 5: Conclusions and Future Work

## 5.1 Main conclusions

Having developed a phenomenological theory, simple lattice models and combined with available all-atom models we obtained the following main results:

1. We have successfully extended the lattice model developed previously by Li. et al. to study the aggregation of polypeptide chains in the presence of various types of foreign surfaces. The simplicity of lattice models allowed us to obtain the dependence of the aggregation rate of proteins on the roughness of hydrophobic and hydrophilic surfaces. Due to the competition between entropy and energy, a moderately absorbing smooth surface accelerates the aggregation process, while weakly and strongly absorbing surfaces slow it down. Our observations are in good agreement with the experiment of Vacha et.al.[132]. If the roughness is sufficiently high protein self-assembly is completely inhibited, which is in good agreement with the experimental work of Shezada et al.[9]. For moderately absorbing surfaces, we predicted that a slightly rough surface could catalyze aggregation but not prevent it. It would be interesting to test this effect experimentally.
2. Using REMD with the all-atom model and implicit water we calculated the beta content of the Aβ42 monomer and its 19 mutants. Comparing with their experimental aggregation rate, for the first time, we disclosed the exponential dependence of aggregation rate on beta-content of monomer. Thus the beta content of monomer is one of the important factors that govern the protein aggregation kinetics. This factor provides an indirect way to estimate the fibril formation time using only the beta-content of monomer, which can be easily calculated from all-atom simulations. This result is valuable because estimating the fibril formation time of proteins using all-atom models is impractical with current computing power.
3. We have developed a phenomenological analytical theory that well describes the logistic mechanism of monomer dissociation from fibrils in both cases, with and without the possibility of reunification of the released monomers with the parent cluster. We have shown that, during thermal degradation, the number of associated chains, which can be measured by tryptophan fluorescence, decays more slowly than the fibril content measured by ThT fluorescence. Above a certain threshold, the logistic function becomes single exponential, and this aggregate size behavior is consistent with experiment. We performed lattice and all-atom simulations that confirmed our analytical theory. It has been experimentally shown that the time dependence of the fibril content, which is proportional to the ThT fluorescence signal, is described by a bi-exponential function. To gain a deeper understanding of this behavior, we performed lattice simulations to study the free energy profile as a function of various reactions coordinates. We discovered that

the bi-exponential kinetics is associated with two pronounced maxima in the free energy profile plotted as a function of the fraction of fibril contacts, while the logistic mechanism occurs when the free energy profile, plotted as a function of the fraction of bound chains, contains one global maximum together with some shallow traps.

## 5.2 Future work

This dissertation was aimed at unraveling the various factors that govern the kinetics of protein aggregation using homemade lattice models and all-atom models, but my work was mainly focused on developing and conducting simulations with lattice models. Using the advantages of a simple lattice model, we plan to consider the problem of fibril polymorphism, i.e. study the conversion between different fibril morphologies and the relationship between morphology and fibril formation time. Recently it was demonstrated that Ostwald's rule, known from the occurrence of crystal polymorphs, is valid for the assembly of synthetic polymers [264]. This rule states that the less stable polymorph is formed before the more stable form. We will check whether this is also true for proteins with the help of lattice models. Another interesting problem concerns the secondary nucleation mechanism for fibril formation. We will use lattice models to investigate the effect of a preformed fibril template on the fibril formation rate.

We have developed lattice models to study the self-assembly of polypeptide chains on the surface. A possible continuation of this work is the implementation of the lattice model of the lipid bilayer and the study of its effect on protein aggregation. Finally, in this dissertation, we have proposed a picture of the kinetics of protein aggregation on rough surfaces based largely on general considerations such as competition between energy and entropy factors. Thus, a more detailed analysis of this process could be considered in the future.

# References


1. Chiti, F.; Dobson, C.M. Protein Misfolding, Amyloid Formation, and Human Disease: A Summary of Progress Over the Last Decade. *Annu. Rev. Biochem.* **2017**, *86*, 27-68, doi:10.1146/annurev-biochem-061516-045115.
2. Nasica-Labouze, J.; Nguyen, P.H.; Sterpone, F.; Berthoumieu, O.; Buchete, N.V.; Cote, S.; De Simone, A.; Doig, A.J.; Faller, P.; Garcia, A.; et al. Amyloid beta Protein and Alzheimer's Disease: When Computer Simulations Complement Experimental Studies. *Chem Rev* **2015**, *115*, 3518-3563, doi:10.1021/cr500638n.
3. Chiti, F.; Dobson, C.M. Protein misfolding, functional amyloid, and human disease. *Annu Rev Biochem* **2006**, *75*, 333-366, doi:10.1146/annurev.biochem.75.101304.123901.
4. Wang, W.; Nema, S.; Teagarden, D. Protein aggregation-Pathways and influencing factors. *Int. J. Pharm.* **2010**, *390*, 89-99, doi:https://doi.org/10.1016/j.ijpharm.2010.02.025.
5. Wang, W.; Roberts, C.J. Protein aggregation – Mechanisms, detection, and control. *Int. J. Pharm.* **2018**, *550*, 251-268, doi:https://doi.org/10.1016/j.ijpharm.2018.08.043.
6. Mahler, H.-C.; Friess, W.; Grauschopf, U.; Kiese, S. Protein aggregation: Pathways, induction factors and analysis. *J. Pharm. Sci.* **2009**, *98*, 2909-2934, doi:https://doi.org/10.1002/jps.21566.
7. Li, M.S.; Klimov, D.K.; Straub, J.E.; Thirumalai, D. Probing the mechanisms of fibril formation using lattice models. *J. Chem. Phys.* **2008**, *129*, 175101.
8. Li, M.S.; Co, N.T.; Reddy, G.; Hu, C.-K.; E.Straub, J.; Thirumalai, D. Factors governing fibrillogenesis of polypeptide chains revealed by lattice models. *Phys. Rev. Lett.* **2010**, *105*, 218101.
9. Shezad, K.; Zhang, K.; Hussain, M.; Dong, H.; He, C.; Gong, X.; Xie, X.; Zhu, J.; Shen, L. Surface Roughness Modulates Diffusion and Fibrillation of Amyloid-β Peptide. *Langmuir* **2016**, *32*, 8238-8244, doi:10.1021/acs.langmuir.6b01756.
10. Kardos, J.; Micsonai, A.; Pál-Gábor, H.; Petrik, É.; Gráf, L.; Kovács, J.; Lee, Y.-H.; Naiki, H.; Goto, Y. Reversible Heat-Induced Dissociation of β2-Microglobulin Amyloid Fibrils. *Biochemistry* **2011**, *50*, 3211-3220, doi:10.1021/bi2000017.
11. Co, N.T.; Li, M.S. Effect of Surface Roughness on Aggregation of Polypeptide Chains: A Monte Carlo Study. *Biomolecules* **2021**, *11*, doi:10.3390/biom11040596.
12. Thu, T.T.M.; Co, N.T.; Tu, L.A.; Li, M.S. Aggregation rate of amyloid beta peptide is controlled by beta-content in monomeric state. *J. Chem. Phys.* **2019**, *150*, 225101, doi:10.1063/1.5096379.
13. Co, N.T.; Lan, P.D.; Quoc Huy, P.D.; Li, M.S. Heat-induced degradation of fibrils: Exponential vs logistic kinetics. *J Chem Phys* **2020**, *152*, 115101, doi:10.1063/1.5144305.
14. Levinthal, C. *Mossbauer Spectroscopy in Biological Systems: Proceeding of a meeting held at Allerton House, Monticello, Illinois*; Munck, J.T.P.D.B.a.E., Ed.; University of Illinois Press: 1969; pp. 22–24.
15. Onuchic, J.N.; Wolynes, P.G. Theory of protein folding. *Curr. Opin. Struct. Biol.* **2004**, *14*, 70-75, doi:https://doi.org/10.1016/j.sbi.2004.01.009.
16. Dill, K.A.; Chan, H.S. From Levinthal to pathways to funnels.Nat. struct. biol. **1997**, *4*, 10-19, doi:10.1038/nsb0197-10.
17. Ke, P.C.; Zhou, R.; Serpell, L.C.; Riek, R.; Knowles, T.P.J.; Lashuel, H.A.; Gazit, E.; Hamley, I.W.; Davis, T.P.; Fändrich, M.; et al. Half a century of amyloids: past, present and future. *Chem. Soc. Rev.* **2020**, *49*, 5473-5509, doi:10.1039/C9CS00199A.
18. Yan, X.; Zhu, P.; Li, J. Self-assembly and application of diphenylalanine-based nanostructures. *Chem. Soc. Rev.* **2010**, *39*, 1877-1890, doi:10.1039/B915765B.
19. Dehsorkhi, A.; Castelletto, V.; Hamley, I.W. Self-assembling amphiphilic peptides. *J. Pept. Sci.* **2014**, *20*, 453-467, doi:https://doi.org/10.1002/psc.2633.

20. Wei, G.; Su, Z.; Reynolds, N.P.; Arosio, P.; Hamley, I.W.; Gazit, E.; Mezzenga, R. Self-assembling peptide and protein amyloids: from structure to tailored function in nanotechnology. *Chem. Soc. Rev.* **2017**, *46*, 4661-4708, doi:10.1039/C6CS00542J.
21. Knowles, T.P.J.; Buehler, M.J. Nanomechanics of functional and pathological amyloid materials. *Nat. Nanotechnol.* **2011**, *6*, 469-479, doi:10.1038/nnano.2011.102.
22. Knowles, T.P.J.; Mezzenga, R. Amyloid Fibrils as Building Blocks for Natural and Artificial Functional Materials. *Adv. Mater.***2016**, *28*, 6546-6561, doi:https://doi.org/10.1002/adma.201505961.
23. Hartl, F.U.; Hayer-Hartl, M. Converging concepts of protein folding in vitro and in vivo.*Nat. Struct. Mol. Biol* **2009**, *16*, 574-581, doi:10.1038/nsmb.1591.
24. Arosio, P.; Knowles, T.P.J.; Linse, S. On the lag phase in amyloid fibril formation.*Phys. Chem. Chem. Phys.* **2015**, *17*, 7606-7618, doi:10.1039/C4CP05563B.
25. Ilie, I.M.; Caflisch, A. Simulation Studies of Amyloidogenic Polypeptides and Their Aggregates. *Chem. Rev.* **2019**, *119*, 6956-6993, doi:10.1021/acs.chemrev.8b00731.
26. Nguyen, P.H.; Li, M.S.; Stock, G.; Straub, J.E.; Thirumalai, D.J.*PNAS*. Monomer adds to preformed structured oligomers of Aβ-peptides by a two-stage dock-lock mechanism. **2007**, *104*, 111-116.
27. Cohen, S.I.A.; Vendruscolo, M.; Dobson, C.M.; Knowles, T.P.J. From Macroscopic Measurements to Microscopic Mechanisms of Protein Aggregation. *J. Mol. Biol.***2012**, *421*, 160-171, doi:https://doi.org/10.1016/j.jmb.2012.02.031.
28. Linse, S. Monomer-dependent secondary nucleation in amyloid formation. *Biophys. Rev.* **2017**, *9*, 329-338, doi:10.1007/s12551-017-0289-z.
29. Nicoud, L.; Lazzari, S.; Balderas Barragán, D.; Morbidelli, M. Fragmentation of Amyloid Fibrils Occurs in Preferential Positions Depending on the Environmental Conditions. *J. Phys. Chem. B* **2015**, *119*, 4644-4652, doi:10.1021/acs.jpcb.5b01160.
30. Co, N.T.; Li, M.S.; Krupa, P. Computational Models for the Study of Protein Aggregation. In *Computer Simulations of Aggregation of Proteins and Peptides*, Li, M.S., Kloczkowski, A., Cieplak, M., Kouza, M., Eds.; Springer US: New York, NY, 2022; pp. 51-78.
31. Eanes, E.D.; Glenner, G.G. X-ray Diffraction Studies on Amyloid Filaments. *J. Histochem. Cytochem.* **1968**, *16*, 673-677, doi:10.1177/16.11.673.
32. Spencer, R.G.S.; Auger, M.; McDermott, A.E.; Griffin, R.G.; Halverson, K.J.; Lansbury, P.T. An Unusual Peptide Conformation May Precipitate Amyloid Formation in Alzheimer's Disease: Application of Solid-State NMR to the Determination of Protein Secondary Structure. *Biochemistry* **1991**, *30*, 10382-10387, doi:10.1021/bi00107a004.
33. Schmidt, A.; Annamalai, K.; Schmidt, M.; Grigorieff, N.; Fändrich, M. Cryo-EM reveals the steric zipper structure of a light chain-derived amyloid fibril. *PNAS* **2016**, *113*, 6200, doi:10.1073/pnas.1522282113.
34. Kouza, M.; Co, N.T.; Li, M.S.; Kmiecik, S.; Kolinski, A.; Kloczkowski, A.; Buhimschi, I.A. Kinetics and mechanical stability of the fibril state control fibril formation time of polypeptide chains: A computational study. *J. Chem. Phys.* **2018**, *148*, 215106, doi:10.1063/1.5028575.
35. Lu, J.-X.; Qiang, W.; Yau, W.-M.; Schwieters, Charles D.; Meredith, Stephen C.; Tycko, R. Molecular Structure of β-Amyloid Fibrils in Alzheimer's Disease Brain Tissue. *Cell* **2013**, *154*, 1257-1268, doi:https://doi.org/10.1016/j.cell.2013.08.035.
36. Paravastu, A.K.; Leapman, R.D.; Yau, W.-M.; Tycko, R. Molecular structural basis for polymorphism in Alzheimer's β-amyloid fibrils. *PNAS* **2008**, *105*, 18349-18354, doi:10.1073/pnas.0806270105.
37. Wälti, M.A.; Ravotti, F.; Arai, H.; Glabe, C.G.; Wall, J.S.; Böckmann, A.; Güntert, P.; Meier, B.H.; Riek, R. Atomic-resolution structure of a disease-relevant Aβ(1–42) amyloid fibril. *PNAS* **2016**, *113*, E4976-E4984, doi:10.1073/pnas.1600749113.

38. Gremer, L.; Schölzel, D.; Schenk, C.; Reinartz, E.; Labahn, J.; Ravelli, R.B.G.; Tusche, M.; Lopez-Iglesias, C.; Hoyer, W.; Heise, H.; et al. Fibril structure of amyloid-β(1-42) by cryo-electron microscopy. *Science* **2017**, *358*, 116-119, doi:doi:10.1126/science.aao2825.
39. Xi, W.; Vanderford, E.K.; Hansmann, U.H.E. Out-of-Register Aβ42 Assemblies as Models for Neurotoxic Oligomers and Fibrils. *J. Chem. Theory Comput.* **2018**, *14*, 1099-1110, doi:10.1021/acs.jctc.7b01106.
40. Hamley, I.W. The Amyloid Beta Peptide: A Chemist's Perspective. Role in Alzheimer's and Fibrillization. *Chem. Rev.* **2012**, *112*, 5147-5192, doi:10.1021/cr3000994.
41. Bisi, N.; Feni, L.; Peqini, K.; Pérez-Peña, H.; Ongeri, S.; Pieraccini, S.; Pellegrino, S. α-Synuclein: An All-Inclusive Trip Around its Structure, Influencing Factors and Applied Techniques. *Front. Chem* **2021**, *9*, doi:10.3389/fchem.2021.666585.
42. Iwasaki, Y. The Braak hypothesis in prion disease with a focus on Creutzfeldt–Jakob disease. *Neuropathology* **2020**, *40*, 436-449, doi:https://doi.org/10.1111/neup.12654.
43. Jadoul, M.; Drüeke, T.B. β2 microglobulin amyloidosis: an update 30 years later.*Nephrol. Dial. Transplant.***2016**, *31*, 507-509, doi:10.1093/ndt/gfv318.
44. Nasr, S.H.; Dasari, S.; Mills, J.R.; Theis, J.D.; Zimmermann, M.T.; Fonseca, R.; Vrana, J.A.; Lester, S.J.; McLaughlin, B.M.; Gillespie, R.; et al. Hereditary Lysozyme Amyloidosis Variant p.Leu102Ser Associates with Unique Phenotype. *J. Am. Soc. Nephrol.* **2017**, *28*, 431-438, doi:10.1681/ASN.2016090951.
45. Zorgati, H.; Larsson, M.; Ren, W.; Sim Adelene, Y.L.; Gettemans, J.; Grimes Jonathan, M.; Li, W.; Robinson Robert, C. The role of gelsolin domain 3 in familial amyloidosis (Finnish type). *PNAS* **2019**, *116*, 13958-13963, doi:10.1073/pnas.1902189116.
46. Marzban, L.; Park, K.; Verchere, C.B. Islet amyloid polypeptide and type 2 diabetes. *Exp. Gerontol.* **2003**, *38*, 347-351, doi:https://doi.org/10.1016/S0531-5565(03)00004-4.
47. Häggqvist, B.; Näslund, J.; Sletten, K.; Westermark Gunilla, T.; Mucchiano, G.; Tjernberg Lars, O.; Nordstedt, C.; Engström, U.; Westermark, P. Medin: An integral fragment of aortic smooth muscle cell-produced lactadherin forms the most common human amyloid. *PNAS* **1999**, *96*, 8669-8674, doi:10.1073/pnas.96.15.8669.
48. D'Souza, A.; Theis, J.D.; Vrana, J.A.; Dogan, A. Pharmaceutical amyloidosis associated with subcutaneous insulin and enfuvirtide administration. *Amyloid* **2014**, *21*, 71-75, doi:10.3109/13506129.2013.876984.
49. Ohashi, T.; Lemmon, C.A.; Erickson, H.P. Fibronectin Conformation and Assembly: Analysis of Fibronectin Deletion Mutants and Fibronectin Glomerulopathy (GFND) Mutants. *Biochemistry* **2017**, *56*, 4584-4591, doi:10.1021/acs.biochem.7b00589.
50. Castelletti, F.; Donadelli, R.; Banterla, F.; Hildebrandt, F.; Zipfel, P.F.; Bresin, E.; Otto, E.; Skerka, C.; Renieri, A.; Todeschini, M.; et al. Mutations in FN1 cause glomerulopathy with fibronectin deposits. *PNAS* **2008**, *105*, 2538-2543, doi:10.1073/pnas.0707730105.
51. Soto, C. Protein misfolding and disease; protein refolding and therapy. *FEBS Lett.***2001**, *498*, 204-207, doi:https://doi.org/10.1016/S0014-5793(01)02486-3.
52. LaFerla, F.M.; Hall, C.K.; Ngo, L.; Jay, G. Extracellular deposition of beta-amyloid upon p53-dependent neuronal cell death in transgenic mice. *J. Clin. Investig.* **1996**, *98*, 1626-1632, doi:10.1172/JCI118957.
53. de Oliveira, G.A.P.; Marques, M.A.; Pedrote, M.M.; Silva, J.L. High pressure studies on the misfolding and aggregation of p53 in cancer and of α-synuclein in Parkinson's disease. *High Press. Res.* **2019**, *39*, 193-201, doi:10.1080/08957959.2019.1576173.
54. Riek, R.; Eisenberg, D.S. The activities of amyloids from a structural perspective. *Nature* **2016**, *539*, 227-235, doi:10.1038/nature20416.
55. Blanco, L.P.; Evans, M.L.; Smith, D.R.; Badtke, M.P.; Chapman, M.R. Diversity, biogenesis and function of microbial amyloids. *Trends Microbiol.* **2012**, *20*, 66-73, doi:10.1016/j.tim.2011.11.005.

56. Martellini, J.A.; Cole, A.L.; Svoboda, P.; Stuchlik, O.; Chen, L.-M.; Chai, K.X.; Gangrade, B.K.; Sørensen, O.E.; Pohl, J.; Cole, A.M. HIV-1 enhancing effect of prostatic acid phosphatase peptides is reduced in human seminal plasma. *PloS One* **2011**, *6*, e16285-e16285, doi:10.1371/journal.pone.0016285.
57. Bolisetty, S.; Boddupalli, C.S.; Handschin, S.; Chaitanya, K.; Adamcik, J.; Saito, Y.; Manz, M.G.; Mezzenga, R. Amyloid Fibrils Enhance Transport of Metal Nanoparticles in Living Cells and Induced Cytotoxicity. *Biomacromolecules* **2014**, *15*, 2793-2799, doi:10.1021/bm500647n.
58. Cheetham, A.G.; Zhang, P.; Lin, Y.-a.; Lock, L.L.; Cui, H. Supramolecular Nanostructures Formed by Anticancer Drug Assembly. *J. Am. Chem. Soc.* **2013**, *135*, 2907-2910, doi:10.1021/ja3115983.
59. Bongiovanni, M.N.; Scanlon, D.B.; Gras, S.L. Functional fibrils derived from the peptide TTR1-cycloRGDfK that target cell adhesion and spreading. *Biomaterials* **2011**, *32*, 6099-6110, doi:https://doi.org/10.1016/j.biomaterials.2011.05.021.
60. Tanaka, H.; Herland, A.; Lindgren, L.J.; Tsutsui, T.; Andersson, M.R.; Inganäs, O. Enhanced Current Efficiency from Bio-Organic Light-Emitting Diodes Using Decorated Amyloid Fibrils with Conjugated Polymer. *Nano Lett.* **2008**, *8*, 2858-2861, doi:10.1021/nl801510z.
61. Bolisetty, S.; Mezzenga, R. Amyloid–carbon hybrid membranes for universal water purification. *Nat. Nanotechnol.* **2016**, *11*, 365-371, doi:10.1038/nnano.2015.310.
62. Tompa, P. Intrinsically unstructured proteins. *Trends Biochem. Sci.* **2002**, *27*, 527-533, doi:https://doi.org/10.1016/S0968-0004(02)02169-2.
63. Rajan, R.; Ahmed, S.; Sharma, N.; Kumar, N.; Debas, A.; Matsumura, K. Review of the current state of protein aggregation inhibition from a materials chemistry perspective: special focus on polymeric materials. *Adv. Mater.* **2021**, *2*, 1139-1176, doi:10.1039/D0MA00760A.
64. Franks, F.; Hatley, R.H.M.; Friedman, H.L. The thermodynamics of protein stability: Cold destabilization as a general phenomenon. *Biophys. Chem.* **1988**, *31*, 307-315, doi:https://doi.org/10.1016/0301-4622(88)80037-1.
65. Wang, W.; Roberts, C.J. Non-Arrhenius Protein Aggregation. *AAPS J.* **2013**, *15*, 840-851, doi:10.1208/s12248-013-9485-3.
66. Kayser, J.J.; Arnold, P.; Steffen-Heins, A.; Schwarz, K.; Keppler, J.K. Functional ethanol-induced fibrils: Influence of solvents and temperature on amyloid-like aggregation of beta-lactoglobulin.*J. Food Eng.* **2020**, *270*, 109764, doi:https://doi.org/10.1016/j.jfoodeng.2019.109764.
67. Sabaté, R.; Gallardo, M.; Estelrich, J. Temperature dependence of the nucleation constant rate in β amyloid fibrillogenesis. *Int. J. Biol. Macromol.***2005**, *35*, 9-13, doi:https://doi.org/10.1016/j.ijbiomac.2004.11.001.
68. Kusumoto, Y.; Lomakin, A.; Teplow, D.B.; Benedek, G.B. Temperature dependence of amyloid beta-protein fibrillization. *PNAS* **1998**, *95*, 12277-12282, doi:10.1073/pnas.95.21.12277.
69. Privalov, P.L. Cold Denaturation of Protein. *Crit. Rev. Biochem. Mol. Biol.* **1990**, *25*, 281-306, doi:Cold Denaturation of Protein
70. Luan, B.; Shan, B.; Baiz, C.; Tokmakoff, A.; Raleigh, D.P. Cooperative Cold Denaturation: The Case of the C-Terminal Domain of Ribosomal Protein L9. *Biochemistry* **2013**, *52*, 2402-2409, doi:10.1021/bi3016789.
71. Esfandiary, R.; Parupudi, A.; Casas-Finet, J.; Gadre, D.; Sathish, H. Mechanism of Reversible Self-Association of a Monoclonal Antibody: Role of Electrostatic and Hydrophobic Interactions. *J. Pharm. Sci.* **2015**, *104*, 577-586, doi:https://doi.org/10.1002/jps.24237.
72. Oliva, A.; Fariña, J.B.; Llabrés, M. Pre-study and in-study validation of a size-exclusion chromatography method with different detection modes for the analysis of monoclonal antibody aggregates. *J. Chromatogr. B* **2016**, *1022*, 206-212, doi:https://doi.org/10.1016/j.jchromb.2016.04.022.

73. Smith, M.; Sharp, J.; Roberts, C. Nucleation and growth of insulin fibrils in bulk solution and at hydrophobic polystyrene surfaces. *Biophys. J.* **2007**, *93*, 2143-2151.
74. Manno, M.; Craparo, E.F.; Podestà, A.; Bulone, D.; Carrotta, R.; Martorana, V.; Tiana, G.; San Biagio, P.L. Kinetics of different processes in human insulin amyloid formation. *J. Mol. Biol.***2007**, *366*, 258-274.
75. Chakroun, N.; Hilton, D.; Ahmad, S.S.; Platt, G.W.; Dalby, P.A. Mapping the Aggregation Kinetics of a Therapeutic Antibody Fragment. *Mol. Pharm.* **2016**, *13*, 307-319, doi:10.1021/acs.molpharmaceut.5b00387.
76. Sahin, Z.; Demir, Y.K.; Kayser, V. Global kinetic analysis of seeded BSA aggregation. *European J. Pharm. Sci.* **2016**, *86*, 115-124, doi:https://doi.org/10.1016/j.ejps.2016.03.007.
77. Saluja, A.; Sadineni, V.; Mungikar, A.; Nashine, V.; Kroetsch, A.; Dahlheim, C.; Rao, V.M. Significance of unfolding thermodynamics for predicting aggregation kinetics: a case study on high concentration solutions of a multi-domain protein. *Pharm. Res.* **2014**, *31*, 1575-1587.
78. Co, N.T.; Hu, C.K.; Li, M.S. Dual effect of crowders on fibrillation kinetics of polypeptide chains revealed by lattice models. *J Chem Phys* **2013**, *138*, 185101, doi:10.1063/1.4804299.
79. Fields, G.B.; Alonso, D.O.V.; Stigter, D.; Dill, K.A. Theory for the aggregation of proteins and copolymers.*J. Phys. Chem.* **1992**, *96*, 3974-3981, doi:10.1021/j100189a013.
80. Alford, J.R.; Kendrick, B.S.; Carpenter, J.F.; Randolph, T.W. High concentration formulations of recombinant human interleukin-1 receptor antagonist: II. Aggregation kinetics. *J Pharm Sci* **2008**, *97*, 3005-3021, doi:10.1002/jps.21205.
81. Tjernberg, L.O.; Pramanik, A.; Björling, S.; Thyberg, P.; Thyberg, J.; Nordstedt, C.; Berndt, K.D.; Terenius, L.; Rigler, R. Amyloid β-peptide polymerization studied using fluorescence correlation spectroscopy.*Chem. Biol.* **1999**, *6*, 53-62.
82. Sabaté, R.; Estelrich, J. Evidence of the existence of micelles in the fibrillogenesis of β-amyloid peptide. *J. Phys. Chem. B* **2005**, *109*, 11027-11032.
83. Novo, M.; Freire, S.; Al-Soufi, W. Critical aggregation concentration for the formation of early Amyloid-β (1–42) oligomers. *Sci. Rep.* **2018**, *8*, 1783, doi:10.1038/s41598-018-19961-3.
84. Kar, K.; Jayaraman, M.; Sahoo, B.; Kodali, R.; Wetzel, R. Critical nucleus size for disease-related polyglutamine aggregation is repeat-length dependent.Nat. Struct. Mol. Biol **2011**, *18*, 328-336, doi:10.1038/nsmb.1992.
85. Sabaté, R.; Estelrich, J. Aggregation characteristics of ovalbumin in β-sheet conformation determined by spectroscopy. *Biopolymers* **2002**, *67*, 113-120, doi:https://doi.org/10.1002/bip.10061.
86. Meisl, G.; Yang, X.; Frohm, B.; Knowles, T.P.J.; Linse, S. Quantitative analysis of intrinsic and extrinsic factors in the aggregation mechanism of Alzheimer-associated Aβ-peptide. *Sci. Rep.* **2016**, *6*, 18728, doi:10.1038/srep18728.
87. Deva, T.; Lorenzen, N.; Vad, B.S.; Petersen, S.V.; Thørgersen, I.; Enghild, J.J.; Kristensen, T.; Otzen, D.E. Off-pathway aggregation can inhibit fibrillation at high protein concentrations. *Biochim. Biophys. Acta* **2013**, *1834*, 677-687, doi:https://doi.org/10.1016/j.bbapap.2012.12.020.
88. Powers, E.T.; Powers, D.L. Mechanisms of Protein Fibril Formation: Nucleated Polymerization with Competing Off-Pathway Aggregation. *Biophys. J.* **2008**, *94*, 379-391, doi:https://doi.org/10.1529/biophysj.107.117168.
89. Zapadka, K.L.; Becher, F.J.; Gomes dos Santos, A.L.; Jackson, S.E. Factors affecting the physical stability (aggregation) of peptide therapeutics. *Interface Focus* **2017**, *7*, 20170030, doi:10.1098/rsfs.2017.0030.
90. Saha, S.; Deep, S. Protein aggregation: elucidation of the mechanism and determination of associated thermodynamic and kinetic parameters. *Curr. Phys. Chem.* **2014**, *4*, 114-136.
91. Cohen, S.I.A.; Linse, S.; Luheshi, L.M.; Hellstrand, E.; White, D.A.; Rajah, L.; Otzen, D.E.; Vendruscolo, M.; Dobson, C.M.; Knowles, T.P.J. Proliferation of amyloid-β42 aggregates occurs through a secondary nucleation mechanism. *PNAS* **2013**, *110*, 9758-9763, doi:doi:10.1073/pnas.1218402110.

92. Niraula, T.N.; Konno, T.; Li, H.; Yamada, H.; Akasaka, K.; Tachibana, H. Pressure-dissociable reversible assembly of intrinsically denatured lysozyme is a precursor for amyloid fibrils. *PNAS* **2004**, *101*, 4089, doi:10.1073/pnas.0305798101.
93. Torrent, J.; Alvarez-Martinez, M.T.; Harricane, M.-C.; Heitz, F.; Liautard, J.-P.; Balny, C.; Lange, R. High Pressure Induces Scrapie-like Prion Protein Misfolding and Amyloid Fibril Formation. *Biochemistry* **2004**, *43*, 7162-7170, doi:10.1021/bi049939d.
94. Cordeiro, Y.; Foguel, D.; Silva, J.L. Pressure–temperature folding landscape in proteins involved in neurodegenerative diseases and cancer. *Biophys. Chem.* **2013**, *183*, 9-18, doi:https://doi.org/10.1016/j.bpc.2013.06.002.
95. Kim, Y.S.; Randolph, T.W.; Seefeldt, M.B.; Carpenter, J.F. High-pressure studies on protein aggregates and amyloid fibrils. *Meth. Enzymol.***2006**, *413*, 237-253, doi:10.1016/s0076-6879(06)13013-x.
96. Roche, J.; Caro, J.A.; Norberto, D.R.; Barthe, P.; Roumestand, C.; Schlessman, J.L.; Garcia, A.E.; García-Moreno E, B.; Royer, C.A. Cavities determine the pressure unfolding of proteins. *PNAS* **2012**, *109*, 6945, doi:10.1073/pnas.1200915109.
97. de Oliveira, G.A.P.; Silva, J.L. A hypothesis to reconcile the physical and chemical unfolding of proteins. *PNAS* **2015**, *112*, E2775, doi:10.1073/pnas.1500352112.
98. Hamann, S.D. The role of electrostriction in high pressure chemistry (Modern aspects of physical chemistry at high pressure : the 50th commemorative volume). *Rev Phys Chem JPN* **1980**, *50*, 147-168.
99. St. John, R.J.; Carpenter, J.F.; Randolph, T.W. High pressure fosters protein refolding from aggregates at high concentrations. *PNAS* **1999**, *96*, 13029, doi:10.1073/pnas.96.23.13029.
100. Foguel, D.; Silva, J.L. New Insights into the Mechanisms of Protein Misfolding and Aggregation in Amyloidogenic Diseases Derived from Pressure Studies. *Biochemistry* **2004**, *43*, 11361-11370, doi:10.1021/bi048864a.
101. Randolph, T.W.; Seefeldt, M.; Carpenter, J.F. High hydrostatic pressure as a tool to study protein aggregation and amyloidosis. *Biochim. Biophys. Acta* **2002**, *1595*, 224-234, doi:https://doi.org/10.1016/S0167-4838(01)00346-6.
102. Kobayashi, S.; Tanaka, Y.; Kiyono, M.; Chino, M.; Chikuma, T.; Hoshi, K.; Ikeshima, H. Dependence pH and proposed mechanism for aggregation of Alzheimer's disease-related amyloid-β(1–42) protein. *J. Mol. Struct.* **2015**, *1094*, 109-117, doi:https://doi.org/10.1016/j.molstruc.2015.03.023.
103. López de la Paz, M.; Goldie, K.; Zurdo, J.; Lacroix, E.; Dobson, C.M.; Hoenger, A.; Serrano, L. De novo designed peptide-based amyloid fibrils. *PNAS* **2002**, *99*, 16052, doi:10.1073/pnas.252340199.
104. Hoyer, W.; Antony, T.; Cherny, D.; Heim, G.; Jovin, T.M.; Subramaniam, V. Dependence of α-Synuclein Aggregate Morphology on Solution Conditions. *J. Mol. Biol.***2002**, *322*, 383-393, doi:https://doi.org/10.1016/S0022-2836(02)00775-1.
105. Raman, B.; Chatani, E.; Kihara, M.; Ban, T.; Sakai, M.; Hasegawa, K.; Naiki, H.; Rao, C.M.; Goto, Y. Critical Balance of Electrostatic and Hydrophobic Interactions Is Required for β2-Microglobulin Amyloid Fibril Growth and Stability. *Biochemistry* **2005**, *44*, 1288-1299, doi:10.1021/bi048029t.
106. vandenAkker, C.C.; Engel, M.F.M.; Velikov, K.P.; Bonn, M.; Koenderink, G.H. Morphology and Persistence Length of Amyloid Fibrils Are Correlated to Peptide Molecular Structure. *J. Am. Chem. Soc.* **2011**, *133*, 18030-18033, doi:10.1021/ja206513r.
107. Marek, P.J.; Patsalo, V.; Green, D.F.; Raleigh, D.P. Ionic strength effects on amyloid formation by amylin are a complicated interplay among Debye screening, ion selectivity, and Hofmeister effects. *Biochemistry* **2012**, *51*, 8478-8490, doi:10.1021/bi300574r.
108. Abelein, A.; Jarvet, J.; Barth, A.; Gräslund, A.; Danielsson, J. Ionic Strength Modulation of the Free Energy Landscape of Aβ40 Peptide Fibril Formation. *J. Am. Chem. Soc.* **2016**, *138*, 6893-6902, doi:10.1021/jacs.6b04511.

109. Priyanka, B.; Venkata, S.K.M. Effect of Ionic Strength on the Aggregation Propensity of Aβ1-42 Peptide: An In-silico Study. *Curr. Chem. Biol.* **2020**, *14*, 216-226, doi:http://dx.doi.org/10.2174/2212796814999200818103157.
110. Tsai, A.M.; van Zanten, J.H.; Betenbaugh, M.J. Electrostatic effect in the aggregation of heat-denatured RNase A and implications for protein additive design. *Biotechnol. Bioeng.* **1998**, *59*, 281-285, doi:https://doi.org/10.1002/(SICI)1097-0290(19980805)59:3<281::AID-BIT3>3.0.CO;2-7.
111. Arakawa, T.; Timasheff, S.N. Mechanism of protein salting in and salting out by divalent cation salts: balance between hydration and salt binding. *Biochemistry* **1984**, *23*, 5912-5923, doi:10.1021/bi00320a004.
112. Curtis, R.A.; Ulrich, J.; Montaser, A.; Prausnitz, J.M.; Blanch, H.W. Protein–protein interactions in concentrated electrolyte solutions. *Biotechnol. Bioeng.* **2002**, *79*, 367-380, doi:https://doi.org/10.1002/bit.10342.
113. Adachi, M.; Noji, M.; So, M.; Sasahara, K.; Kardos, J.; Naiki, H.; Goto, Y. Aggregation-phase diagrams of β 2-microglobulin reveal temperature and salt effects on competitive formation of amyloids versus amorphous aggregates.*J. Biol. Chem.* **2018**, *293*, 14775-14785, doi:10.1074/jbc.RA118.004683.
114. Saha, S.; Deep, S. Switch in the Aggregation Pathway of Bovine Serum Albumin Mediated by Electrostatic Interactions. *J. Phys. Chem. B* **2014**, *118*, 9155-9166, doi:10.1021/jp502435f.
115. Gupta, P.; Deep, S. Salt mediated unusual switching in the aggregation kinetic profile of human carbonic anhydrase. *RSC Adv.* **2015**, *5*, 95717-95726.
116. Zimmerman, S.B.; Trach, S.O. Estimation of macromolecule concentrations and excluded volume effects for the cytoplasm of Escherichia coli. *J. Mol. Biol.***1991**, *222*, 599-620, doi:https://doi.org/10.1016/0022-2836(91)90499-V.
117. Feig, M.; Yu, I.; Wang, P.-h.; Nawrocki, G.; Sugita, Y. Crowding in Cellular Environments at an Atomistic Level from Computer Simulations. *J. Phys. Chem. B* **2017**, *121*, 8009-8025, doi:10.1021/acs.jpcb.7b03570.
118. Ellis, R.J. Macromolecular crowding: obvious but underappreciated. *Trends Biochem. Sci.* **2001**, *26*, 597-604, doi:https://doi.org/10.1016/S0968-0004(01)01938-7.
119. Cabaleiro-Lago, C.; Quinlan-Pluck, F.; Lynch, I.; Dawson, K.A.; Linse, S. Dual effect of amino modified polystyrene nanoparticles on amyloid β protein fibrillation. *ACS Chem. Neurosci.* **2010**, *1*, 279-287, doi:10.1021/cn900027u.
120. Mittal, S.; Singh, L.R. Macromolecular crowding decelerates aggregation of a β-rich protein, bovine carbonic anhydrase: a case study. *J. Biochem.* **2014**, *156*, 273-282, doi:10.1093/jb/mvu039.
121. Ellis, R.J.; Minton, A.P. Protein aggregation in crowded environments. *Biol. Chem.* **2006**, *387*, 485-497, doi:doi:10.1515/BC.2006.064.
122. White, D.A.; Buell, A.K.; Knowles, T.P.J.; Welland, M.E.; Dobson, C.M. Protein Aggregation in Crowded Environments. *J. Am. Chem. Soc.* **2010**, *132*, 5170-5175, doi:10.1021/ja909997e.
123. Magno, A.; Caflisch, A.; Pellarin, R. Crowding Effects on Amyloid Aggregation Kinetics.*J. Phys. Chem. Letters* **2010**, *1*, 3027-3032, doi:10.1021/jz100967z.
124. O'Brien, E.P.; Straub, J.E.; Brooks, B.R.; Thirumalai, D. Influence of Nanoparticle Size and Shape on Oligomer Formation of an Amyloidogenic Peptide.*J. Phys. Chem. Letters* **2011**, *2*, 1171-1177, doi:10.1021/jz200330k.
125. Zhou, Z.; Fan, J.-B.; Zhu, H.-L.; Shewmaker, F.; Yan, X.; Chen, X.; Chen, J.; Xiao, G.-F.; Guo, L.; Liang, Y. Crowded Cell-like Environment Accelerates the Nucleation Step of Amyloidogenic Protein Misfolding.*J. Biol. Chem.* **2009**, *284*, 30148-30158, doi:https://doi.org/10.1074/jbc.M109.002832.
126. Co, N.T.; Hu, C.-K.; Li, M.S. Dual effect of crowders on fibrillation kinetics of polypeptide chains revealed by lattice models. *J. Chem. Phys.* **2013**, *138*, 185101, doi:10.1063/1.4804299.

127. Gao, G.; Zhang, M.; Gong, D.; Chen, R.; Hu, X.; Sun, T. The size-effect of gold nanoparticles and nanoclusters in the inhibition of amyloid-β fibrillation. *Nanoscale* **2017**, *9*, 4107-4113, doi:10.1039/C7NR00699C.
128. Latshaw, D.C., 2nd; Hall, C.K. Effects of hydrophobic macromolecular crowders on amyloid β (16-22) aggregation. *Biophys. J.* **2015**, *109*, 124-134, doi:10.1016/j.bpj.2015.05.032.
129. Musiani, F.; Giorgetti, A. Chapter Two - Protein Aggregation and Molecular Crowding: Perspectives From Multiscale Simulations. *Int. Rev. Cell Mol*, Sandal, M., Ed.; Academic Press: 2017; Volume 329, pp. 49-77.
130. Yang, B.; Adams, D.J.; Marlow, M.; Zelzer, M. Surface-Mediated Supramolecular Self-Assembly of Protein, Peptide, and Nucleoside Derivatives: From Surface Design to the Underlying Mechanism and Tailored Functions. *Langmuir* **2018**, *34*, 15109-15125, doi:10.1021/acs.langmuir.8b01165.
131. Keller, A.; Grundmeier, G. Amyloid aggregation at solid-liquid interfaces: Perspectives of studies using model surfaces. *Appl. Surf. Sci.* **2020**, *506*, 144991, doi:https://doi.org/10.1016/j.apsusc.2019.144991.
132. Vacha, R.; Linse, S.; Lund, M. Surface effects on aggregation kinetics of amyloidogenic peptides. *J Am Chem Soc* **2014**, *136*, 11776-11782, doi:10.1021/ja505502e.
133. Lindberg, D.J.; Wesén, E.; Björkeroth, J.; Rocha, S.; Esbjörner, E.K. Lipid membranes catalyse the fibril formation of the amyloid-β (1–42) peptide through lipid-fibril interactions that reinforce secondary pathways. *Biochim Biophys Acta Biomembr.* **2017**, *1859*, 1921-1929, doi:https://doi.org/10.1016/j.bbamem.2017.05.012.
134. Morriss-Andrews, A.; Brown, F.L.H.; Shea, J.-E. A Coarse-Grained Model for Peptide Aggregation on a Membrane Surface. *J. Phys. Chem. B* **2014**, *118*, 8420-8432, doi:10.1021/jp502871m.
135. Rawat, A.; Langen, R.; Varkey, J. Membranes as modulators of amyloid protein misfolding and target of toxicity. *Biochim Biophys Acta Biomembr.* **2018**, *1860*, 1863-1875, doi:https://doi.org/10.1016/j.bbamem.2018.04.011.
136. Rabe, M.; Soragni, A.; Reynolds, N.P.; Verdes, D.; Liverani, E.; Riek, R.; Seeger, S. On-Surface Aggregation of α-Synuclein at Nanomolar Concentrations Results in Two Distinct Growth Mechanisms. *ACS Chem. Neurosci.* **2013**, *4*, 408-417, doi:10.1021/cn3001312.
137. Lin, Y.-C.; Li, C.; Fakhraai, Z. Kinetics of Surface-Mediated Fibrillization of Amyloid-β (12–28) Peptides. *Langmuir* **2018**, *34*, 4665-4672, doi:10.1021/acs.langmuir.7b02744.
138. Cabaleiro-Lago, C.; Quinlan-Pluck, F.; Lynch, I.; Lindman, S.; Minogue, A.M.; Thulin, E.; Walsh, D.M.; Dawson, K.A.; Linse, S. Inhibition of Amyloid β Protein Fibrillation by Polymeric Nanoparticles. *J. Am. Chem. Soc.* **2008**, *130*, 15437-15443, doi:10.1021/ja8041806.
139. Kang, S.-g.; Huynh, T.; Xia, Z.; Zhang, Y.; Fang, H.; Wei, G.; Zhou, R. Hydrophobic Interaction Drives Surface-Assisted Epitaxial Assembly of Amyloid-like Peptides. *J. Am. Chem. Soc.* **2013**, *135*, 3150-3157, doi:10.1021/ja310989u.
140. Zhang, F.; Du, H.-N.; Zhang, Z.-X.; Ji, L.-N.; Li, H.-T.; Tang, L.; Wang, H.-B.; Fan, C.-H.; Xu, H.-J.; Zhang, Y.; et al. Epitaxial Growth of Peptide Nanofilaments on Inorganic Surfaces: Effects of Interfacial Hydrophobicity/Hydrophilicity.*Angew. Chem. Int. Ed.* **2006**, *45*, 3611-3613, doi:https://doi.org/10.1002/anie.200503636.
141. Ban, T.; Morigaki, K.; Yagi, H.; Kawasaki, T.; Kobayashi, A.; Yuba, S.; Naiki, H.; Goto, Y. Real-time and Single Fibril Observation of the Formation of Amyloid β Spherulitic Structures*.*J. Biol. Chem.* **2006**, *281*, 33677-33683, doi:https://doi.org/10.1074/jbc.M606072200.
142. Huang, R.; Su, R.; Qi, W.; Zhao, J.; He, Z. Hierarchical, interface-induced self-assembly of diphenylalanine: formation of peptide nanofibers and microvesicles. *Nanotechnology* **2011**, *22*, 245609, doi:10.1088/0957-4484/22/24/245609.
143. Chaturvedi, S.K.; Siddiqi, M.K.; Alam, P.; Khan, R.H. Protein misfolding and aggregation: Mechanism, factors and detection. *Process Biochem* **2016**, *51*, 1183-1192, doi:https://doi.org/10.1016/j.procbio.2016.05.015.

144. Breydo, L.; Redington, J.M.; Uversky, V.N. Chapter Four - Effects of Intrinsic and Extrinsic Factors on Aggregation of Physiologically Important Intrinsically Disordered Proteins. In *Int. Rev. Cell Mol*, Sandal, M., Ed.; Academic Press: 2017; Volume 329, pp. 145-185.
145. Krone, M.G.; Baumketner, A.; Bernstein, S.L.; Wyttenbach, T.; Lazo, N.D.; Teplow, D.B.; Bowers, M.T.; Shea, J.-E. Effects of Familial Alzheimer's Disease Mutations on the Folding Nucleation of the Amyloid β-Protein. *J. Mol. Biol.***2008**, *381*, 221-228, doi:https://doi.org/10.1016/j.jmb.2008.05.069.
146. Baumketner, A.; Krone, M.G.; Shea, J.-E. Role of the familial Dutch mutation E22Q in the folding and aggregation of the 15–28 fragment of the Alzheimer amyloid-β protein. *PNAS* **2008**, *105*, 6027-6032, doi:10.1073/pnas.0708193105.
147. Qiang, W.; Yau, W.-M.; Luo, Y.; Mattson, M.P.; Tycko, R. Antiparallel β-sheet architecture in Iowa-mutant β-amyloid fibrils. *PNAS* **2012**, *109*, 4443-4448, doi:10.1073/pnas.1111305109.
148. Kaden, D.; Harmeier, A.; Weise, C.; Munter, L.M.; Althoff, V.; Rost, B.R.; Hildebrand, P.W.; Schmitz, D.; Schaefer, M.; Lurz, R.; et al. Novel APP/Aβ mutation K16N produces highly toxic heteromeric Aβ oligomers. *EMBO Mol. Med.* **2012**, *4*, 647-659, doi:https://doi.org/10.1002/emmm.201200239.
149. Tomiyama, T.; Nagata, T.; Shimada, H.; Teraoka, R.; Fukushima, A.; Kanemitsu, H.; Takuma, H.; Kuwano, R.; Imagawa, M.; Ataka, S.; et al. A new amyloid β variant favoring oligomerization in Alzheimer's-type dementia. *Ann. Neurol.* **2008**, *63*, 377-387, doi:https://doi.org/10.1002/ana.21321.
150. Krüger, R.; Kuhn, W.; Müller, T.; Woitalla, D.; Graeber, M.; Kösel, S.; Przuntek, H.; Epplen, J.T.; Schöls, L.; Riess, O. Ala30Pro mutation in the gene encoding α-synuclein in Parkinson's disease. *Nat. Genet.* **1998**, *18*, 106-108, doi:10.1038/ng0298-106.
151. Polymeropoulos, M.H.; Lavedan, C.; Leroy, E.; Ide, S.E.; Dehejia, A.; Dutra, A.; Pike, B.; Root, H.; Rubenstein, J.; Boyer, R.; et al. Mutation in the α-synuclein gene identified in families with Parkinson's disease. *Science* **1997**, *276*, 2045-2047, doi:10.1126/science.276.5321.2045.
152. Zarranz, J.J.; Alegre, J.; Gómez-Esteban, J.C.; Lezcano, E.; Ros, R.; Ampuero, I.; Vidal, L.; Hoenicka, J.; Rodriguez, O.; Atarés, B.; et al. The New Mutation, E46K, of α-Synuclein Causes Parkinson and Lewy Body Dementia. *Ann. Neurol.* **2004**, *55*, 164-173, doi:10.1002/ana.10795.
153. Hutton, M.; Lendon, C.L.; Rizzu, P.; Baker, M.; Froelich, S.; Houlden, H.; Pickering-Brown, S.; Chakraverty, S.; Isaacs, A.; Grover, A.; et al. Association of missense and 5′-splice-site mutations in tau with the inherited dementia FTDP-17. *Nature* **1998**, *393*, 702-705, doi:10.1038/31508.
154. Kouri, N.; Carlomagno, Y.; Baker, M.; Liesinger, A.M.; Caselli, R.J.; Wszolek, Z.K.; Petrucelli, L.; Boeve, B.F.; Parisi, J.E.; Josephs, K.A.; et al. Novel mutation in MAPT exon 13 (p.N410H) causes corticobasal degeneration. *Acta Neuropathol.* **2014**, *127*, 271-282, doi:10.1007/s00401-013-1193-7.
155. Pickering-Brown, S.M.; Baker, M.; Nonaka, T.; Ikeda, K.; Sharma, S.; Mackenzie, J.; Simpson, S.A.; Moore, J.W.; Snowden, J.S.; De Silva, R.; et al. Frontotemporal dementia with Pick-type histology associated with Q336R mutation in the tau gene. *Brain* **2004**, *127*, 1415-1426, doi:10.1093/brain/awh147.
156. Mirceta, S.; Signore Anthony, V.; Burns Jennifer, M.; Cossins Andrew, R.; Campbell Kevin, L.; Berenbrink, M. Evolution of Mammalian Diving Capacity Traced by Myoglobin Net Surface Charge. *Science* **2013**, *340*, 1234192, doi:10.1126/science.1234192.
157. Bemporad, F.; Ramazzotti, M. Chapter One - From the Evolution of Protein Sequences Able to Resist Self-Assembly to the Prediction of Aggregation Propensity. In *Int. Rev. Cell Mol*, Sandal, M., Ed.; Academic Press: 2017; Volume 329, pp. 1-47.
158. Otzen, D.E.; Kristensen, O.; Oliveberg, M. Designed protein tetramer zipped together with a hydrophobic Alzheimer homology: A structural clue to amyloid assembly. *PNAS* **2000**, *97*, 9907, doi:10.1073/pnas.160086297.
159. Hori, Y.; Hashimoto, T.; Wakutani, Y.; Urakami, K.; Nakashima, K.; Condron, M.M.; Tsubuki, S.; Saido, T.C.; Teplow, D.B.; Iwatsubo, T. The Tottori (D7N) and English (H6R) Familial

Alzheimer Disease Mutations Accelerate Aβ Fibril Formation without Increasing Protofibril Formation.*J. Biol. Chem.* **2007**, *282*, 4916-4923, doi:https://doi.org/10.1074/jbc.M608220200.
160. Ono, K.; Condron, M.M.; Teplow, D.B. Effects of the English (H6R) and Tottori (D7N) familial Alzheimer disease mutations on amyloid beta-protein assembly and toxicity. *The J. Biol. Chem.* **2010**, *285*, 23186-23197, doi:10.1074/jbc.M109.086496.
161. de Rosa, M.; Barbiroli, A.; Giorgetti, S.; Mangione, P.P.; Bolognesi, M.; Ricagno, S. Decoding the Structural Bases of D76N ß2-Microglobulin High Amyloidogenicity through Crystallography and Asn-Scan Mutagenesis. *PloS one* **2015**, *10*, e0144061-e0144061, doi:10.1371/journal.pone.0144061.
162. Gazit, E. A possible role for π-stacking in the self-assembly of amyloid fibrils. *FASEB J* **2002**, *16*, 77-83, doi:https://doi.org/10.1096/fj.01-0442hyp.
163. Adler-Abramovich, L.; Gazit, E. The physical properties of supramolecular peptide assemblies: from building block association to technological applications. *Chem. Soc. Rev.* **2014**, *43*, 6881-6893, doi:10.1039/C4CS00164H.
164. Bowerman, C.J.; Ryan, D.M.; Nissan, D.A.; Nilsson, B.L. The effect of increasing hydrophobicity on the self-assembly of amphipathic β-sheet peptides. *Mol. Biosyst.* **2009**, *5*, 1058-1069, doi:10.1039/B904439F.
165. Senguen, F.T.; Lee, N.R.; Gu, X.; Ryan, D.M.; Doran, T.M.; Anderson, E.A.; Nilsson, B.L. Probing aromatic, hydrophobic, and steric effects on the self-assembly of an amyloid-β fragment peptide. *Mol. Biosyst.* **2011**, *7*, 486-496, doi:10.1039/C0MB00080A.
166. Nam, H.B.; Kouza, M.; Zung, H.; Li, M.S. Relationship between population of the fibril-prone conformation in the monomeric state and oligomer formation times of peptides: Insights from all-atom simulations. *J. Chem. Phys.* **2010**, *132*, 04B613.
167. Sciarretta, K.L.; Gordon, D.J.; Petkova, A.T.; Tycko, R.; Meredith, S.C. Aβ40-Lactam (D23/K28) models a conformation highly favorable for nucleation of amyloid. *Biochemistry* **2005**, *44*, 6003-6014.
168. Sgourakis, N.G.; Yan, Y.; McCallum, S.A.; Wang, C.; Garcia, A.E. The Alzheimer's peptides Aβ40 and 42 adopt distinct conformations in water: a combined MD/NMR study. *J. Mol. Biol.***2007**, *368*, 1448-1457.
169. Yang, M.; Teplow, D.B. Amyloid β-protein monomer folding: free-energy surfaces reveal alloform-specific differences. *J. Mol. Biol.***2008**, *384*, 450-464.
170. Morriss-Andrews, A.; Shea, J.-E. Computational Studies of Protein Aggregation: Methods and Applications. *Annu. Rev. Phys. Chem.* **2015**, *66*, 643-666, doi:10.1146/annurev-physchem-040513-103738.
171. Weiner, P.K.; Kollman, P.A. AMBER: Assisted model building with energy refinement. A general program for modeling molecules and their interactions.*J. Comput. Chem.* **1981**, *2*, 287-303, doi:https://doi.org/10.1002/jcc.540020311.
172. Brooks, B.R.; Bruccoleri, R.E.; Olafson, B.D.; States, D.J.; Swaminathan, S.; Karplus, M. CHARMM: A program for macromolecular energy, minimization, and dynamics calculations.*J. Comput. Chem.* **1983**, *4*, 187-217, doi:https://doi.org/10.1002/jcc.540040211.
173. Hermans, J.; Berendsen, H.J.C.; Van Gunsteren, W.F.; Postma, J.P.M. A consistent empirical potential for water–protein interactions. *Biopolymers* **1984**, *23*, 1513-1518, doi:https://doi.org/10.1002/bip.360230807.
174. Jorgensen, W.L.; Tirado-Rives, J. The OPLS [optimized potentials for liquid simulations] potential functions for proteins, energy minimizations for crystals of cyclic peptides and crambin. *J. Am. Chem. Soc.* **1988**, *110*, 1657-1666, doi:10.1021/ja00214a001.
175. Mark, P.; Nilsson, L. Structure and Dynamics of the TIP3P, SPC, and SPC/E Water Models at 298 K.*J. Phys. Chem. A* **2001**, *105*, 9954-9960, doi:10.1021/jp003020w.
176. Izadi, S.; Anandakrishnan, R.; Onufriev, A.V. Building Water Models: A Different Approach.*J. Phys. Chem. Letters* **2014**, *5*, 3863-3871, doi:10.1021/jz501780a.

177. Tsui, V.; Case, D.A. Theory and applications of the generalized born solvation model in macromolecular simulations. *Biopolymers* **2000**, *56*, 275-291, doi:https://doi.org/10.1002/1097-0282(2000)56:4<275::AID-BIP10024>3.0.CO;2-E.
178. Stein, C.J.; Herbert, J.M.; Head-Gordon, M. The Poisson–Boltzmann model for implicit solvation of electrolyte solutions: Quantum chemical implementation and assessment via Sechenov coefficients. *J. Chem. Phys.* **2019**, *151*, 224111, doi:10.1063/1.5131020.
179. Robustelli, P.; Piana, S.; Shaw David, E. Developing a molecular dynamics force field for both folded and disordered protein states. *PNAS* **2018**, *115*, E4758-E4766, doi:10.1073/pnas.1800690115.
180. Yu, L.; Li, D.-W.; Brüschweiler, R. Balanced Amino-Acid-Specific Molecular Dynamics Force Field for the Realistic Simulation of Both Folded and Disordered Proteins. *J. Chem. Theory Comput.* **2020**, *16*, 1311-1318, doi:10.1021/acs.jctc.9b01062.
181. Liu, H.; Song, D.; Lu, H.; Luo, R.; Chen, H.-F. Intrinsically disordered protein-specific force field CHARMM36IDPSFF. *Chem Biol Drug Des* **2018**, *92*, 1722-1735, doi:https://doi.org/10.1111/cbdd.13342.
182. Nasica-Labouze, J.; Reviews, J.C.; et al. Amyloid beta-protein and Alzheimer's disease: when computer simulations complement experimental studies. **2015**, *115*, 3518-3563.
183. Berendsen, H.J.C.; van der Spoel, D.; van Drunen, R. GROMACS: A message-passing parallel molecular dynamics implementation. *Comput. Phys. Commun.* **1995**, *91*, 43-56, doi:https://doi.org/10.1016/0010-4655(95)00042-E.
184. Case, D.A.; Cheatham Iii, T.E.; Darden, T.; Gohlke, H.; Luo, R.; Merz Jr, K.M.; Onufriev, A.; Simmerling, C.; Wang, B.; Woods, R.J. The Amber biomolecular simulation programs.*J. Comput. Chem.* **2005**, *26*, 1668-1688, doi:https://doi.org/10.1002/jcc.20290.
185. Phillips, J.C.; Hardy, D.J.; Maia, J.D.C.; Stone, J.E.; Ribeiro, J.V.; Bernardi, R.C.; Buch, R.; Fiorin, G.; Hénin, J.; Jiang, W.; et al. Scalable molecular dynamics on CPU and GPU architectures with NAMD. *J. Chem. Phys.* **2020**, *153*, 044130-044130, doi:10.1063/5.0014475.
186. Marrink, S.J.; Risselada, H.J.; Yefimov, S.; Tieleman, D.P.; de Vries, A.H. The MARTINI Force Field: Coarse Grained Model for Biomolecular Simulations. *J. Phys. Chem. B* **2007**, *111*, 7812-7824, doi:10.1021/jp071097f.
187. Monticelli, L.; Kandasamy, S.K.; Periole, X.; Larson, R.G.; Tieleman, D.P.; Marrink, S.-J. The MARTINI Coarse-Grained Force Field: Extension to Proteins. *J. Chem. Theory Comput.* **2008**, *4*, 819-834, doi:10.1021/ct700324x.
188. Derreumaux, P. From polypeptide sequences to structures using Monte Carlo simulations and an optimized potential. *J. Chem. Phys.* **1999**, *111*, 2301-2310, doi:10.1063/1.479501.
189. Maupetit, J.; Tuffery, P.; Derreumaux, P. A coarse-grained protein force field for folding and structure prediction. *Proteins* **2007**, *69*, 394-408, doi:https://doi.org/10.1002/prot.21505.
190. Liwo, A.; Ołdziej, S.; Pincus, M.R.; Wawak, R.J.; Rackovsky, S.; Scheraga, H.A. A united-residue force field for off-lattice protein-structure simulations. I. Functional forms and parameters of long-range side-chain interaction potentials from protein crystal data.*J. Comput. Chem.* **1997**, *18*, 849-873, doi:https://doi.org/10.1002/(SICI)1096-987X(199705)18:7<849::AID-JCC1>3.0.CO;2-R.
191. Khalili, M.; Liwo, A.; Jagielska, A.; Scheraga, H.A. Molecular Dynamics with the United-Residue Model of Polypeptide Chains. II. Langevin and Berendsen-Bath Dynamics and Tests on Model α-Helical Systems. *J. Phys. Chem. B* **2005**, *109*, 13798-13810, doi:10.1021/jp058007w.
192. Davtyan, A.; Schafer, N.P.; Zheng, W.; Clementi, C.; Wolynes, P.G.; Papoian, G.A. AWSEM-MD: Protein Structure Prediction Using Coarse-Grained Physical Potentials and Bioinformatically Based Local Structure Biasing. *J. Phys. Chem. B* **2012**, *116*, 8494-8503, doi:10.1021/jp212541y.
193. Chen, M.; Schafer, N.P.; Zheng, W.; Wolynes, P.G. The Associative Memory, Water Mediated, Structure and Energy Model (AWSEM)-Amylometer: Predicting Amyloid Propensity and Fibril

Topology Using an Optimized Folding Landscape Model. *ACS Chem. Neurosci.* **2018**, *9*, 1027-1039, doi:10.1021/acschemneuro.7b00436.
194. Chen, X.; Chen, M.; Schafer, N.P.; Wolynes, P.G. Exploring the interplay between fibrillization and amorphous aggregation channels on the energy landscapes of tau repeat isoforms. *PNAS* **2020**, *117*, 4125, doi:10.1073/pnas.1921702117.
195. Mousseau, N.; Derreumaux, P. Exploring the Early Steps of Amyloid Peptide Aggregation by Computers. *Acc. Chem. Res.* **2005**, *38*, 885-891, doi:10.1021/ar050045a.
196. Song, W.; Wei, G.; Mousseau, N.; Derreumaux, P. Self-Assembly of the β2-Microglobulin NHVTLSQ Peptide Using a Coarse-Grained Protein Model Reveals a β-Barrel Species. *J. Phys. Chem. B* **2008**, *112*, 4410-4418, doi:10.1021/jp710592v.
197. De Simone, A.; Derreumaux, P. Low molecular weight oligomers of amyloid peptides display β-barrel conformations: A replica exchange molecular dynamics study in explicit solvent. *J. Chem. Phys.* **2010**, *132*, 165103, doi:10.1063/1.3385470.
198. Chiricotto, M.; Melchionna, S.; Derreumaux, P.; Sterpone, F. Multiscale Aggregation of the Amyloid Aβ16–22 Peptide: From Disordered Coagulation and Lateral Branching to Amorphous Prefibrils.*J. Phys. Chem. Letters* **2019**, *10*, 1594-1599, doi:10.1021/acs.jpclett.9b00423.
199. Rojas, A.; Liwo, A.; Browne, D.; Scheraga, H.A. Mechanism of fiber assembly: treatment of Aβ peptide aggregation with a coarse-grained united-residue force field. *J. Mol. Biol.***2010**, *404*, 537-552, doi:10.1016/j.jmb.2010.09.057.
200. Rojas, A.V.; Liwo, A.; Scheraga, H.A. A study of the α-helical intermediate preceding the aggregation of the amino-terminal fragment of the β amyloid peptide (Aβ(1-28)).*J. Phys. Chem.. B* **2011**, *115*, 12978-12983, doi:10.1021/jp2050993.
201. Nguyen, H.L.; Krupa, P.; Hai, N.M.; Linh, H.Q.; Li, M.S. Structure and Physicochemical Properties of the Aβ42 Tetramer: Multiscale Molecular Dynamics Simulations. *J. Phys. Chem. B* **2019**, *123*, 7253-7269, doi:10.1021/acs.jpcb.9b04208.
202. Vácha, R.; Frenkel, D. Relation between molecular shape and the morphology of self-assembling aggregates: a simulation study. *Biophys. J.* **2011**, *101*, 1432-1439, doi:10.1016/j.bpj.2011.07.046.
203. Bieler, N.S.; Knowles, T.P.J.; Frenkel, D.; Vácha, R. Connecting Macroscopic Observables and Microscopic Assembly Events in Amyloid Formation Using Coarse Grained Simulations. *PLoS Comput. Biol.* **2012**, *8*, e1002692, doi:10.1371/journal.pcbi.1002692.
204. Šarić, A.; Chebaro, Y.C.; Knowles, T.P.J.; Frenkel, D. Crucial role of nonspecific interactions in amyloid nucleation. *PNAS* **2014**, *111*, 17869, doi:10.1073/pnas.1410159111.
205. Michaels, T.C.T.; Šarić, A.; Curk, S.; Bernfur, K.; Arosio, P.; Meisl, G.; Dear, A.J.; Cohen, S.I.A.; Dobson, C.M.; Vendruscolo, M.; et al. Dynamics of oligomer populations formed during the aggregation of Alzheimer's Aβ42 peptide. *Nat. Chem.* **2020**, *12*, 445-451, doi:10.1038/s41557-020-0452-1.
206. Ilie, I.M.; den Otter, W.K.; Briels, W.J. A coarse grained protein model with internal degrees of freedom. Application to α-synuclein aggregation. *J. Chem. Phys.* **2016**, *144*, 085103, doi:10.1063/1.4942115.
207. Ilie, I.M.; den Otter, W.K.; Briels, W.J. The attachment of α-synuclein to a fiber: A coarse-grain approach. *J. Chem. Phys.* **2017**, *146*, 115102, doi:10.1063/1.4978297.
208. Barz, B.; Urbanc, B. Minimal model of self-assembly: emergence of diversity and complexity.*J. Phys. Chem.. B* **2014**, *118*, 3761-3770, doi:10.1021/jp412819j.
209. Hoang, T.X.; Trovato, A.; Seno, F.; Banavar, J.R.; Maritan, A. Geometry and symmetry presculpt the free-energy landscape of proteins. *PNAS* **2004**, *101*, 7960, doi:10.1073/pnas.0402525101.
210. Auer, S.; Dobson, C.M.; Vendruscolo, M. Characterization of the nucleation barriers for protein aggregation and amyloid formation.*HFSP J.* **2007**, *1*, 137-146, doi:10.2976/1.2760023.
211. Auer, S.; Meersman, F.; Dobson, C.M.; Vendruscolo, M. A Generic Mechanism of Emergence of Amyloid Protofilaments from Disordered Oligomeric Aggregates. *PLoS Comput. Biol.* **2008**, *4*, e1000222, doi:10.1371/journal.pcbi.1000222.

212. Hung, N.B.; Le, D.-M.; Hoang, T.X. Sequence dependent aggregation of peptides and fibril formation. *J. Chem. Phys.* **2017**, *147*, 105102, doi:10.1063/1.5001517.
213. Mioduszewski, Ł.; Cieplak, M. Disordered peptide chains in an α-C-based coarse-grained model.Phys. Chem. Chem. Phys. **2018**, *20*, 19057-19070, doi:10.1039/C8CP03309A.
214. Mioduszewski, Ł.; Cieplak, M. Protein droplets in systems of disordered homopeptides and the amyloid glass phase.Phys. Chem. Chem. Phys. **2020**, *22*, 15592-15599, doi:10.1039/D0CP01635G.
215. Pellarin, R.; Caflisch, A. Interpreting the Aggregation Kinetics of Amyloid Peptides. *J. Mol. Biol.***2006**, *360*, 882-892, doi:https://doi.org/10.1016/j.jmb.2006.05.033.
216. Pellarin, R.; Schuetz, P.; Guarnera, E.; Caflisch, A. Amyloid Fibril Polymorphism Is under Kinetic Control. *J. Am. Chem. Soc.* **2010**, *132*, 14960-14970, doi:10.1021/ja106044u.
217. Pellarin, R.; Guarnera, E.; Caflisch, A. Pathways and Intermediates of Amyloid Fibril Formation. *J. Mol. Biol.***2007**, *374*, 917-924, doi:https://doi.org/10.1016/j.jmb.2007.09.090.
218. Friedman, R.; Pellarin, R.; Caflisch, A. Amyloid Aggregation on Lipid Bilayers and Its Impact on Membrane Permeability. *J. Mol. Biol.***2009**, *387*, 407-415, doi:https://doi.org/10.1016/j.jmb.2008.12.036.
219. Friedman, R.; Caflisch, A. Surfactant Effects on Amyloid Aggregation Kinetics. *J. Mol. Biol.***2011**, *414*, 303-312, doi:https://doi.org/10.1016/j.jmb.2011.10.011.
220. Bellesia, G.; Shea, J.-E. Self-assembly of β-sheet forming peptides into chiral fibrillar aggregates. *J. Chem. Phys.* **2007**, *126*, 245104, doi:10.1063/1.2739547.
221. Bellesia, G.; Shea, J.-E. Diversity of kinetic pathways in amyloid fibril formation. *J. Chem. Phys.* **2009**, *131*, 111102, doi:10.1063/1.3216103.
222. Morriss-Andrews, A.; Shea, J.-E. Kinetic pathways to peptide aggregation on surfaces: The effects of β-sheet propensity and surface attraction. *J. Chem. Phys.* **2012**, *136*, 065103, doi:10.1063/1.3682986.
223. Irbäck, A.; Jónsson, S.Æ.; Linnemann, N.; Linse, B.; Wallin, S. Aggregate Geometry in Amyloid Fibril Nucleation.*Phys. Rev. Lett.* **2013**, *110*, 058101, doi:10.1103/PhysRevLett.110.058101.
224. Zhang, J.; Muthukumar, M. Simulations of nucleation and elongation of amyloid fibrils. *J. Chem. Phys.* **2009**, *130*, 035102-035102, doi:10.1063/1.3050295.
225. Abeln, S.; Vendruscolo, M.; Dobson, C.M.; Frenkel, D. A Simple Lattice Model That Captures Protein Folding, Aggregation and Amyloid Formation. *PLOS ONE* **2014**, *9*, e85185, doi:10.1371/journal.pone.0085185.
226. Ni, R.; Abeln, S.; Schor, M.; Cohen Stuart, M.A.; Bolhuis, P.G. Interplay between Folding and Assembly of Fibril-Forming Polypeptides.*Phys. Rev. Lett.* **2013**, *111*, 058101, doi:10.1103/PhysRevLett.111.058101.
227. Tran, T.T.; Nguyen, P.H.; Derreumaux, P. Lattice model for amyloid peptides: OPEP force field parametrization and applications to the nucleus size of Alzheimer's peptides. *J. Chem. Phys.* **2016**, *144*, 205103, doi:10.1063/1.4951739.
228. Kouza, M.; Co, N.T.; Nguyen, P.H.; Kolinski, A.; Li, M.S. Preformed template fluctuations promote fibril formation: Insights from lattice and all-atom models. *J. Chem. Phys.* **2015**, *142*, 145104, doi:10.1063/1.4917073.
229. Co, N.T.; Li, M.S. New method for determining size of critical nucleus of fibril formation of polypeptide chains. *J. Chem. Phys.* **2012**, *137*, 095101, doi:10.1063/1.4749257.
230. Koliński, A. Protein modeling and structure prediction with a reduced representation. *Acta Biochim. Pol.* **2004**, *51*.
231. Zambrano, R.; Jamroz, M.; Szczasiuk, A.; Pujols, J.; Kmiecik, S.; Ventura, S. AGGRESCAN3D (A3D): server for prediction of aggregation properties of protein structures. *Nucleic Acids Res.* **2015**, *43*, W306-W313, doi:10.1093/nar/gkv359.
232. Metropolis, N.; Ulam, S. The Monte Carlo Method. *J Am Stat Assoc* **1949**, *44*, 335-341, doi:10.1080/01621459.1949.10483310.

233. Betancourt, M.R.; Thirumalai, D. Pair potentials for protein folding: Choice of reference states and sensitivity of predicted native states to variations in the interaction schemes. *Protein Sci.* **1999**, *8*, 361-369, doi:10.1110/ps.8.2.361.
234. Nosé, S. A molecular dynamics method for simulations in the canonical ensemble. *Mol. Phys.* **1984**, *52*, 255-268, doi:10.1080/00268978400101201.
235. Van Gunsteren, W.F.; Berendsen, H.J. A leap-frog algorithm for stochastic dynamics. *Mol Simul* **1988**, *1*, 173-185.
236. Ryckaert, J.-P.; Ciccotti, G.; Berendsen, H.J.C. Numerical integration of the cartesian equations of motion of a system with constraints: molecular dynamics of n-alkanes. *J. Comput. Phys.* **1977**, *23*, 327-341, doi:https://doi.org/10.1016/0021-9991(77)90098-5.
237. Wu, X.; Brooks, B.R. Self-guided Langevin dynamics simulation method.*Chem. Phys. Lett.* **2003**, *381*, 512-518.
238. Darden, T.; York, D.; Pedersen, L. Particle mesh Ewald: An N·log(N) method for Ewald sums in large systems. *J. Chem. Phys.* **1993**, *98*, 10089-10092, doi:10.1063/1.464397.
239. Grubmüller, H.; Heymann, B.; Tavan, P. Ligand binding: molecular mechanics calculation of the streptavidin-biotin rupture force. *Science* **1996**, *271*, 997-999.
240. Binning, G.; Quate, C.; Gerber, C. Atomic force microscope.*Phys. Rev. Lett.*. **1986**.
241. Bustamante, C.J.; Chemla, Y.R.; Liu, S.; Wang, M.D. Optical tweezers in single-molecule biophysics. *Nat. Rev. Dis. Primers* **2021**, *1*, 25, doi:10.1038/s43586-021-00021-6.
242. Sarkar, R.; Rybenkov, V.V. A Guide to Magnetic Tweezers and Their Applications.*Front. Phys.* **2016**, *4*, doi:10.3389/fphy.2016.00048.
243. Kumar, S.; Li, M.S. Biomolecules under mechanical force. *Phys. Rep.* **2010**, *486*, 1-74, doi:https://doi.org/10.1016/j.physrep.2009.11.001.
244. Ruggeri, F.S.; Šneideris, T.; Vendruscolo, M.; Knowles, T.P.J. Atomic force microscopy for single molecule characterisation of protein aggregation. *Arch. Biochem. Biophys.***2019**, *664*, 134-148, doi:https://doi.org/10.1016/j.abb.2019.02.001.
245. Izrailev, S.; Stepaniants, S.; Balsera, M.; Oono, Y.; Schulten, K. Molecular dynamics study of unbinding of the avidin-biotin complex. *Biophys. J.* **1997**, *72*, 1568-1581.
246. Isralewitz, B.; Izrailev, S.; Schulten, K. Binding pathway of retinal to bacterio-opsin: a prediction by molecular dynamics simulations. *Biophys. J.* **1997**, *73*, 2972-2979.
247. Heinig, M.; Frishman, D. STRIDE: a web server for secondary structure assignment from known atomic coordinates of proteins. *Nucleic Acids Res.* **2004**, *32*, W500-W502, doi:10.1093/nar/gkh429.
248. Turner, P. XMGRACE, Version 5.1. 19. *Center for Coastal and Land-Margin Research, Oregon Graduate Institute of Science and Technology, Beaverton, OR* **2005**.
249. Harrington, B.e.a. Inkscape. **2004**.
250. Lin, Y.C.; Li, C.; Fakhraai, Z. Kinetics of Surface-Mediated Fibrillization of Amyloid-beta (12-28) Peptides. *Langmuir* **2018**, *34*, 4665-4672, doi:10.1021/acs.langmuir.7b02744.
251. Rabe, M.; Soragni, A.; Reynolds, N.P.; Verdes, D.; Liverani, E.; Riek, R.; Seeger, S. On-surface aggregation of alpha-synuclein at nanomolar concentrations results in two distinct growth mechanisms. *ACS Chem Neurosci* **2013**, *4*, 408-417, doi:10.1021/cn3001312.
252. Lindberg, D.J.; Wesen, E.; Bjorkeroth, J.; Rocha, S.; Esbjorner, E.K. Lipid membranes catalyse the fibril formation of the amyloid-beta (1-42) peptide through lipid-fibril interactions that reinforce secondary pathways. *Biochim Biophys Acta Biomembr* **2017**, *1859*, 1921-1929, doi:10.1016/j.bbamem.2017.05.012.
253. Cabaleiro-Lago, C.; Lynch, I.; Dawson, K.A.; Linse, S. Inhibition of IAPP and IAPP(20-29) fibrillation by polymeric nanoparticles. *Langmuir* **2010**, *26*, 3453-3461, doi:10.1021/la902980d.
254. Mahmoudi, M.; Akhavan, O.; Ghavami, M.; Rezaee, F.; Ghiasi, S.M.A. Graphene oxide strongly inhibits amyloid beta fibrillation. *Nanoscale* **2012**, *4*, 7322-7325, doi:10.1039/C2NR31657A.

255. Kang, S.G.; Huynh, T.; Xia, Z.; Zhang, Y.; Fang, H.; Wei, G.; Zhou, R. Hydrophobic interaction drives surface-assisted epitaxial assembly of amyloid-like peptides. *J Am Chem Soc* **2013**, *135*, 3150-3157, doi:10.1021/ja310989u.
256. Zhang, F.; Du, H.N.; Zhang, Z.X.; Ji, L.N.; Li, H.T.; Tang, L.; Wang, H.B.; Fan, C.H.; Xu, H.J.; Zhang, Y.; et al. Epitaxial growth of peptide nanofilaments on inorganic surfaces: effects of interfacial hydrophobicity/hydrophilicity. *Angew Chem Int Ed Engl* **2006**, *45*, 3611-3613, doi:10.1002/anie.200503636.
257. CO, N.T.; VIET, M.H.; MINH, P.; TRUONG, M.K.; LI, M.S. Key factors governing fibril formation of proteins: insights from simulations and experiments. *TASK QUARTERLY* **2014**, *18*, 245-254.
258. Chiti, F.; Stefani, M.; Taddei, N.; Ramponi, G.; Dobson, C.M. Rationalization of the effects of mutations on peptide andprotein aggregation rates. *Nature* **2003**, *424*, 805-808, doi:10.1038/nature01891.
259. Benilova, I.; Karran, E.; De Strooper, B. The toxic Aβ oligomer and Alzheimer's disease: an emperor in need of clothes.*Nat. Neurosci* **2012**, *15*, 349.
260. Ostermeier, L.; de Oliveira, G.A.P.; Dzwolak, W.; Silva, J.L.; Winter, R. Exploring the polymorphism, conformational dynamics and function of amyloidogenic peptides and proteins by temperature and pressure modulation. *Biophys. Chem.* **2021**, *268*, 106506, doi:https://doi.org/10.1016/j.bpc.2020.106506.
261. Gruning, C.S.R.; Klinker, S.; Wolff, M.; Schneider, M.; Toksoz, K.; Klein, A.N.; Nagel-Steger, L.; Willbold, D.; Hoyer, W.J.J.B.C. The off-rate of monomers dissociating from amyloid-Î² protofibrils. **2013**, *203*, 37104-37111.
262. Li, M.S.; Klimov, D.K.; Straub, J.E.; Thirumalai, D. Probing the mechanisms of fibril formation using lattice models. *J Chem Phys* **2008**, *129*, 175101.
263. Pearlman, D.A.; Case, D.A.; Caldwell, J.W.; Ross, W.S.; Cheatham, T.E.; DeBolt, S.; Ferguson, D.; Seibel, G.; Kollman, P. AMBER, a package of computer programs for applying molecular mechanics, normal mode analysis, molecular dynamics and free energy calculations to simulate the structural and energetic properties of molecules. *Comput. Phys. Commun.* **1995**, *91*, 1-41, doi:https://doi.org/10.1016/0010-4655(95)00041-D.
264. Levin, A.; Mason, T.O.; Adler-Abramovich, L.; Buell, A.K.; Meisl, G.; Galvagnion, C.; Bram, Y.; Stratford, S.A.; Dobson, C.M.; Knowles, T.P.J.; et al. Ostwald's rule of stages governs structural transitions and morphology of dipeptide supramolecular polymers. *Nat. Commun.* **2014**, *5*, 5219, doi:10.1038/ncomms6219.